TECHNICAL UNIVERSITY OF LIBEREC
Faculty of Textile Engineering

Stabilizace sono syntetizovaného fotocatalistu na textil a rozvoj multifunkčních nanokompozitů

Disertační práce

Studijní program: P3106 – Textile Engineering

Studijní obor: 3106V015 – Textile Technics and Materials Engineering

Autor práce: **Muhammad Tayyab Noman, M.Sc.**

Vedoucí práce: Ing. Jana Šašková, Ph.D.

TECHNICAL UNIVERSITY OF LIBEREC
Faculty of Textile Engineering

STABILIZATION OF SONO SYNTHESIZED PHOTOCATALYST ON TEXTILES AND DEVELOPMENT OF MULTIFUNCTIONAL NANOCOMPOSITES

Dissertation

Study programme: P3106 – Textile Engineering

Study branch: 3106V015 – Textile Technics and Materials Engineering

Author: **Muhammad Tayyab Noman, M.Sc.**

Supervisor: Ing. Jana Šašková, Ph.D.

Prohlášení

Byl jsem seznámen s tím, že na mou disertační práci se plně vztahuje zákon č. 121/2000 Sb., o právu autorském, zejména § 60 – školní dílo.

Beru na vědomí, že Technická univerzita v Liberci (TUL) nezasahuje do mých autorských práv užitím mé disertační práce pro vnitřní potřebu TUL.

Užiji-li disertační práci nebo poskytnu-li licenci k jejímu využití, jsem si vědom povinnosti informovat o této skutečnosti TUL; v tomto případě má TUL právo ode mne požadovat úhradu nákladů, které vynaložila na vytvoření díla, až do jejich skutečné výše.

Disertační práci jsem vypracoval samostatně s použitím uvedené literatury a na základě konzultací s vedoucím mé disertační práce a konzultantem.

Současně čestně prohlašuji, že tištěná verze práce se shoduje s elektronickou verzí, vloženou do IS STAG.

Datum:

Podpis:

Preface

This dissertation is the result of my own work and includes nothing which is the outcome of work done in collaboration. The presented work was undertaken at the Department of Material Engineering, Technical University of Liberec, Czech Republic. No other part of this dissertation has been submitted for a degree to this or any other university. This dissertation contains approximately 26900 words, 39 figures and 19 tables.

The work discussed in this dissertation has already been published in the following:

1. M.T. Noman, J. Wiener, J. Saskova, M.A. Ashraf, M. Vikova, H. Jamshaid, P. Kejzlar, "In-situ development of highly photocatalytic multifunctional nanocomposites by ultrasonic acoustic method", ***Ultrasonics Sonochemistry***, 40 (2018) 41-56. **Impact factor: 6.012**.
2. M.T. Noman, J. Militky, J. Wiener, J. Saskova, M.A. Ashraf, H. Jamshaid, M. Azeem, "Sonochemical synthesis of highly crystalline photocatalyst for industrial applications", ***Ultrasonics***, 83 (2018) 203-213. **Impact factor: 2.377.**
3. M.T. Noman, M.A. Ashraf, H. Jamshaid, A. Ali, "A novel green stabilization of TiO_2 nanoparticles onto cotton", ***Fibers and Polymers*** (Accepted). **Impact factor: 1.353.**

Muhammad Tayyab Noman, M.Sc.

Student ID: T14000555

Abstract

Nanoparticles (NPs) with smaller size and higher crystallinity exert a remarkable influence on the photocatalytic performance of a photocatalyst. This dissertation is about the synthesis and stabilization of a novel photocatalyst to enhance the functional properties of textiles. Moreover, an in-situ Ultrasonic Acoustic Method (UAM) is used to develop novel Cotton-TiO_2 (CT) multifunctional nanocomposites.

Highly photo active pure anatase form of TiO_2 (titanium dioxide, titania) NPs with average particle size 4 *nm* have been successfully synthesized by Ultrasonic Acoustic Method (UAM). The effects of process variables i.e. precursors concentration and sonication time were investigated based on Central Composite Design (CCD) and Response Surface Methodology (RSM). The characteristics of the Resulting Nanoparticles (RNP) were analysed by Scanning Electron Microscopy (SEM), Dynamic Light Scattering (DLS), Transmission Electron Microscopy (TEM), X-ray Diffractometry (XRD) and Raman Spectroscopy. Photocatalytic experiments were performed with Methylene Blue (MB) dye which is considered as a model organic pollutant in textile industry. A comparative analysis between the developed photocatalyst and commercially available photocatalyst Degussa P25 was performed for photocatalytic performance against dye removal efficiency. The rapid removal of MB in case of RNP indicates their higher photocatalytic activity than P25. Maximum dye removal efficiency 99 % was achieved with optimal conditions i.e. Titanium Tetraisopropoxide (TTIP) conc. 10 *mL*, Ethylene Glycol (EG) conc. 4 *mL* and sonication time 1 *h*. Interestingly, no significant difference was found in the photocatalytic performance of RNP after calcination. Moreover, self-cleaning efficiency of RNP deposited on cotton was evaluated in RGB (Red, Green, Blue) colour space. The obtained results indicate the significant impact of ultrasonic

irradiations on the photocatalytic performance of pure anatase form than any other hybrid type of TiO_2 NPs.

In another experiment, facile embedding of the Resulting Nanoparticles (RNP) onto cotton fabric has been successfully attained by Ultraviolet (UV) light irradiations. The adhesion of NPs with fibre surface, tensile behaviour and physicochemical changes before and after UV treatment were investigated by SEM, Energy Dispersive X-ray (EDX) and Inductive Couple Plasma-Atomic Emission (ICP-AES) Spectroscopies. Experimental variables i.e. dosage of TiO_2 NPs, temperature of the system and time of UV irradiations were optimised by CCD and RSM. Moreover, two different mathematical models were developed for incorporated TiO_2 onto cotton and tensile strength of cotton after UV treatment, and further used to testify the obtained results. Self-clean fabric through a synergistic combination of cotton with highly photo active TiO_2 NPs was produced. Stability against UV irradiations and self-cleaning properties of the produced fabric were evaluated.

Finally, Cotton-TiO_2 (CT) nanocomposites with multifunctional properties were synthesized by an in-situ Ultrasonic Acoustic Method (UAM). Ultrasonic irradiations were used as a potential tool to develop CT nanocomposites at low temperature in the presence of Titanium Tetrachloride (TTC) and Isopropanol (ISP). The synthesized samples were characterized by XRD, SEM, EDX and ICP-AES methods. Functional properties i.e. Ultraviolet Protection Factor (UPF), self-cleaning, washing durability, antimicrobial and tensile strength of the CT nanocomposites were evaluated by different methods. CCD and RSM were employed to evaluate the effects of selected variables on responses. The results confirm the simultaneous formation and incorporation of anatase TiO_2 with average crystallite size of 4 *nm* on cotton fabric with excellent photocatalytic properties. The sustained self-cleaning efficiency of CT

nanocomposites even after 30 home launderings indicates their excellent washing durability. Significant effects were obtained during statistical analysis for selected variables on the formation and incorporation of TiO_2 NPs on cotton and photocatalytic properties of CT nanocomposites.

Keywords

TiO_2; Anatase; Photocatalysis; Sonochemical synthesis; Dyes degradation; Ultrasonic irradiations; Ethylene glycol; Response surfaces; Self-stabilization; Self-cleaning; Nanoparticles; Ultrasonic acoustic method; Ultraviolet protection factor; Nanocomposites

Abstrakt

Nanočástice (NP) s menší velikostí a vyšší krystalinitou mají významný vliv na fotokatalytický výkon fotokatalyzátoru. Tato práce se zabývá syntézou a stabilizací nového fotokatalyzátoru pro zvýšení funkčních vlastností textilií. Navíc je použita ultrazvuková akustická metoda in-situ pro vývoj nových multifunkčních nanokompozitů bavlna-TiO_2 (CT).

Ultrazvukovou akustickou metodou byly úspěšně syntetizovány nanočástice oxidu titaničitého (TiO_2) ve formě čistého anatasu, které mají průměrnou velikost 4 nm a jsou vysoce fotoaktivní. Za pomoci metody centrálního kompozitního designu (CCD) a metody povrchové odezvy (RSM) byl zkoumán vliv procesních proměnných (koncentrace prekurzorů a doba sonizace) na výsledný produkt. Vlastnosti připravených nanočástic (RNP) byly analyzovány skenovací elektronovou mikroskopií (SEM), dynamickým rozptylem světla (DLS), transmisní elektronovou mikroskopií (TEM), rentgenovou difraktometrií (XRD) a Ramanovou spektroskopií. V experimentech ověřujících fotokatalytické vlastností byla použita metylenová modř (MB), která je považována za model organické znečišťující látky v textilním průmyslu. Pro posouzení fotokatalytických vlastností (účinnost v odstraňování barviva) byla provedena srovnávací analýza vyvinutého fotokatalyzátoru s komerčně dostupným fotokatalyzátorem Degussa P25. Rychlé odstranění MB v případě RNP naznačuje jejich vyšší fotokatalytickou aktivitu než P25. Za optimálních podmínek (10ml titanium tetraisopropoxidu (TTIP), 4ml etylenglykolu (EG) konc. a doba sonizace 1 h) byla dosažena maximální účinnost odstraňování barviva 99%. Je zajímavé, že při kalcinaci nebyl nalezen žádný významný rozdíl ve fotokatalytickém výkonu RNP. Samočisticí účinnost RNP aplikovaných na bavlnu byla navíc vyhodnocena v barevném prostoru RGB. Získané výsledky ukazují na významný vliv

ultrazvukového působení na fotokatalytický výkon čistého anatasu než na jakýkoli jiný hybridní typ nanočástic oxidu titaničitého.

V dalším experimentu bylo dosaženo povrchové fixace RNP na bavlněnou tkaninu ultrafialovým zářením (UV). Adheze nanočástic na povrchu vlákna, tahové chování a fyzikálně chemické změny před UV ozářením a po něm, byly zkoumány pomocí spektrometrů SEM, Energy Dispersive X-ray (EDX) a spektroskopií s induktivní dvojitou plazmovou atomovou emisí (ICP-AES). Experimentální proměnné, tj. množství nanočástic TiO_2, teplota systému a doba UV záření byly optimalizovány pomocí CCD a RSM. Také byly vyvinuty dva matematické modely pro aplikaci TiO_2 na bavlnu a pevnost v tahu bavlny po UV ozáření. Modely byly dále použity k potvrzení získaných výsledků. Byla vyrobena samočistící tkanina synergickou kombinací bavlny s vysoce fotoaktivními nanočásticemi TiO_2. Byla hodnocena stabilita při UV záření a samočisticí vlastnosti vyrobené tkaniny.

Nakonec byly ultrazvukovou akustickou metodou in situ připraveny nanokompozity bavlna-TiO_2 (CT) s multifunkčními vlastnostmi. Působení ultrazvuku bylo použito jako potenciální nástroj pro vývoj CT nanokompozitů při nízké teplotě v přítomnosti tetrachloridu titaničitého (TTC) a isopropanolu (ISP). Syntetizované vzorky byly charakterizovány metodami XRD, SEM, EDX a ICP-AES. Dále byly sledovány funkční vlastnosti jako ultrafialový ochranný faktor (UPF), samočisticí schopnosti, stálost v praní, antimikrobiální vlastnosti a pevnost CT nanokompozitů v tahu. Pro vyhodnocení vybraných vlivů byly využity metody CCD a RSM. Výsledky potvrzují současně vznik a inkorporaci anatasového TiO_2 s průměrnou velikostí krystalů 4 nm na bavlněnou tkaninu, vzniká materiál s vynikajícími fotokatalytickými vlastnostmi. Samočisticí účinnost CT nanokompozitů i po 30 cyklech praní naznačuje jejich

vynikající životnost. Při statistické analýze vybraných proměnných v přípravě a fixaci TiO_2 na bavlnu byly ověřeny jejich významné účinky na fotokatalytické vlastnosti CT nanokompozitů.

Klíčová slova

TiO_2; Anatas; Fotokatalýza; Sonochemická syntéza; Degradace barviv; Ultrazvukové ozařování; Etylenglykol; Odpovídající povrchy; Samostabilizace; Samočistění; Nanočástice; Ultrazvukové akustické metody; Faktor ochrany proti ultrafialovému záření; Nanokompozity

Введение

Наночастицы с меньшим размером и высокой кристалличностью оказывают выдающееся влияние на фотокаталитическую активность фотокатализа. Данная диссертация рассказывает о синтезе и стабилизации неизведанного фотокатализатора для повышения функциональных свойств текстиля. Более того, для разработки мультифункциональных нанокомпозитов Cotton-TiO_2 (Хлопок Диоксид Титана) используется ультразвуковой акустический метод in-situ.

Высоко фото активная чистая анатазная форма наночастиц TiO_2 (Диоксид Титана), размер частиц которых составляет в среднем 4*нм*, были успешно синтезированы с помощью ультразвукового акустического метода. Воздействия переменных процесса, т.е. концентрации прекурсоров и время разрушения ультразвуком, были исследованы на базе Центрального композиционного плана и Методологии расчета на основе поверхности отклика. Характеристики полученных наночастиц были анализированы с помощью Растрового электронного микроскопа, Динамического рассеяния света, Просвечивающего электронного микроскопа, Дифракционного рентгеновского анализа и Рамановской спектроскопии. Фотокаталитические эксперименты были выполнены с красителем Метиленовый синий, который считается образцовым органическим загрязнителем в текстильной индустрии. Сравнительный анализ полученного фотокатализа и коммерчески доступного фотокатализа Degussa P25 был проведён для фотокаталитического действия против эффективности удаления красителя. Быстрое удаление красителя Метиленовый синий в случае полученных наночастиц указывает на его более высокую фотокаталитическую активность, чем имеет P25. Максимальная эффективность удаления красителя 99% была достигнута в оптимальных условиях, т.е.

концентрат Тетраизопропоксида Титана 10мл, концентрат Этиленгриколя 4мл и время разрушения ультразвуком 1 час. Интересно, но значительной разницы в фотокаталитическом действии полученных частиц после обжигания выявлено не было. Более того, эффективность самоочищения полученных наночастиц, депонированных на хлопке, была оценена в КЗС (Красный, Зеленый, Синий) цветовой модели. Полученные результаты указывают на более существенное влияние ультразвукового облучения на фотокаталитическое действие чистой анатазной формы, чем у других гибридов наночастиц Диоксида Титана.

В результате другого эксперимента было достигнуто лёгкое внедрение полученных наночастиц в хлопковую ткань с помощью Ультрафиолетового светового облучения. Сцепление наночастиц с поверхностью волокна, растяжимость и физико-химические изменения до и после облучения были исследованы Растровым электронным микроскопом, Рентгеноспектральным анализатором и Атомно-эмиссионной спектроскопией с индуктивно связанной плазмой. Экспериментальные переменные, т.е. дозировка наночастиц TiO_2, температура системы и время Ультрафиолетового облучения, были оптимизированы с помощью Центрального композиционного плана и Методологии расчета на основе поверхности отклика. Более того, для силы растяжимости хлопка после УФ облучения и TiO_2, внедренного в хлопок, были разработаны две разные математические модели, которые в дальнейшем использовались для тестирования результатов. Самоочищающаяся ткань из синергетической комбинации хлопка с высоко фото активными наночастицами TiO_2 была произведена, ее устойчивость против УФ облучению и самоочищающиеся свойства подтверждены.

Наконец, нанокомпозиты Cotton-TiO_2 о с мультифункциональными свойствами были синтезированы ультразвуковым акустическим методом in-situ. Ультразвуковые излучения использовались как потенциальное средство разработки нанокомпозитов Cotton-TiO_2 при низкой температуре с Тетрахлоридом титана и Изопропиловым спиртом. Синтезированные образцы были охарактеризованы с помощью Дифракционного рентгеновского анализа, Растрового электронного микроскопа, Рентгеноспектрального анализатора и Атомно-эмиссионной спектроскопии с индуктивно связанной плазмой. Функциональные свойства, т.е. Ультрафиолетовый коэффициент защиты, самоочищаемость, стойкость к стирке, антимикробный фактор и предел прочности, были оценены разными методами. Центральный композиционный плана и Методология расчета на основе поверхности отклика были применены для оценки эффектов выбранных переменных от реакций. Результаты подтвердили одновременное образование и объединение анатаза TiO_2 со средним размером кристаллита 4нм с хлопковой тканью с потрясающими фотокаталитическими свойствами. Самоочищающееся свойство нанокомпозитов Cotton-TiO_2 сохраняет свою эффективность даже после 30 домашних стирок. Значимые эффекты были получены в течение статистического анализа выбранных переменных на образовании и объединении наночастиц TiO_2 с хлопком и фотокаталитических свойств нанокомпозитов Cotton-TiO_2.

Ключевые слова

TiO_2; Анатаз; Фотокатализ; Сонохимический анализ; Деградация красителей; Ультразвуковые излучения; Этиленгликоль; Поверхности отклика; Самостабилизация;

Самоочищение; Наночастицы; Ультразвуковой акустический метод; Ультрафиолетовый коэффициент защиты; Нанокомпозиты.

الملخص

الجسيمات النانوية (NPs) ذات الحجم الأصغر والتبلور العالي تبذل تأثيراً ملحوظاً على آداء التحفيز الضوئي للحفاز الضوئي. هذه الرسالة تدور حول تخليق وتثبيت حفاز ضوئي جديد لتعزيز الخصائص الوظيفية للمنسوجات. وعلاوة على ذلك ، يتم إستخدام طريقة بالموجات فوق الصوتية في الموقع لتطوير تركيبات نانونية جديدة متعددة الوظائف من القطن-TiO_2 (CT).

تم تخليق حساس للضوء عالي النقاء من هيكل آناتاز من TiO_2 (ثاني أكسيد التيتانيوم، وتيتانيا) NPs بنجاح بمتوسط حجم جسيمات 4 نانومتر عن طريق الموجات فوق الصوتية (UAM). وقد تم دراسة تأثير متغيرات العمليات، أي تركيز السلائف، وزمن الصوتنة، على أساس تصميم المركب المركزي (CCD)، وطريقة أسطح الإستجابة (RSM). تم تحليل خصائص الجسيمات النانوية الناتجة(RNP) بواسطة الميكروسكوب الإلكتروني الماسح (SEM)، وتشتيت الضوء الديناميكى (DLS)، والميكروسكوب الإلكتروني النافذ (TEM)، وجهاز قياس إنكسار الأشعة السيني (XRD)، ومطياف رامان. وأجريت تجارب التحفيز الضوئي بإستخدام صبغة الميثيلين الأزرق (MB) التي تعتبر ملوثًا عضويًا نموذجيًا في صناعة المنسوجات. وتم إجراء تحليل مقارن بين الحفاز الضوئي المطور والحفاز الضوئي المتوفر تجارياً ديجوسا P25 لآداء التحفيز الضوئي ضد كفاءة إزالة الصبغة. وتشير سرعة إزالة الـ MB في حالة الـ RNP إلى نشاطهم التحفيز الضوئي الأعلى من P25. وتم تحقيق الحد الأقصى لكفاءة إزالة الصبغة بنسبة 99% مع الظروف المثلى، أي تيتانيوم تيترايسوبروبوكسيد(TTIP) بتركيز 10 مل، وإيثيلين جلايكول (EG) بتركيز 4 مل، وزمن صوتنة 1 ساعة. ومن المثير للإهتمام أنه لم يتم العثور على إختلاف بارز في الآداء التحفيزي لـ RNP بعد التكليس. وعلاوة على ذلك ، تم تقييم كفاءة التنظيف الذاتي للـ RNP المترسب على القطن في حيز اللون RGB (الأحمر، والأخضر، والأزرق). وتشير النتائج التي تم الحصول عليها إلى التأثير الملحوظ للإشعاعات فوق الصوتية على الآداء التحفيزي لهيكل آناتاز النقي عن أي نوع هجين آخر من TiO_2 NPs.

وفي تجربة أخرى ، تم تحقيق الطمر السطحي للجسيمات النانوية الناتجة (RNP) على قماش قطني بنجاح بواسطة الآشعة فوق البنفسجية (UV). وتم فحص إلتصاق NPs مع سطح الألياف، وسلوك متانة الشد، والتغيرات الفيزيوكيميائية قبل وبعد المعالجة بالآشعة فوق البنفسجية بإستخدام SEM، والأشعة السينية المشتتة للطاقة EDX، ومطياف الإنبعاث الحثي لزوج البلازما-الذرى (ICP-AES). وتم تحديد القيم المثلى للمتغيرات التجريبية، أي جرعة الـ TiP_2 NPs، ودرجة حرارة

النظام، وزمن إشعاع الآشعة فوق البنفسجية بواسطة الـ CCD و RSM. وعلاوة على ذلك، تم تطوير نموذجين رياضيين مختلفين لدمج TiO_2 على القطن، وتم إستخدام قوة شد القطن بعد المعالجة بالآشعة فوق البنفسجية لتؤكد النتائج التي تم الحصول عليها. وتم إنتاج قماش نظيف ذاتيًا من خلال مزيج منشط من القطن مع حساس للضوء عالي TiO_2 NPs. وتم تقييم درجة الثبات ضد الآشعة فوق البنفسجية وخصائص التنظيف الذاتي للقماش المنتج.

وأخيراً، تم تخليق مركبات نانوية من القطن (CT) TiO_2 ذات خصائص متعددة الوظائف بواسطة طريقة فوق صوتية في المكان. وإستخدمت الإشعاعات فوق الصوتية كآداة محتملة لتطوير المركبات النانوية CT عند درجة حرارة منخفضة في وجود تيترا كلورايد التيتانيوم (TTC)، وأيسوبروبانول (ISP). وتم وصف العينات المركبة بإستخدام الـ XRD، وSEM، وEDX، وICP-AES. وتم تقييم الخصائص الوظيفية، أى معامل الحماية من الأشعة فوق البنفسجية (UPF)، والتنظيف الذاتي، والثبات ضد الغسيل، ومقاومة الميكروبات، ومتانة الشد للمركبات النانوية CT باستخدام طرق مختلفة. وتم إستخدام CCDوRSM لتقييم تأثيرات المتغيرات المختارة على الإستجابات. والنتائج تؤكد التشكيل المتزامن ودمج الـ TiO_2 آناتاز بمتوسط حجم تبلور 4 نانومتر على قماش قطنى مع خصائص تحفيز ضوئى ممتازة. وتشير كفاءة التنظيف الذاتي المستمرة للمركبات النانوية CT حتى بعد 30 عملية غسيل منزلية إلى الثبات الممتاز ضد الغسيل. وتم الحصول على تأثيرات هامة خلال التحليل الإحصائي للمتغيرات المختارة على تكوين ودمج TiP_2 NPs على القطن وخواص التحفيز الضوئى للمركبات النانوية CT.

الكلمات الدالة

TIO_2، آناتاز، تحفيز ضوئي، تخليق سونوكيميائى، تدهور الأصباغ، الإشعاع بالموجات فوق الصوتية، إيثلين جلايكول، أسطح الإستجابة، التوازن الذاتى، التنظيف الذاتي، الجسيمات النانوية، طريقة الموجات فوق الصوتية، معامل الحماية من الأشعة فوق البنفسجية، المركبات النانوية.

Acknowledgement

"Life is not easy for any of us. But what of that? We must have perseverance, and above all, confidence in ourselves. We must believe that we are gifted for something and that this thing must be attained."

(Marie Curie)

If one were to consider the significant milestones in their own lives, it would become necessary to also consider those who have made these milestones possible. Here, I will do my best to acknowledge the people who have made this dissertation a reality. First and foremost, I would like to thank *Prof. Ing. Jiří Militký, CSc.* for his persistence, guidance and advice. I would like to extend my deepest appreciation and gratitude to my supervisor *Ing. Jana Šašková, Ph.D.* and research consultant *Prof. Ing. Jakub Wiener, Ph.D.* for their significant contributions to the experimental work. I would like to express my utmost gratitude to all members of Technical University of Liberec especially *Ing. Blanka Tomková, Ph.D., doc. RNDr. Miroslav Brzezina, CSc., Ing. Jana Drašarová, Ph.D., Ing. Gabriela Krupincová, Ph.D., doc. Rajesh Mishra, Ph.D., B. Tech., Ing. Marie Kašparová, Ph.D., Mrs. Bohumila Keilová and Mrs. Hana Musilova* for their moral support and assistance in different aspects.

I wish to acknowledge *Muhammad Azeem Ashraf*, who has been a wonderful friend and confidant throughout my life. Last but not the least, I would like to thank my nurturing parents, vivacious siblings and friends for all their prayers, undying love, guidance, support and encouragement. Thank you all for your support throughout this long journey.

Contents

List of Figures

List of Tables

List of Abbreviations

Acronyms	Description
NPs	Nanoparticles
NMs	Nanomaterials
NST	Nanoscience or Nanotechnology
SEM	Scanning Electron Microscopy
EDX	Energy Dispersive X-ray Spectroscopy
ISP	Isopropanol
TTC	Titanium Tetrachloride
TTIP	Titanium Tetraisopropoxide
ICP-AES	Inductive Couple Plasma-Atomic Emission Spectroscopy
EG	Ethylene Glycol
MB	Methylene Blue
CCD	Central Composite Design
RSM	Response Surface Methodology
CT	Cotton-TiO_2
DLS	Dynamic Light Scattering
UPF	Ultraviolet Protection Factor
TEM	Transmission Electron Microscopy
TiO_2	Titanium Dioxide, Titania
UAM	Ultrasonic Acoustic Method
RGB	Red, Green, Blue
RNP	Resulting Nanoparticles
XRD	X-ray Diffractometry
UV	Ultraviolet
nm	Nanometre
mL	Millilitre
h	Hour
°C	Degree Celsius
K	Kelvin
MPa	Mega Pascals
Ks^{-1}	Kelvin Per Second
mjm^{-2}	Milli Joule Per Square Meter
$TiCl_4$	Titanium Tetra Chloride
m^2g^{-1}	Meter Square Per Gram
gm^{-2}	Gram Per Square Meter
%	Percent/percentage
rpm	Revolutions Per Minute
kHz	Kilo Hertz
W	Watts
min	Minutes
kV	Kilo Volts
mA	Milli Ampere
g	Gram
gL^{-1}	Gram Per Litre

mgL^{-1}	Milligram Per Litre
Wm^{-2}	Watts Per Square Meter
cm	Centimetre
w/v	Weight/Volume
kN	Kilo Newton
$mmin^{-1}$	Meters Per Minute
M	Molar
NaCl	Sodium Chloride
L	Lightness
Wcm^{-2}	Watts Per Square Centimetre
v/v	Volume/Volume
cm^{-1}	Per Centimetre
eV	Electron Volts
conc.	Concentration
$OH^{\bullet}$	Hydroxyl Radical
$^{\bullet}O_2^-$	Super Oxide Anion
Ti	Titanium
ppm	Parts Per Million
N	Newton
°	Degree
S. aureus	Staphylococcus aureus
E. coli	Escherichia coli
JCPDS	Joint Committee on Powder Diffraction Standards

Chapter 1

1 Introduction

Nano Science or Nanotechnology (NST) manipulates matter on nanoscale by keeping at least one dimension less than 100 *nm* to develop products with extremely novel properties and functions. NST has gained much attention in recent years due to its fundamentals i.e. surface area to volume ratio and quantum confinement effect [1; 2]. Advances in NST have shown tremendous impact in the field of pharmaceuticals, materials science, energy, electronics and textiles [3-12]. NST encompasses two principal approaches: (1) ‘‘Top-down” approach through which larger assemblies are reduced to nanoscale by using different techniques i.e. grinding, milling, drilling, crushing etc. and (2) ‘‘Bottom-up” approach in which products are engineered through self-assembly of atoms or molecules by wet techniques i.e. sol-gel, hydrothermal and chemical vapour deposition etc. [13].

Scientists have admitted that Nanomaterials (NMs) play a prominent role in producing products with novel properties [14-23]. Researchers are successfully using numerous kinds of NMs in textile industry [24-38]. TiO_2 is the most significant and effective material which has been extensively employed in this field. The most significant reasons of its use in multiple applications are high photocatalytic activity, non-toxicity and chemical stability. TiO_2 is the only naturally occurring oxide of titanium metal at atmospheric pressure. It has three naturally existed polymorphic forms i.e. rutile, anatase, and brookite. All three polymorphs have same chemical structure but differ in their geometry and crystal form. The crystallization temperature for anatase is 300-400 $^{\circ}C$ while at high temperatures i.e. 800-1050 $^{\circ}C$, it directly transforms

itself into the rutile phase [39]. Rutile is mostly used in light scattering while anatase is used in photocatalysis due to its higher photocatalytic activity which is associated to its crystal lattice [40]. Matthews investigated the phenomenon of higher photocatalytic activity of anatase TiO_2 and explained that it happens due to the arrangement of TiO_6 octahedron. In rutile, TiO_6 octahedron shows an irregular orthorhombic distortion while in anatase, octahedron exhibits its symmetry lower than orthorhombic. Moreover, each octahedron exhibits two sharing edges in rutile and four sharing edges connection with the neighbouring octahedron in anatase respectively. These differences in octahedron arrangement make the crystal structures of the two up given polymorphs different and increases photocatalytic performance of anatase than rutile [41]. The surface chemistry of anatase and rutile by TiO_6 octahedron distortion, difference between lattice parameters and space groups is illustrated in *Figure 1-1* [42]. The role of anatase TiO_2 as a photocatalyst in self-cleaning and self-sterilizing coatings, photo degradation of organic toxins, gas sensors, biomedicines, energy, air and water purification are of great importance [43-50].

The methods used in the synthesis of NMs have a remarkable role in developing more precise and robust products with enhanced functional properties. Researchers have used different methods for the preparation of NMs [51-75]. Sonochemical synthesis is a promising route that enhances physical and chemical properties of a material through acoustic cavitation i.e. rapid formation, growth and collapse of unstable bubbles. The enhanced local conditions i.e. temperature (>5000 *K*), pressure (>20 *MPa*) and cooling rate (>10^{10} Ks^{-1}) induce exceptional properties into sonicated solutions that diminish metal ions to metals or metal oxides NPs [76]. The key advantages of using this method are its simplicity and energy efficiency. This method

has been efficiently used as an outstanding tool for low temperature synthesis of nanocrystalline TiO_2 [77; 78].

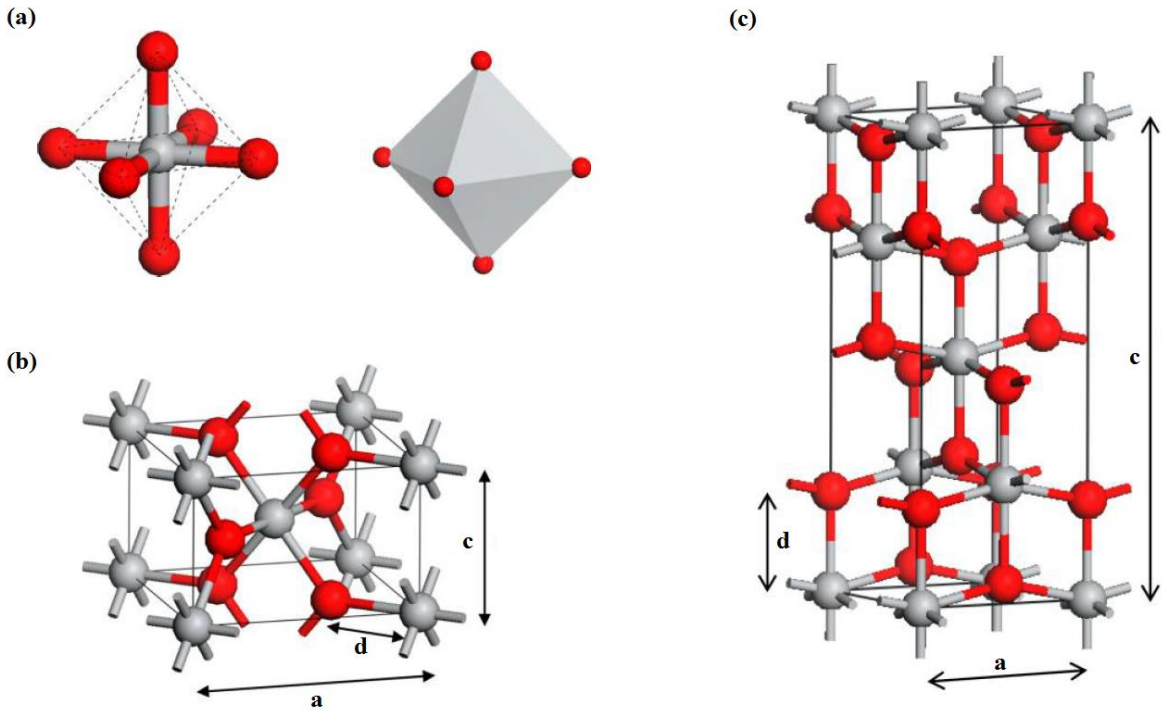

Figure 1-1 (a) Schematic representation of the distorted TiO_6 octahedron of TiO_2 (anatase and rutile). (b) Tetragonal structure of rutile described by using two cell edge parameters, a and c, and one internal parameter, d. (c) Tetragonal structure of anatase described by using two cell edge parameters, a and c, and one internal parameter, d. [42].

Photocatalysis is a dynamic mechanism and the most intrinsic feature of TiO_2 NMs that triggers a series of oxidation and reduction reactions. In photocatalysis, materials absorb light energy and break down the molecules into their fragments i.e. atoms, ions and radicals. The principle behind photocatalysis is the conversion of light energy into chemical energy to produce radicals and other unstable chemical compounds. The primary oxidizing species formed during

photocatalysis are hydroxyl radicals and superoxide anions [79; 80]. The general mechanism of photocatalysis on the surface of pure TiO_2 is described in *Figure 1-2* [17].

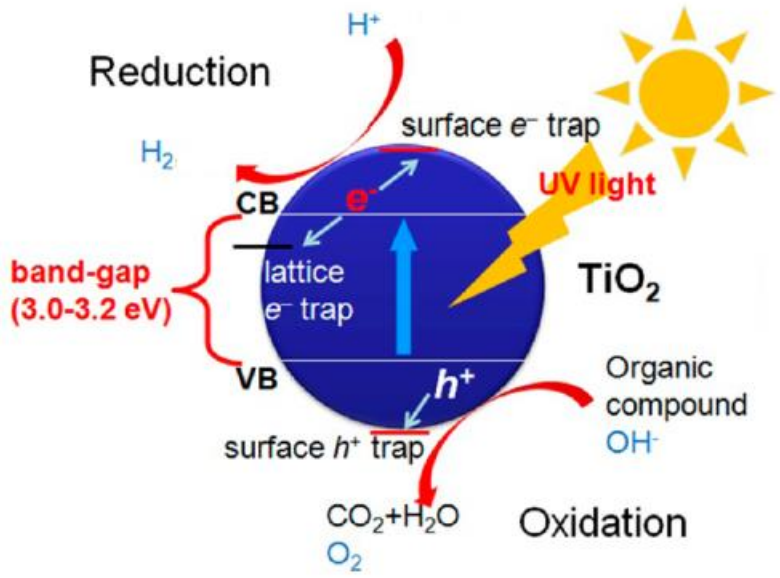

Figure 1-2 Mechanism of photocatalysis on the surface of TiO_2. Reactions occur in the following steps: (a) absorption of photon to produce electron-hole pair; (b) migration of separated charges towards the surface; (c) redox reactions with adsorbed reactants. [17].

1.1 Problem Statement

In textiles, the stabilization of NMs has been introduced during the last decade. Cheng et al. reported that there is almost no attraction between textile substrates (polymeric materials) and metal oxides particles (inorganic materials). This happens due to the difference in surface energy of the two above mentioned materials that produces repellence on their interfaces [81]. The values of surface energy for cotton and TiO_2 are 40-46 mjm^{-2} and $39x10^{-32}$ mjm^{-2} respectively. So, the stabilization of NPs on textiles is not permanent particularly against

washing. Researchers have been utilising different methods that require different steps for the stabilization of inorganic NMs on textile surfaces that are very time consuming and costly for large scale production. Regardless of the above-mentioned dilemma, researchers continued their efforts and used different approaches to embed or stabilize TiO_2 NPs on the surface of textiles [25; 82-86].

1.2 Research Objectives

The primary aims and overall objectives of this dissertation are:

- Synthesize TiO_2 Nanoparticles (NPs) in anatase form by Ultrasonic Acoustic Method (UAM) with novel reagents and incorporate them on textiles by two different approaches i.e. dip-pad-dry and UV induced stabilization and further utilised them as an efficient photocatalyst in multiple applications such as dyes degradation, self-cleaning, UV protecting clothes and antimicrobial finishes etc.

- Comparison of the developed photocatalyst with commercially available photocatalyst named Degussa P25 for higher photocatalytic efficiency.

- In-situ fabrication of Cotton-TiO_2 (CT) nanocomposites through UAM by using $TiCl_4$ or titanium tetrachloride (TTC) as a novel reagent.

- Analyse the role of ultrasonic irradiations and TiO_2 on the surface and structural properties of CT nanocomposites.

- Improve the characterization of pristine cotton by incorporation ultrafine TiO_2 NPs onto cotton.

- A comparative analysis of the developed method with conventional method explains the benefits of novel Ultrasonic Acoustic Method in textiles and composites industries.

- Durability of successfully deposited TiO_2 NPs on cotton fabric is evaluated against washing to investigate the colouring effect of applied materials on fabric.

- Optimization of the process variables by Central Composite Design (CCD) and Response Surface Methodology (RSM) to obtain more precise and accurate results.

- Analysis of the obtained results through regression and quadratic functions enhances the significance of the experiments and the development of mathematical models to predict the responses at any given point.

- Evaluation and increment in the efficiency of the functional properties i.e. Ultraviolet Protection Factor (UPF), dyes degradation efficiency, tensile strength etc., of the developed CT nanocomposites for their efficient use in different applications.

1.3 Dissertation Outline

Chapter 1 provides a detailed introduction about the dissertation theme that contains current state of the problem and research objectives. **Chapter 2** provides state of the art and discusses related work in previous literatures. The main body of the dissertation is in chapter 3 and chapter 4. **Chapter 3** describes the experimental conditions, materials, synthesis, design of experiments, methods, characterizations, modulations and formulas that utilised during the research work. **Chapter 4** explains a detailed chemical, mathematical and statistical analysis of the results derived from different experiments. In the end, **Chapter 5** concludes the dissertation and suggests some avenues for further research.

Chapter 2

2 Overview of the Current State of Problem

This **Chapter** enlightens the experimental investigations relevant to this dissertation that is divided into two main sections. The first section provides a comprehensive information about the synthesis mechanisms, experimental conditions, relevant parameters, used reagents and the relevant literature regarding synthesis methods mostly used in the fabrication of TiO_2 nanoparticles (NPs) while the applications are in the second section.

Ethylene Glycol (EG) has been extensively used in the synthesis of metal oxide nanomaterials (NMs) as it has strong reducing power and high boiling point [72; 87-89]. Many researchers have utilized EG in the synthesis of metal oxides by developing glycolated precursors because of its ability to coordinate with transition metal ions [90-92]. Mo and Chen described the role of EG as a cross-linking reagent to permit the formation of crack-free films in sol-gel process [93]. Kakihana et al. have synthesized powders of $LaMnO_{3+d}$ through in-situ polyesterification between citric acid and EG [94]. Lee et al. investigated the role of EG in the synthesis of barium titanate and barium orthotitanate powders through complex polymerization [95].

Hassani et al. investigated the sonocatalytic degradation of ciprofloxacin by utilizing synthesized TiO_2 NPs on montmorillonite and concluded that sonocatalytic process affects the degradation efficiency of ciprofloxacin and hydroxyl radicals produced by TiO_2 NPs play a major role in sonocatalytic phenomenon [96]. Fathinia et al. investigated the photocatalytic ozonation kinetic characteristics under different operational parameters and developed different kinetic models with TiO_2 NPs thin film for photocatalytic ozonation of

phenazopyridine in a mixed semi-batch photoreactor and found significant results among the predicting capability of all proposed models [97].

Abidi et al. reported sol-gel stabilization of TiO_2 on cotton fabric that improves UV scattering properties of cotton. They further used curing process to stabilize the developed nanosol on cotton [25]. Perelshtein et al. reported an ultrasonic assisted stabilization of TiO_2 NPs on cotton fabric to impart antimicrobial properties. Their results revealed that TiO_2 in its anatase and rutile form provides significant antimicrobial effects against microorganisms [86]. El-Rafie et al. and Hebeish et al. incorporated green synthesized silver NPs on cotton fabric in the presence of a binder by using a simple pad-dry-cure process. Their results revealed that cotton fabrics incorporated with silver NPs synthesized by green materials exhibit significant antimicrobial effects against Staphylococcus aureus (S. aureus) and Escherichia coli (E. coli) [82; 98]. Karimi et al. reported the fixation of nano TiO_2 and graphene oxide onto cotton fabric through oven heating and explained the synergetic effects of TiO_2/graphene nanocomposites on the photocatalytic efficiency of cotton fabric [84]. Long et al. developed fabrics with self-cleaning properties by stabilizing platinum modified TiO_2 NPs on cotton through dip-coating method that displayed significantly higher photocatalytic performance for methyl orange and coffee stain [85].

Gashti and Almasian reported the stabilization of carbon nanotubes on cotton fabric by UV radiations in order to develop flame retardant carbon/cellulose composites coatings [99]. In another study, Gashti et al. reported the incorporation of silica/kaolinite network on cotton surface through UV irradiations using succinic acid as a cross-linking agent to create a thermal resistant hydrophobic surface for cellulose based textiles [100]. Maleki et al. investigated the photodegradation of humic substances with zinc oxide (ZnO) NPs stabilized on glass plates

under UV irradiations. They used chemical precipitation method for the synthesis of ZnO NPs. They concluded that acidic conditions are more favourable than alkaline conditions for the photodegradation of humic substances and the photocatalytic performance can be enhanced by increasing the power of UV lamp and surface area of glass plates [101].

Huang et al. utilized titanium tetraisopropoxide (TTIP) and titanium tetrachloride (TTC) as titanium sources to synthesize anatase and rutile phase of TiO_2 through sonication process respectively [102]. Guo et al. harnessed high intensity ultrasonic waves for the synthesis of TiO_2 NPs at 90 $^{\circ}C$ and explained that ultrasonic waves can use as an efficient tool for low temperature synthesis of nanocrystalline TiO_2 [62]. Ghows and Enterazi used low intensity ultrasonic waves at low temperature for the synthesis of TiO_2 NPs by the hydrolysis of titanium precursor [103]. Prasad et al. reported ultrasonic assisted sol-gel synthesis of nano size TiO_2 [104]. Their study showed that ultrasonic acoustic waves reduces the crystallite size and temperature for anatase-rutile phase transformation [105]. Babu et al. investigated the effects of electron transferring of graphene oxide on copper doped TiO_2 nanocomposites via ultrasonic assisted wet impregnation technique and found that copper oxide doping increases the photocatalytic activity of TiO_2 by reducing the band gap energy and the loading of graphene oxide extends the lifetime of photo-generated charge carriers [106]. Vinoth et al. reported that the absorption capacity of TiO_2 is extendable to visible light region by loading graphene oxide which prevents electron-hole pair recombination rate by changing the optical band gap. They synthesized AgI-Meso TiO_2 on reduced graphene oxide sheets by ultrasonic assisted method [107].

Karthik et al. developed a visible light active catechol-TiO_2 carbonaceous polymer by a simple photosynthetic process that exhibits superior photocatalytic efficiency for H_2 production and

Cr(vi) reduction via ligand to metal charge transition which leads to fabricate stable inorganic-organic hybrid materials for light harvesting till visible region for energy applications [108]. Xu et al. prepared hollow TiO_2 microtubes with assembled radially aligned nanowires by using polyester fibers via multistep process i.e. sol-gel, solution preparation and calcination. They reported that photodegradation of Rhodamine B for nanowires assembled hollow structures is significantly higher as compared to TiO_2 NPs prepared by sol-gel method and it happened due to the presence of abundant surface hydroxyl groups [109]. Zhang et al. reviewed the one-dimensional hybrid heterostructures TiO_2 for photocatalytic applications and summarized their potential in heterogeneous photocatalysis, hydrogen production, photo electrocatalysis and CO_2 reduction [110].

During the last decade, the immobilization of NPs on textile substrates have been investigated by different methods but a few dealt with an in-situ Ultrasonic Acoustic Method (UAM). This method is useful to enhance washing durability and finishing processes but regardless of the benefits of UAM, sol-gel method is used mostly for the synthesis and deposition of NPs on textile substrates. Many researchers have reported the low temperature nucleation and growth of anatase TiO_2 on cotton fabrics. They concluded that cotton fabric with TiO_2 NPs in anatase form produces multifunctional properties such as self-cleaning, UV protection and antimicrobial properties [31; 111]. With sol-gel method, Uddin et al. deposited TiO_2 NPs on cotton fabric at low temperature which induced UV protecting and self-cleaning properties to cotton fabric [112]. All reviewed paper discussed above involved two-step developments initiated with synthesis and followed by deposition procedure. However, Pereleshtein et al. reported a one-step synthesis and deposition of TiO_2 NPs on cotton fabric. They concluded that

ultrasonic irradiations have ability to produce crystalline form of TiO_2 without subsequent heating [86].

The first section of this dissertation represents the unique demonstration that metal alkoxide such as TTIP interact with EG under ultrasonic irradiations and synthesize pure anatase form of TiO_2 NPs with smaller size and higher crystallinity that enhances the photocatalytic performance of the developed photocatalyst. In addition to the precursors discussed here, it is believed that this approach is a generic one and can be extendable for other titanium precursors and synthesis routes. The stabilization of TiO_2 NPs on cotton by UV light is investigated in the second section.

An in-situ method for the development of cotton-TiO_2 (CT) nanocomposites is presented in the last section. Ultrasonic homogenizer was utilized for simultaneous synthesis and deposition of anatase TiO_2 on cotton fabric for multifunctional properties and applications. This study was conducted to investigate the synergistic role of sono synthesized TiO_2 NPs on cotton fabric and to explain the influence of ultrasonic irradiations on photocatalytic, UV protection, self-cleaning, antimicrobial and tensile properties of the CT nanocomposites. The variables i.e. concentrations of Titanium Tetrachloride (TTC) and Isopropanol (ISP), and ultrasonic irradiations time, were optimized accurately by Central Composite Design (CCD) to achieve the optimal conditions and functional properties.

Chapter 3

3 *Materials and Methods*

This **Chapter** consists the materials and methodology for the synthesis of TiO_2 NPs (RNP) as an efficient photocatalyst than Degussa P25; the incorporation or stabilization of RNP onto cotton by UV light irradiations; and an in-situ development of multifunctional Cotton-TiO_2 (CT) nanocomposites that has been divided into three sections respectively.

3.1 Experiments for the Synthesis of TiO_2 NPs (RNP)

This section explains the experimental part for the synthesis of TiO_2 NPs (RNP) in pure anatase form and the characterization techniques used in this study.

3.1.1 Materials for the Synthesis of TiO_2 NPs

Titanium Tetraisopropoxide (TTIP) with chemical formula $Ti(OC_3H_7)_4$, Ethylene Glycol (EG) with chemical formula $HOCH_2CH_2OH$, Methylene Blue (MB) dye with chemical formula $C_{16}H_{18}ClN_3S$ and Ethanol with chemical formula C_2H_5OH were received from Sigma-Aldrich. Commercially available photocatalyst named P25 (99.9 %) composed of 80 % anatase and 20 % rutile with specific surface area 59 m^2g^{-1} and average particle size 18 *nm* was received from Degussa corporation. 100 % pure Plain weave cotton fabric with fabric mass 115 gm^{-2} was received from Department of Material Engineering, Technical University of Liberec, Czech Republic. All reagents were of analytical standard and used as received.

3.1.2 Design of Experiment for the Synthesis of TiO_2 NPs

A Central Composite Design (CCD) is a set of experimental design with three different design points i.e. factorial points (±1), centre point (0) and star/axial points (±α) which is beneficial in Response Surface Methodology (RSM) to fit a quadratic model in order to estimate the effect

of curvature or to find out the maximum and minimum of a variable. In CCD, the centre point is replicated for getting more precision of the experiment. The general form of a CCD with three input variables/factors (A, B, C) and their coded values (±1), centre point (0) and axial/star points (±α) is illustrated in *Figure 3-1*. For 3 factors CCD, the value of α is 1.68.

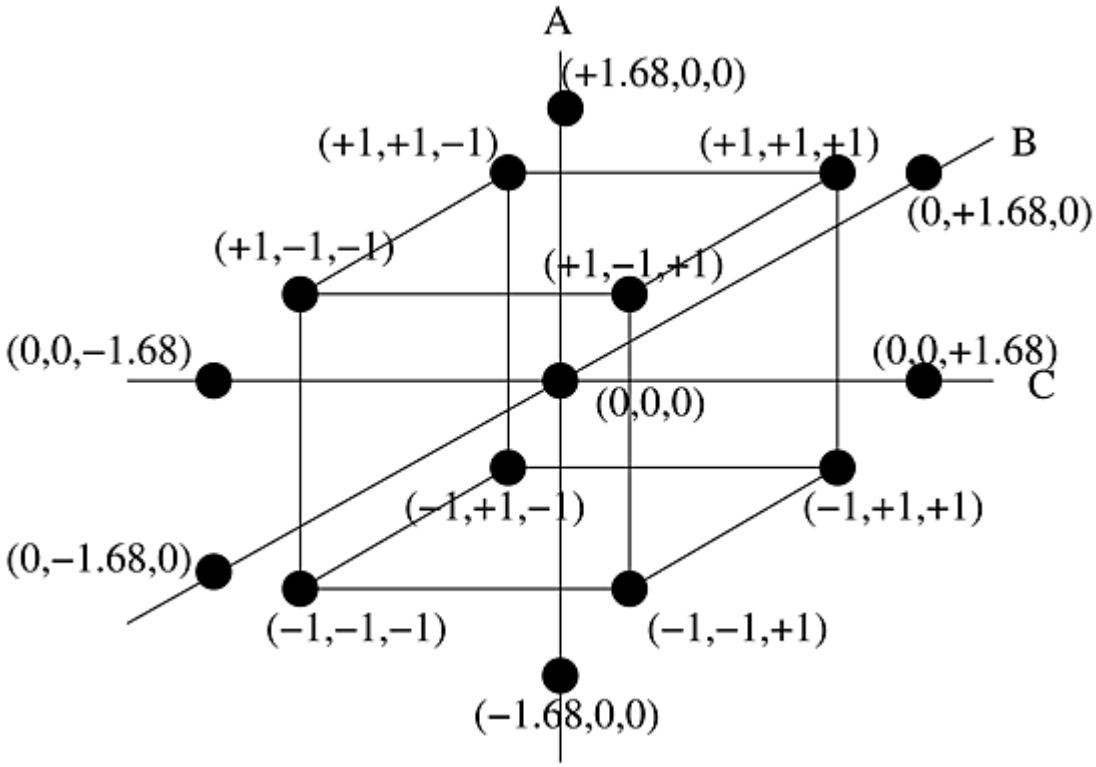

Figure 3-1 General form of a three factors central composite design with coded values.

Table 3-1 shows the input variables (factors) with their coded values (minimum, maximum) and their central points whereas ***Table 3-2*** illustrates the factors level setting in their coded form based on CCD.

Table 3-1 The 3-factors CCD matrix for experimental variables with coded values for the synthesis of TiO_2 NPs

Factor	Name	Unit	Coded Values		Central Point	Mean	Std. Dev.
A	TTIP	*mL*	-1=4	1=8	6	6	1.8
B	EG	*mL*	-1=3	1=5	4	4	0.9
C	Sonication Time	*h*	-1=1	1=3	2	2	0.8

Design-Expert version 10 by Stat-Ease corporation was used for statistical analysis throughout the experiments. The influence of variables on the results including: Y=MB removal [%] was adjusted by using a quadratic Equation 1:

$$Y = b_0 + \sum b_i X_i + \sum b_{i.j} X_i X_j + \sum b_{i.i} X_i^2 \quad i \geq j \quad i,j = 1,2,3 \qquad [1]$$

Where b_0 is the coefficient of constant term, b_i represents the coefficient of linear term that explains the persuade of the variables, b_{ii} is the coefficient of quadratic term and b_{ij} represents the coefficient of two factors interaction [78; 113; 114].

Table 3-2 The 3-factors general CCD matrix for experimental variables with coded values and factors level setting for the synthesis of TiO_2 NPs

Experimental Trial	Factors Level Setting		
	A	B	C
1	-1	-1	-1
2	1	-1	-1
3	-1	1	-1
4	1	1	-1
5	-1	-1	1
6	1	-1	1
7	-1	1	1
8	1	1	1
9	-α	0	0
10	α	0	0
11	0	-α	0
12	0	α	0
13	0	0	-α
14	0	0	α
15	0	0	0
16	0	0	0
17	0	0	0
18	0	0	0
19	0	0	0
20	0	0	0

3.1.3 Methodology for the Synthesis of TiO_2 NPs

In the experimental part, liquid TTIP was added drop by drop into a beaker containing 50 *mL* ethanol with simultaneous addition of EG into the running solution with TTIP:EG ratio 2:1 under continuous magnetic stirring at 500 *rpm*. The temperature of the solution was adjusted to 80 $^{\circ}C$ by using the hot plate equipped with magnetic stirrer. The purpose of continuous mixing was to homogenize the solution throughout the experiment. TTIP was a slightly viscous alkoxide and tried to settle down. The solution was then sonicated for different time intervals based on CCD under ultrasonic homogeniser system (Bandelin Sonopuls HD 3200, 20 kH_Z, 200 *W*, 50 *%* efficiency) to complete the reaction mechanism. The resulting white flocculates were washed several times with ethanol to remove impurities. The white flocculates were then centrifuged at 6000 *rpm* for 5 *min* to separate solid particles. The centrifuged solid was dried at 100 $^{\circ}C$ for 2 *h* in an oven and then further characterized. In order to emphasize the fundamental influence of ultrasonic irradiations, similar sample was developed by conventional magnetic stirring method in which EG was added to a solution containing TTIP and ethanol under same experimental conditions. The same procedure was repeated without sonication. The XRD analysis of this sample exhibited an amorphous nature as no characteristic peaks obtained so the results of this sample are not included in the results and discussions section. The experimental setup is shown in *Figure 3-2*.

3.1.4 Characterization of Resulting Nanoparticles (RNP)

Scanning Electron Microscopic (SEM) images were processed by Vegas-Tescan microscope with an accelerating voltage 2 *kV*. SEM images were developed at high magnifications 5.0 *kX* for investigating the morphological changes. All samples were first covered with gold coatings to increase the quality of the image. Transmission Electron Microscopy (TEM) study was

carried out with a JEOL (JEM-2000CX) microscope with an accelerating voltage 200 *kV*. The samples were developed by putting a drop of suspension onto a carbon coated copper grid which is further dried in air to eliminate the solvent. Powder X-ray Diffraction (XRD) patterns were collected by X'Pert PRO X-ray diffractometer using Cu Kα radiation λ=0.15406 *nm* with a scanning angle (*2θ*) range 10-70°, under voltage and current of 40 *kV* and 30 *mA* respectively. The size of the crystals was calculated through the line broadening of the plane reflection by Scherer's crystallite equation as presented in Equation 2:

$$D = \frac{K\lambda}{\beta Cos\theta} \quad [2]$$

Where *D* represents the crystallite size and λ is the wavelength of the X-ray radiations. *K* is the shape constant with a constant value i.e. 0.89 and β is the full line width at half-maximum height [112; 115]. Malvern zeta sizer nano ZS was used to determine the size distribution of the Resulting Nanoparticles (RNP) through Dynamic Light Scattering (DLS) technology. The specific surface area was measured by BET (Brunauer, Emmett, Teller) method using Micromeritics Gemini VII 2390. Raman method was used to identify the molecular vibrational scattering of a material when it is subjected to laser light that further explain the purity of a material. Thermo scientific DXR Raman spectroscope was used to detect the purity of anatase form for RNP. It should be noted that all results discussed here bonded with RNP under optimal conditions TTIP 10 *mL*, EG 4 *mL* and sonication time 1 *h*. The UV-Vis absorption spectrum of RNP was measured on UV-1600PC Spectrophotometer to calculate the absorption intensities. The experiment was performed in liquid form as 0.1 *g* of RNP was mixed in 100 *mL* of distilled H_2O and sonicated for 5 *min* to make a homogenous solution. The experiment was also repeated for P25 to make a comparison.

3.1.5 Photocatalytic Performance of RNP

The photocatalytic performance of RNP and P25 was studied by decolouration of MB solution under UV irradiations. In this experiment, 0.5 gL^{-1} of RNP was mixed with 100 *mL* solution containing 50 mgL^{-1} MB. The suspension was magnetically stirred in the dark for 30 *min* to reach an adsorption equilibrium. The results of initial experiments demonstrated that the adsorption equilibrium of MB with RNP takes place in 30 *min*. The UV light source was a 500 *W* UV lamp. The intensity of UV light was 30 Wm^{-2} based on distance (10 *cm*) from lamp to the surface of solution. The residual concentration of MB in the solution was measured by using spectrophotometer at a maximum wavelength of 668 *nm*. The colour removal efficiency (*CR%*) was calculated by Equation 3:

$$CR\% = [\frac{C_o - C}{C_o}] \times 100 \quad [3]$$

Where C_o and C represents the initial and final concentration of MB in the solution, respectively. Experiment was repeated three times and mean values were taken for precision of the results. The initial spectrum of dye solution without RNP was taken as standard or controlled sample. After adding RNP, the suspension was kept under the influence of UV light for a specific period of time. An aliquot was pulled out by a syringe after a fix time interval to measure the *CR%*. The same experiment was performed with P25 to compare the photoactivity.

3.1.6 Self-cleaning Efficiency of RNP

Self-cleaning efficiency of RNP deposited on cotton fabric was evaluated on the basis of colour change and degradation activity of MB stain under daylight irradiations for 24 *h*. Cotton fabric was immersed in RNP solution and pad-dry method was used to develop samples. Moreover, the experiment was conducted by taking swatches (5x5 *cm*) from each sample as well as P25

and blank sample (untreated cotton) and placed on a flat surface. All samples were stained by dropping 0.01 % (*w/v*) solution of MB and left in the dark for 30 *min* to achieve adsorption-desorption equilibrium. Furthermore, all stained samples were dried in air and then self-cleaning efficiency was evaluated by the removal of MB stain at different time intervals of daylight irradiations. The maximum exposure time for daylight irradiations was 24 *h*. The change in colour before and after irradiations was considered as self-cleaning efficiency which was evaluated in RGB colour space according to Equation 4:

$$\Delta RGB = [\Delta R^2 + \Delta B^2 + \Delta G^2]^{1/2} \quad [4]$$

The lower ΔRGB value corresponds to lower self-cleaning efficiency and vice versa.

3.2 Experiments for the Stabilization of TiO_2 NPs onto Cotton

This section explains the experimental part for the stabilization of TiO_2 NPs (RNP) onto cotton fabric by UV light irradiations and the characterization techniques used in this study.

3.2.1 Materials for the Stabilization of TiO_2 NPs onto Cotton

100 % pure cotton fabric (plain weave with fabric mass 115 gm^{-2}) was used as received from Department of Material Engineering, Technical University of Liberec, Czech Republic. The fabric was first washed with 1 gL^{-1} non-ionic detergent in a washing bath with fabric-liquor ratio 1:40. The fabric was then cut into (12.5x12.5 *cm*) uniform samples. TiO_2 NPs with average particle size 4 *nm* and specific surface area 150 m^2g^{-1} were used in this study as synthesized and reported in our up given investigation [116]. Distilled water was used throughout the study.

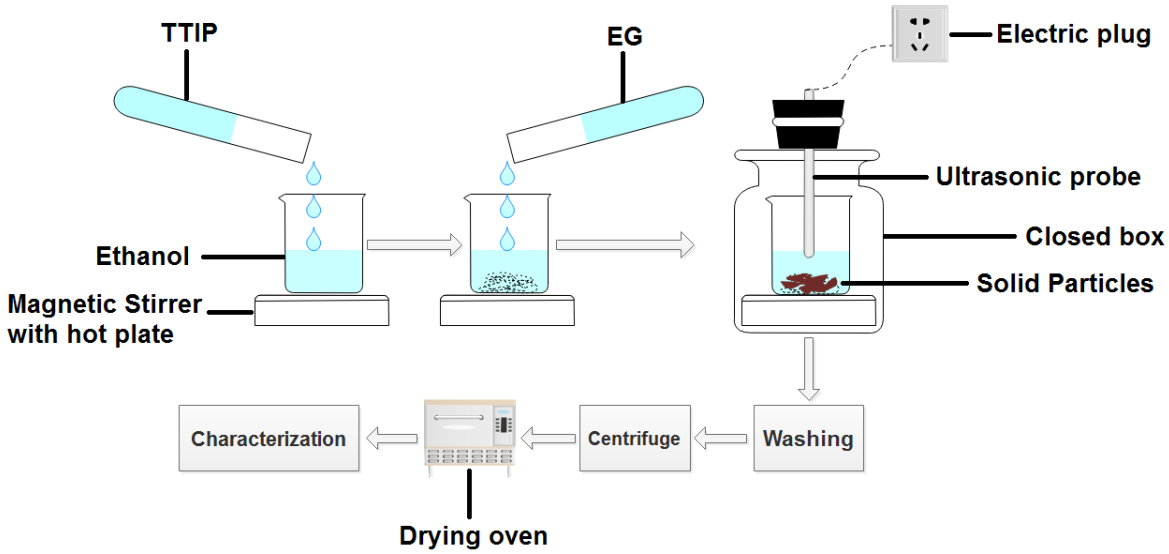

Figure 3-2 Schematic representation of the synthesis of TiO_2 nanoparticles via Ultrasonic Acoustic Method.

3.2.2 Design of Experiment for the Stabilization of TiO_2 NPs onto Cotton

The experimental design for the stabilization of TiO_2 NPs onto cotton is based on CCD. The general form of CCD is discussed in detail in the section 3.1.2. The input variables (factors) with their coded values (minimum, maximum) and central points for the stabilization of TiO_2 NPs onto cotton are given in ***Table 3-3*** whereas the factors level setting in coded form based on CCD for the stabilization of TiO_2 NPs onto cotton is illustrated in ***Table 3-4***.

Table 3-3 The 3-factors CCD matrix for experimental variables with coded values for the stabilization of TiO_2 NPs onto cotton

Factor	Name	Unit	Coded Values		Central Point	Mean	Std. Dev.
A	TiO_2 Dosage	gL^{-1}	-1=4	1=8	6	6	1.8
B	Temperature	$^{\circ}C$	-1=30	1=60	45	45	12.6
C	UV Irradiation Time	*min*	-1=40	1=120	80	80	33.9

3.2.3 Suspension and Deposition of TiO_2 NPs onto Cotton

A suspension of TiO_2 NPs with distilled water was developed by ultrasonic homogeniser. The concentration of TiO_2 NPs varying from 2 gL^{-1} to 10 gL^{-1} according to CCD. Dip-pad-dry method was used to embed TiO_2 NPs onto cotton fabric. All samples were immersed in suspension for 2 *min*, squeezed on padder (Mathis, Switzerland) under pressure 3 *kN* with velocity 1 $mmin^{-1}$ and finally dried in an oven at 60 $^{\circ}C$ for 30 *min*. These samples were named as TiO_2 treated samples whereas pristine samples (untreated cotton) were called untreated samples.

3.2.4 Stabilization of TiO_2 NPs onto Cotton through UV Light

To investigate the adhesion, incorporation and surface changes, all TiO_2 treated and untreated samples were irradiated under UV light for different time intervals ranging from 15 *min* to 150 *min* according to CCD. An open system was developed consisting a polypropylene box and a special holder for samples enclosed in it as shown in *Figure 3-3*. To find out the crucial role to UV light, TiO_2 treated samples without UV irradiations were also used in leaching and self-cleaning processes for comparison.

3.2.5 Characterization of the Developed Samples

The morphological changes on the surface of TiO_2 treated samples, untreated samples and samples 1-20, were observed by UHR-SEM Zeiss Ultra Plus with an accelerating voltage 2 *kV* equipped with an Energy Dispersive X-ray (EDX) Spectrometer Oxford X-max 20. The charging effect was eliminated by the use of charge compensator (local N_2 injection). EDX analysis of the samples was performed at 10 *kV* accelerating voltage to confirm the elemental configuration of the embedded materials on the surface of cotton. The incorporated amount of TiO_2 NPs on cotton surface after UV irradiations was estimated by Inductive Couple Plasma-

Atomic Emission Spectroscopy (ICP-AES) elemental analysis. Tensile strength of all samples was measured on TIRA test 2300 with CRE (Constant Rate of Extension) according to standard test method ISO 13934-1.

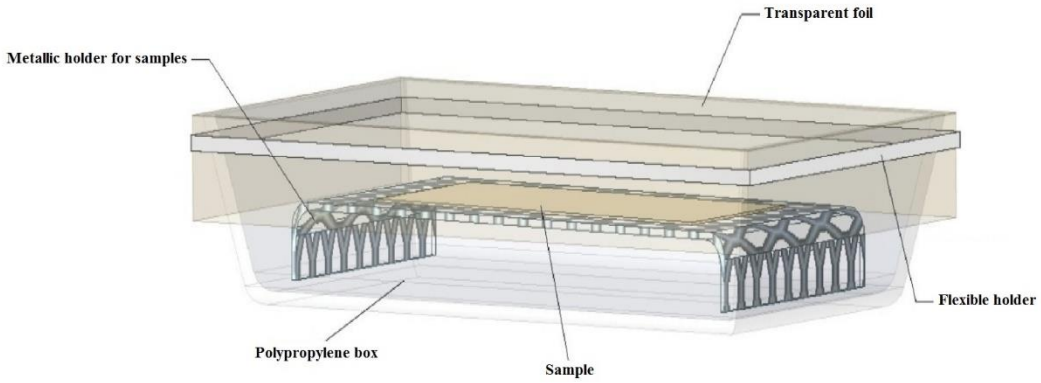

Figure 3-3 Schematic illustration of the experimental setup for embedding of TiO_2 NPs onto cotton.

3.2.6 Durability of Stabilized TiO_2 NPs against Washing and Leaching

The durability of embedded TiO_2 NPs onto cotton fabric against washing was evaluated according to ISO 105 C06 (B1M) standard test method. 4 gL^{-1} detergent was used for each washing cycle at 50 $^{\circ}C$ for 45 *min* time interval. The washed specimens were then rinsed and dried at 60 $^{\circ}C$ for 15 *min* after each washing cycle. A Varian Cary 500 UV-vis-NIR Spectrophotometer was used to evaluate absorption spectra of washing effluents. For leaching, the amount of Ti^{+4} ions presented in the leaching solution was estimated to evaluate the adhesion and stability of the developed samples. For this purpose, different samples were treated with 1*M* NaCl solution at laboratory conditions for 6 *h*. Later, the samples were removed from leaching solution and the amount of Ti^{+4} was estimated by ICP-AES analysis.

Table 3-4 The 3-factors general CCD matrix for experimental variables with coded values and factors level setting for the stabilization of TiO_2 NPs onto cotton

Experimental Trial	Factors Level Setting		
	A	B	C
1	-1	-1	-1
2	1	-1	-1
3	-1	1	-1
4	1	1	-1
5	-1	-1	1
6	1	-1	1
7	-1	1	1
8	1	1	1
9	-α	0	0
10	α	0	0
11	0	-α	0
12	0	α	0
13	0	0	-α
14	0	0	α
15	0	0	0
16	0	0	0
17	0	0	0
18	0	0	0
19	0	0	0
20	0	0	0

3.2.7 Self-cleaning Efficiency of the Stabilized TiO_2 NPs after UV irradiations

Self-cleaning efficiency was evaluated on the basis of degradation activity of coffee stain under daylight irradiations for 12 *h*. The study was conducted by taking swatches (4x4 *cm*) from all samples and a coffee stain was dropped vertically on them. After that, all samples were dried and exposed to daylight irradiations for different time intervals and colour difference was estimated according to Equation 5:

$$\Delta E = [\Delta L^2 + \Delta a^2 + \Delta b^2]^{1/2} \quad [5]$$

Where *L* refers to lightness of the fabric, *a* and *b* stand for red-green colour and yellow-blue colour respectively.

3.3 Experiments for In-situ Development of Multifunctional Cotton-TiO_2 (CT) Nanocomposites

This section explains the experimental part for the development of multifunctional CT nanocomposites and the characterization techniques used in this study.

3.3.1 Materials for Multifunctional CT Nanocomposites

100 % pure plain cotton fabric with mass 115 gm^{-2} was used. The fabric was first washed with detergent in a washing bath containing 1 gL^{-1} nonionic detergent with fabric-liquor ratio 1:60. Temperature of the bath was set at 60 $^{\circ}C$ by digital heating system. After 30 *min* of continuous heating and stirring, the fabric was rinsed with H_2O and dried at 60 $^{\circ}C$ for 30 *min*. Titanium Tetrachloride (TTC) with chemical formula $TiCl_4$, Isopropanol (ISP) with chemical formula $(CH_3)_2CHOH$ and Methylene Blue (MB) with chemical formula $C_{16}H_{18}ClN_3S$ were received from Sigma Aldrich. All chemicals were used without any further processing.

3.3.2 In-situ Synthesis and Deposition of TiO_2 NPs on Cotton

TiO_2 nanocrystalline particles with smaller size have been simultaneously synthesized and deposited on cotton surface by Ultrasonic Acoustic Method (UAM). Distilled water was used throughout the experiments. Cotton fabric was immersed in a vessel containing TTC, ISP and water under ultrasonic system (Bandelin Sonopuls HD 3200, 20 kH_Z, 200 W, 50 % efficiency) to complete the reaction mechanism. TTC was hydrolyzed in the presence of ISP and water. The effective power of ultrasonic waves emitted in the solution was 100 Wcm^{-2} experimentally determined by calorimetric measurement. The detailed mechanism for the development of Cotton-TiO_2 (CT) nanocomposites is described in *Figure 3-4*. In this unique study, varying amount of ISP (0.5-8 mL) was dissolved in 100 mL of distilled H_2O by v/v percentage under continuous stirring in order to make homogeneous solution. The final volume of the running solution was 100 mL adjusted by decreasing the amount of water simultaneously with increased amount of ISP. A squared cotton fabric sample (12x12 cm) was then immersed in the solution for 2-3 min and then drop by drop addition of TTC into the solution bath. The immersed fabric was then sonicated for different time intervals varying from 0.25 h to 4 h. The system temperature was maintained from room temperature to 70 $^{\circ}C$ by using hot plate. In order to get maximum photocatalytic efficiency of the CT nanocomposites, TiO_2 NPs with anatase form were required which were obtained successfully through an In-situ UAM. Some preliminary experiments were performed to find out the optimal values of the variables for the success of this study. According to initial assessment of the preliminary results, we came to know that the temperature of the system increased from room temperature (22 ±2 $^{\circ}C$) to 70 $^{\circ}C$ during the whole experiment. Interestingly, ultrasonic irradiations have no negative effect on the color fastness properties of cotton fabric as the fabric sustained its natural color even at 70 $^{\circ}C$ with longer ultrasonic irradiations time. The treated samples were dried in oven for 2 h at 70 $^{\circ}C$. To

find out the crucial role to ultrasonic irradiations, conventional magnetic stirring was used to prepare similar sample that 10 *mL* TTC, 6 *mL* ISP and cotton fabric (12x12 *cm*) at 70 $^{\circ}C$ were magnetically stirred at 500 *rpm*. This sample was named as sample C. The proposed mechanism of photocatalysis on the surface of CT nanocomposites is described in *Figure 3-5*.

3.3.3 Solid Powder Extraction

After removing the fabric, the solution was centrifuged at 6000 *rpm* for 5 *min* to separate the solid particles from the liquid. The centrifuged solid was washed five times with ethanol to remove trashes and impurities.

3.3.4 Design of Experiment for the Development of CT Nanocomposites

The experimental design for the development of CT nanocomposites is based on CCD. The general form of CCD is discussed in detail in the section 3.1.2. The input variables (factors) with their coded values (minimum, maximum) and central points for the development of CT nanocomposites are given in ***Table 3-5*** whereas the factors level setting in coded form based on CCD for the development of CT Nanocomposites is illustrated in ***Table 3-6***.

Table 3-5 The 3-factors CCD matrix for experimental variables with coded values for the development of CT nanocomposites

Factor	Name	Unit	Coded Values		Central Point	Mean	Std. Dev.
A	TTC	*mL*	-1=4	1=8	6	6	1.8
B	ISP	*mL*	-1=2	1=6	4	4	1.7
C	Sonication Time	*h*	-1=1	1=3	2	2	0.8

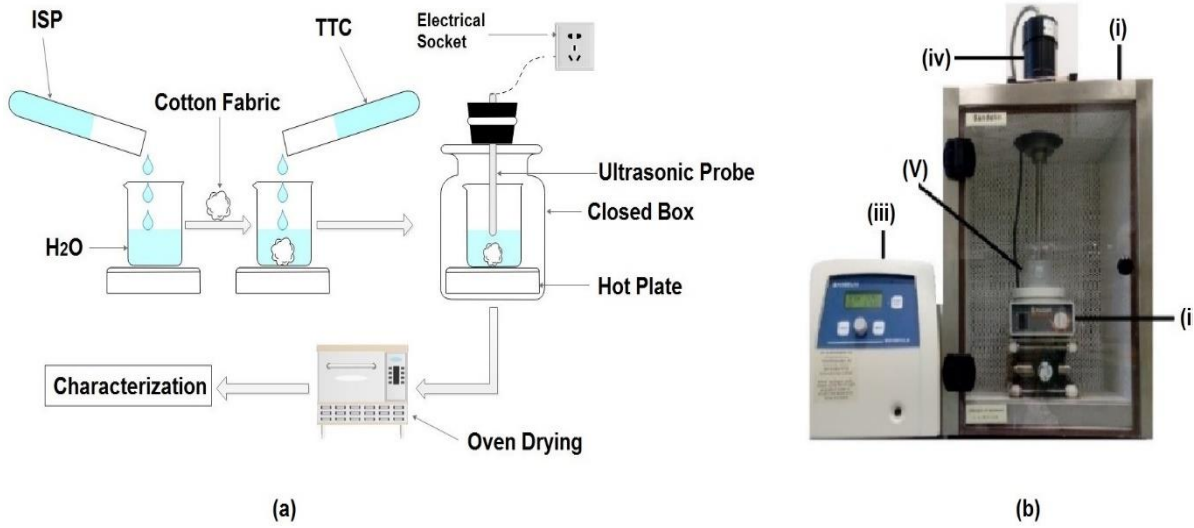

Figure 3-4 (a) Schematic representation for the development of CT nanocomposites; (b) Experimental Setup: (i) closed box (ii) hot plate (iii) ultrasonic wave generator (iv) ultrasonic probe (v) immersed fabric sample.

3.3.5 Characterization of CT Nanocomposites

The morphological changes on the surface of cotton fabric after in-situ deposition of TiO_2 NPs were observed by UHR-SEM Zeiss Ultra Plus with an accelerating voltage 2 *kV* equipped with an Energy Dispersive X-ray (EDX) Spectrometer Oxford X-max 20. The charging effect was eliminated by the use of charge compensator (local N_2 injection). EDX analysis of the resulting CT nanocomposites was performed at 10 *kV* accelerating voltage to confirm the elemental configuration of the deposited materials on the surface of cotton. Perkin Elmer Optima 2100 was use to estimate the relative amount of deposited TiO_2 NPs on cotton surface by ICP-AES elemental analysis. In order to identify the crystal size and crystal structure, XRD patterns were collected by X'Pert PRO X-ray Diffractometer using Cu Kα radiation λ=0.15406 *nm* with a

scanning angle (2θ) range 10-70°, voltage and current of 40 *kV* and 30 *mA* respectively. The observed patterns were analysed and compared with standard patterns of JCPDS card no. (21-1272). The crystallite size was calculated through Equation 2. The UV-Vis absorption spectrum of the solid powder was measured on UV-1600PC Spectrophotometer in order to investigate the photocatalytic activity of the extracted solid powder.

3.3.6 Photocatalytic Activity of the Resulting Solution

After extracting the developed CT nanocomposites from the solution, photocatalytic activity of the resulting solution was evaluated by MB colour change before and after artificial daylight irradiations. For this purpose, 0.01 *%* (*w/v*) MB was mixed with 100 *mL* of the resulting solution containing 1 gL^{-1} TiO_2 NPs. Before irradiations, the suspension was magnetically stirred in the dark for 30 *min* in order to achieve adsorption-desorption equilibrium. After equilibrium, the suspension was exposed to 500 *W* xenon lamp for 2 *h*. The distance between suspension and lamp was 20 *cm*. An aliquot was taken out after a pre-set time interval and UV-Vis absorption spectrum of the extracted aliquot was recorded on UV-1600PC Spectrophotometer. The residual concentration of MB was measured at a maximum wavelength of 668 *nm*. The colour removal efficiency was calculated by Equation 3. For precision of results, experiment was repeated five times and mean values were used for results.

Table 3-6 The 3-factors general CCD matrix for experimental variables with coded values and factors level setting for the development of CT nanocomposites

Experimental Trial	Factors Level Setting		
	A	B	C
1	-1	-1	-1
2	1	-1	-1
3	-1	1	-1
4	1	1	-1
5	-1	-1	1
6	1	-1	1
7	-1	1	1
8	1	1	1
9	-α	0	0
10	α	0	0
11	0	-α	0
12	0	α	0
13	0	0	-α
14	0	0	α
15	0	0	0
16	0	0	0
17	0	0	0
18	0	0	0
19	0	0	0
20	0	0	0

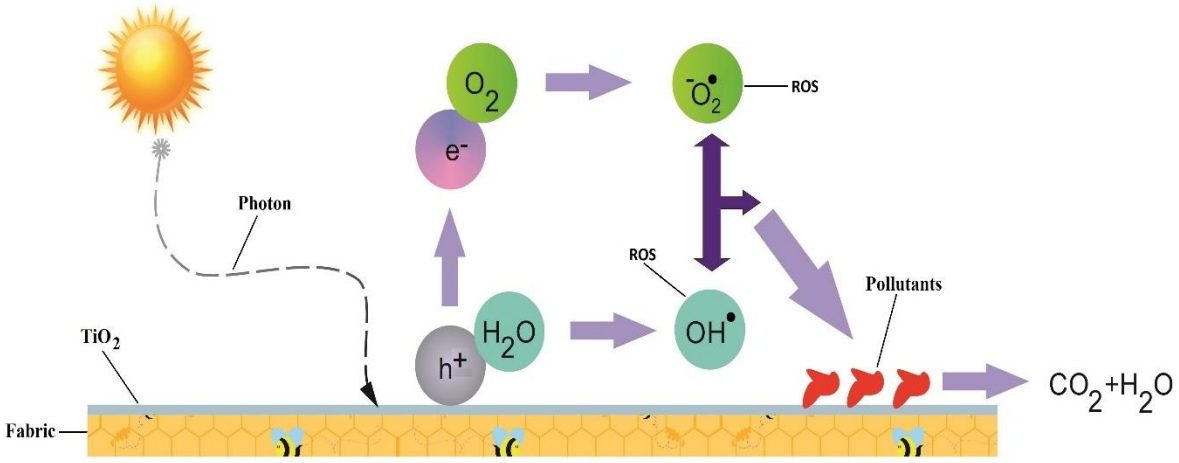

Figure 3-5 Photocatalytic degradation of pollutants on the surface of CT nanocomposites.

3.3.7 UPF Efficiency of CT Nanocomposites

In order to determine the Ultraviolet Protection Factor (UPF) of the developed CT nanocomposites, measurements were conducted according to AS/NZS 4399:1996 with a Varian Cary 500 UV-Vis-NIR Spectrophotometer with integrated sphere. All the treated samples along with sample C and blank sample were placed at the entrance of sphere. For each sample, four measurements were performed with different directions and the average of all four scans was taken as a final UPF value which was calculated by Equation 6.

$$UPF = \frac{\sum_{280}^{400} S_\lambda E_\lambda \Delta_\lambda}{\sum_{280}^{400} S_\lambda E_\lambda \mathrm{T}_\lambda \Delta_\lambda} \qquad [6]$$

In Equation 6, S_λ is the solar spectral irradiance, $E_\lambda$is the relative erythemal spectral response, $\mathrm{T}_\lambda$is the average spectral transmittance of the sample and Δ_λ is the measured wavelength interval in nanometres.

3.3.8 Self-cleaning Efficiency of CT Nanocomposites

Self-cleaning efficiency of the developed CT nanocomposites was evaluated on the basis of colour change and degradation activity of MB stain under daylight irradiations for 24 *h*. The experiment was conducted by taking swatches (5x5 *cm*) from each sample as well as sample C and blank sample and immersed in 0.01 % (*w/v*) of MB solution and left in the dark for 30 *min* to achieve adsorption-desorption equilibrium. Moreover, all samples were dried in air and then exposed to daylight irradiations for different time intervals and colour change was estimated in RGB colour space according to Equation 4.

3.3.9 Antimicrobial Efficiency of CT Nanocomposites

The quantitative antimicrobial efficiency of the developed CT nanocomposites was evaluated against Staphylococcus aureus (S. aureus) and Escherichia coli (E. coli) microorganisms according to AATCC test method 100-2012. This test was employed to measure the ability of nanocomposites to prevent the growth of microorganisms over a 24 *h* period of contact or kill them [117]. The number of viable cells was recorded by counting the bacteria colonies in agar plate before and after treatment and antimicrobial efficiency of the developed CT nanocomposites was reported as percentages of bacteria reduction according to Equation 7.

$$R\% = \left[\frac{(P - Q)}{P}\right] \times 100 \qquad [7]$$

In Equation 7, P and Q represents the total numbers of bacteria colonies recovered from untreated and treated specimen and $R\%$ is the percentage reduction of bacteria colonies.

3.3.10 Washing Durability of CT Nanocomposites

Finishing applications have a colouring effect on fabrics so the durability of TiO_2 NPs synthesized by an in-situ UAM on cotton fabric against washing was evaluated according to ISO 105 C06 (B1M). According to the standard test method, each washing cycle completed with 4 gL^{-1} detergent at 50 $^{\circ}C$ for 45 *min* time interval is equal to five home launderings [33]. The washed specimen was then rinsed and dried at 60 $^{\circ}C$ for 15 *min* after each washing cycle. A Varian Cary 500 UV-Vis-NIR Spectrophotometer was used to evaluate absorption spectra of washing effluents.

3.3.11 Tensile Strength of CT Nanocomposites

Tensile strength of the developed CT nanocomposites was tested on TIRA Test 2300 with Constant Rate of Extension (CRE) according to standard test method ISO 13934-1.

Chapter 4

4 Results and Discussions

This **Chapter** explains the results for the synthesis of TiO_2 NPs (RNP); the stabilization of RNP onto cotton by UV light irradiations and an in-situ development of multifunctional Cotton-TiO_2 (CT) nanocomposites in three sections respectively.

4.1 Results and Discussions for the Synthesis of TiO_2 NPs

This section explains the results for the synthesis of TiO_2 NPs (RNP) and discusses their applications in details.

4.1.1 Characterization of Resulting Nanoparticles (RNP)

In Figure 4-1, the results of the SEM analysis are illustrated which indicate that Resulting Nanoparticles (RNP) are more spherical in shape than P25. The size of RNP is much smaller in comparison to P25 as observed in *Figure 4-1*. The average particle size for P25 and RNP were 18 *nm* and 4 *nm* respectively confirmed by particle size distribution as presented in *Figure 4-2*.

TEM analysis of RNP and P25 is described in *Figure 4-3*. The TEM results indicate that the RNP are more spherical in shape with uniform distribution of particles. Moreover, most of the RNP are separated from each other while agglomeration observed in P25. The inset showed a distinct diffraction rings for RNP corresponding to the crystalline phase while for P25, dull fringes and agglomeration observed. These results indicate that RNP are more crystalline in nature than P25. The ratio of agglomeration in the RNP is insignificant which indicates their good photocatalytic activity as compared to P25. The estimated mean particle size through TEM images is around 4 *nm* which is in good agreement with XRD results.

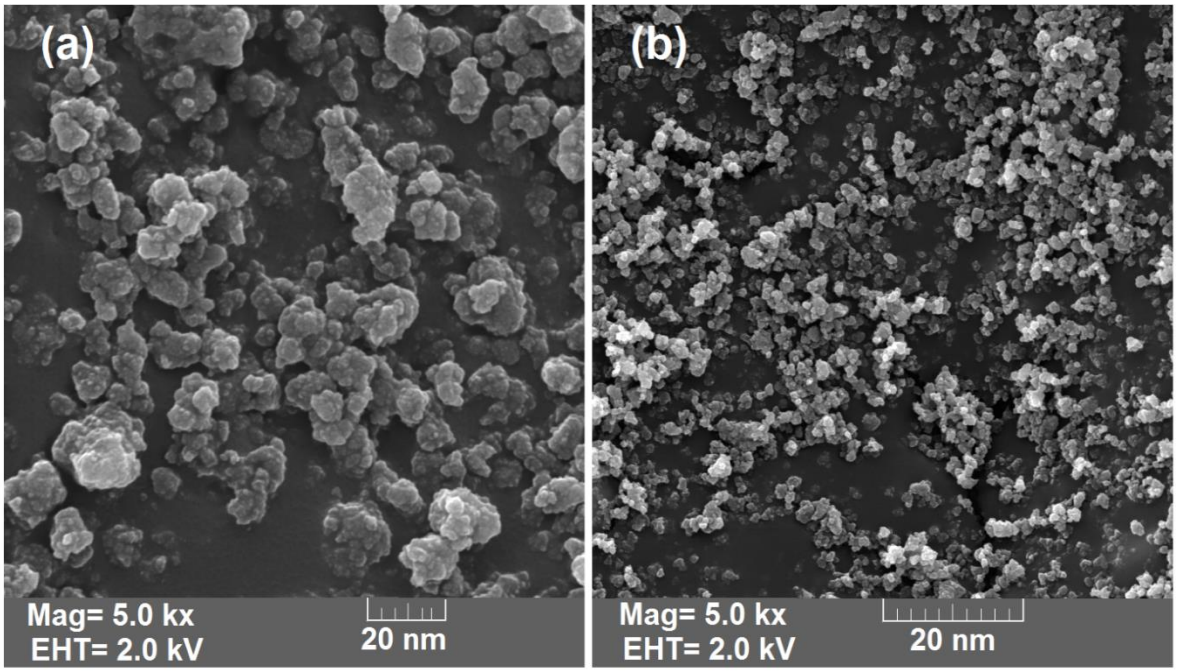

Figure 4-1 SEM images (a) P25, (b) RNP with optimal conditions TTIP 10 mL, EG 4 mL, Sonication time 1 h.

Surface area and volume distribution are two important microstructural parameters depend on the geometrical shape and porosity of the NPs. The up given characteristics of the RNP are investigated by BET method under N_2 atmosphere and the results are written in ***Table 4-1***. It should be noted that the surface area of RNP without calcination is 149 m^2g^{-1} experimentally determined by BET method.

These results indicate a linear relationship between temperature and surface area of the RNP. A large surface area enables RNP to provide more surface-active sites to dyes for the adsorption of reactive molecules on the surface of RNP which enhances the photoactivity of the RNP and leads the photocatalytic process to be more efficient. ***Table 4-1*** describes that the surface area

of RNP is very high as compare to P25. The surface area of P25 is 59 m^2g^{-1} as mentioned in the experimental part.

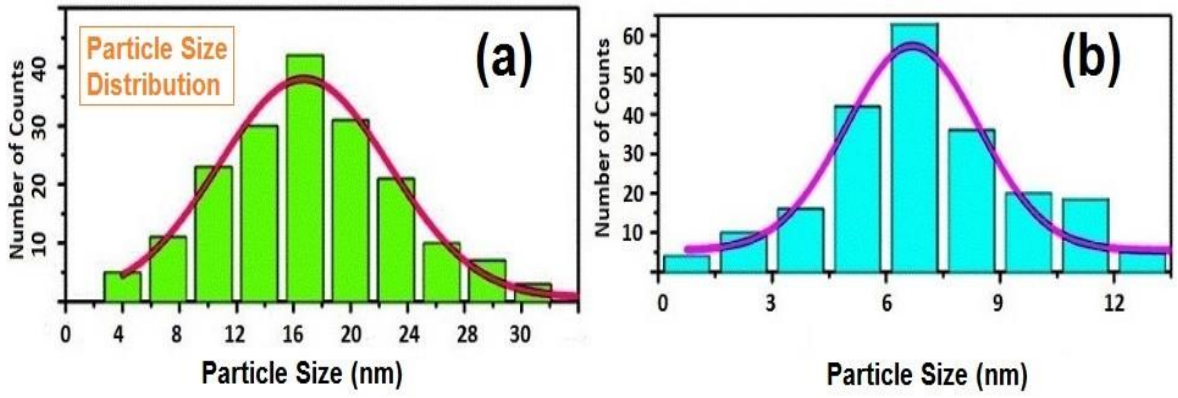

Figure 4-2 Particle size distribution obtained by DLS (a) P25, (b) RNP with optimal conditions TTIP 10 mL, EG 4 mL, Sonication time 1 h.

The results collected by XRD analysis describe that RNP possessed pure anatase phase with all sharp peaks matched with the standard Powder Diffraction card data base JCPDS (21-1272). In *Figure 4-4*, the highest peak obtained at 2θ=25.4° represents the (101) plane reflection which is the characteristic peak for pure anatase form of TiO_2 followed by three more primary peaks at 2θ=38°, 48° and 54° for (004), (200) and (211) planes respectively. The average crystallite size obtained by using Scherrer's equation is 4 *nm*. It can be evaluated by the results that RNP have much smaller size as compared to P25. It could be due to EG content into the crystal lattice of RNP that suppress the crystal growth of RNP.

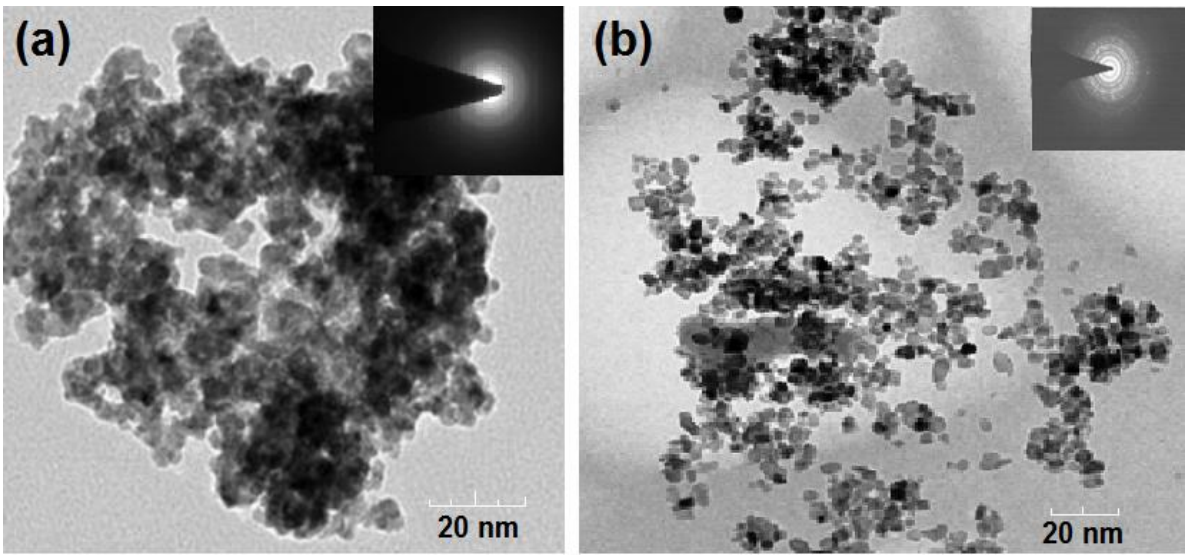

Figure 4-3 TEM images (a) P25, (b) RNP with optimal conditions TTIP 10 mL, EG 4 mL, Sonication time 1 h.

Table 4-1 Summary of microstructural characteristics of RNP

Calcination Temp [$^{\circ}C$]	**Surface Area [m^2g^{-1}]**	**Pore Volume [cm^3g^{-1}]**	**Anatase phase purity [%]**	**Rutile phase purity [%]**
300	149	0.21	100	Not found
400	153	0.18	100	Not found
500	156	0.16	100	Not found
600	158	0.13	100	Not found
700	161	0.10	92	8

Raman spectrum of RNP is presented in *Figure 4-5*. It is observed that the spectrum of the RNP is quite similar to the standard spectrum of the pure anatase TiO_2. The inset is the standard spectrum obtained from spectra library of Raman spectroscopy. Factor group analysis with vibrational modes of crystals explains that pure anatase phase consists of given Raman active

modes i.e. (144 cm^{-1}, 197 cm^{-1}, 399 cm^{-1}, 513 cm^{-1} and 639 cm^{-1}). In *Figure 4-5*, a strong peak at 144 cm^{-1} which is the metaphor of anatase phase can be observed. The Raman spectrum of RNP is consistent with XRD results.

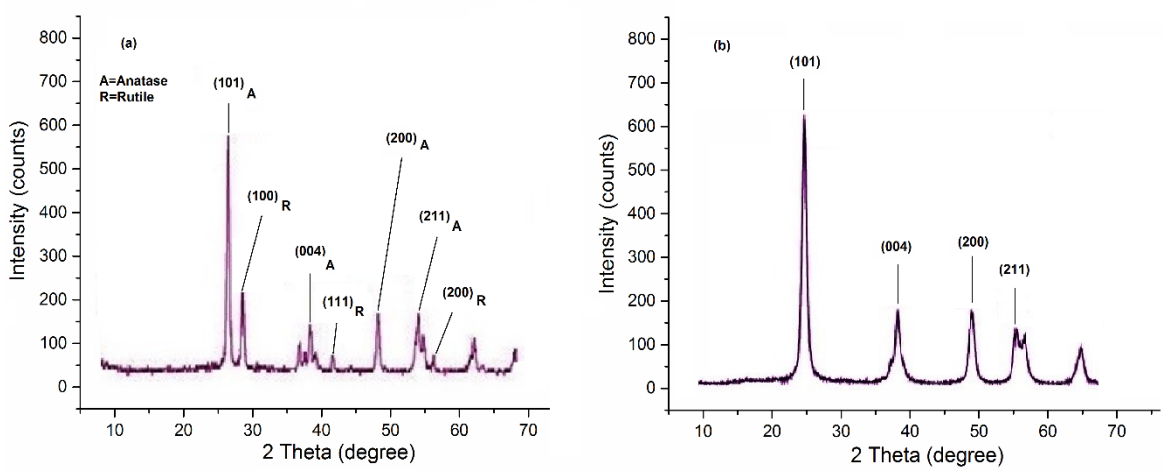

Figure 4-4 XRD pattern (a) P25, (b) RNP with optimal conditions TTIP 10 mL, EG 4 mL, Sonication time 1 h.

The optical photon with energy equal to or more than the band gap of TiO_2 jumped into higher energy state to produce electrons and holes (band gap). This property enables TiO_2 as a photocatalyst under UV irradiations. The effective results are obtained below 400 *nm* as shown in *Figure 4-6*. The maximum absorption efficiency is obtained at 320 *nm* lies in the UV region of the electromagnetic light. The average band gap energy of RNP calculated by Tauc's formula is 3.26 *eV*. We observed same behaviour for P25 and RNP but RNP absorbs more quantity of UV light than P25 as they possess larger surface area confirmed by BET analysis. This spectrum indicates that the behaviour of RNP as a photocatalyst under UV light is much quicker and more precise than P25. It could be due to smaller particle size and larger surface area of RNP. These results are consistent with BET and XRD results. So, RNP can be

considered as a good choice for photocatalyst in UV protecting devices, self-cleaning materials, sunscreens, cosmetics and many other applications etc.

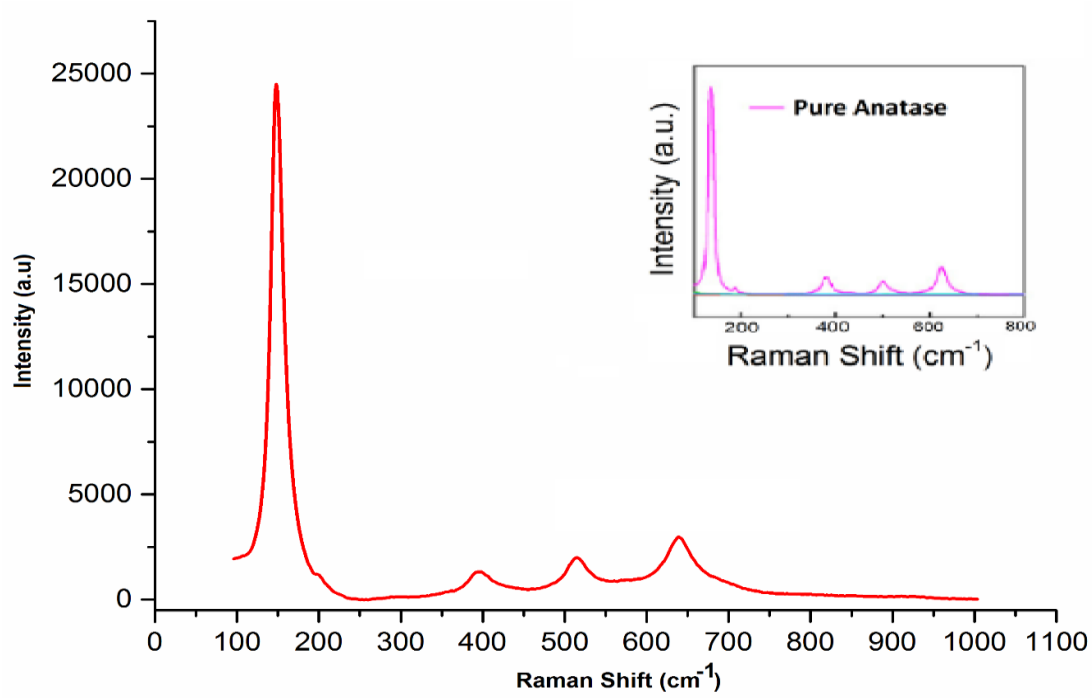

Figure 4-5 Raman Spectrum of RNP with optimal conditions TTIP 10 mL, EG 4 mL, Sonication time 1 h.

4.1.2 Effect of Calcination on RNP

In this stage, sample 4 of RNP was selected and the effect of calcination temperature on photocatalytic activity was optimized and comparison was made with non-calcined sample and P25. Sample 4 before and after calcination is named as non-calcined and calcined sample respectively. *Figure 4-7* illustrates that the non-calcined sample provides approximately two times higher photoactivity than P25. However, there was only 1 % increase in the photocatalytic performance of calcined sample than non-calcined sample. We observed that during calcination, organic substances and other impurities were removed from RNP which

were present as a result during the preparation process. These impurities block the active sites of RNP to some extent and prevent dye molecule from attaching to the active site. This leads to a decrease in photocatalytic degradation process when compared to the calcined samples. It can be seen (*Figure 4-7*) that the maximum dye removal efficiency was attained by samples calcined at 600 $^{\circ}C$ as it provides more surface area for the dye molecule to adsorb on it. We found a small portion of rutile phase above 600 $^{\circ}C$ as mentioned in ***Table 4-1***. This result indicates that EG controls the anatase to rutile phase transformation to a certain temperature. We couldn't find any improvement in the dye removal efficiency above 600 $^{\circ}C$.

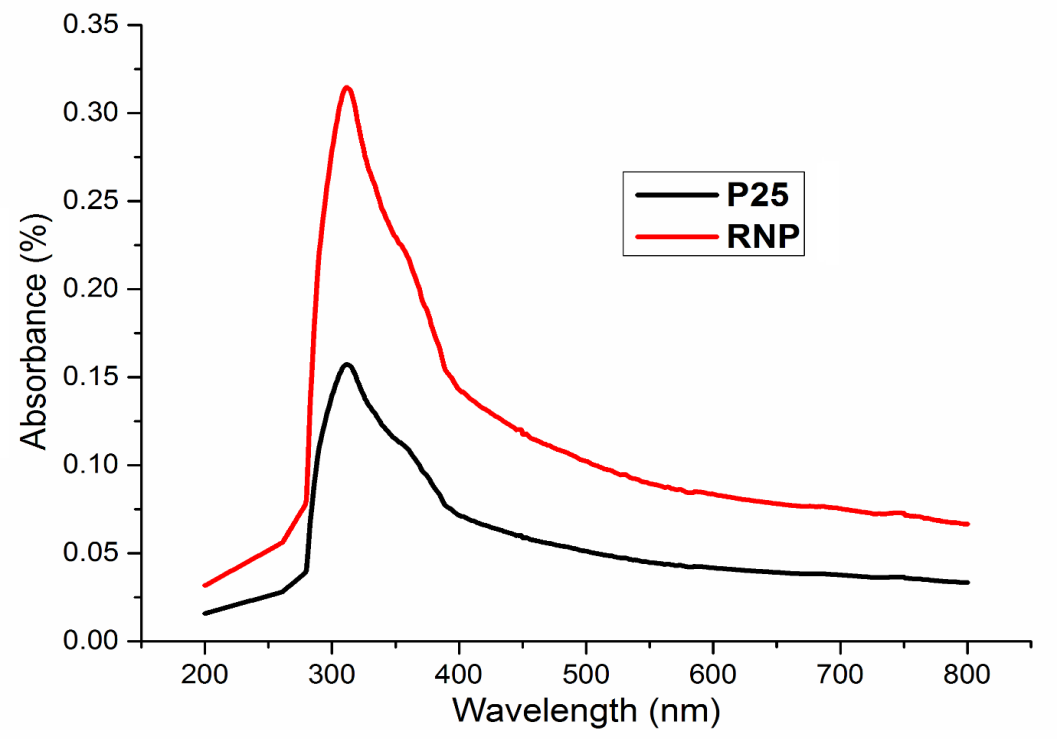

Figure 4-6 UV-Vis absorption spectrum, P25 and RNP with optimal conditions TTIP 10 mL, EG 4 mL, Sonication time 1 h.

4.1.3 Optimization of Experimental Variables for RNP

The design of experiment with different concentrations of TTIP and EG under varying sonication time based on actual values of CCD is presented in ***Table 4-2***. To optimize the effects of independent variables; TTIP, EG and ultrasonic irradiations time were selected as experimental variables and MB removal as a response. Total 20 experimental CCD designed samples were developed as illustrated in ***Table 4-2***. 3D surfaces and contour plots are helpful in identifying the effect of tested variables and the type of interactions between them.

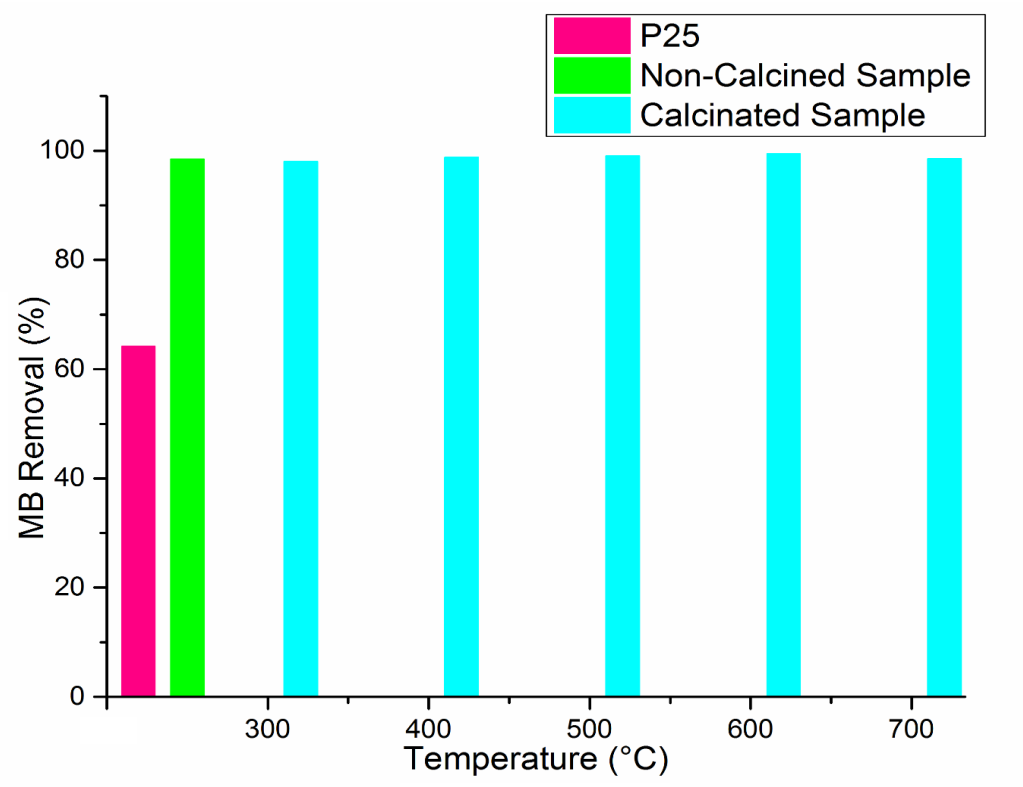

Figure 4-7 Comparison of calcined sample, non-calcined sample and P25 at different temperatures and their effects on photocatalytic activity.

Table 4-2 The 3-factors CCD matrix based on actual values for experimental variables and response, Y=MB Removal, for the synthesis of TiO_2 NPs

Sample	TTIP Conc. [*mL*]	EG Conc. [*mL*]	Sonication Time [*h*]	MB Removal [*%*] Experimental	MB Removal [*%*] Predicted
1	6	4	2	67	64
2	6	4	0.25	57	58
3	4	3	1	33	32
4	10	4	1	99	98
5	4	5	3	47	46
6	8	3	1	72	73
7	8	3	3	91	91
8	6	4	2	63	64
9	2	4	2	21	23
10	6	6	2	81	81
11	6	4	2	62	64
12	6	4	2	62	64
13	6	4	2	63	64
14	4	5	1	50	49
15	8	5	3	74	74
16	4	3	3	72	71
17	6	4	4	72	73
18	6	2	2	81	81
19	6	4	2	64	64
20	8	5	2	85	86

The response surfaces and contour plots were drawn by Design-Expert 10 to evaluate the interactive relationships between the selected variables and MB removal efficiency. The effect of precursor's concentrations and ultrasonic irradiations time on the photocatalytic removal of MB is presented in *Figure 4-8*.

The CCD results indicate that the photocatalytic activity of RNP increased with the increase in TTIP and EG concentrations up to 10 *mL* and 4 *mL* respectively. It can be seen in ***Table 4-2*** that MB removal rate increased from 33 % to 91 %, 33 % to 85 % and 33 % to 91 % by increasing the TTIP and EG concentration and sonication time up to their maximum level. However, the best outcome 99 % was achieved with optimal conditions i.e. TTIP 10 *mL*, EG 4 *mL* and sonication time 1 *h*., whereas, the predicted response value for MB removal at optimal conditions (Sample 4) was 98 %.

A mathematical model (Equation 8) was developed in order to evaluate the obtained results and the relationship between independent variables and response surfaces. The related response of the model was a function of independent variables. This model is useful in predicting the responses for a given value of independent variables i.e. TTIP conc., EG conc. and ultrasonic irradiations time. Based on this model, response surfaces and contour plots were drawn as illustrated in *Figure 4-8*. MB removal on the basis of developed model is calculated by Equation 8:

$$Y = -30.2 + 14.8(TTIP) - 20.5(EG) + 60.9(Time) + 1.0(TTIP * EG) - 2.6(TTIP * Time) - 10.6(EG * Time) - 0.4(TTIP)^2 + 4.4(EG)^2 + 0.3(Time)^2 \quad [8]$$

Analysis of variance (ANOVA) was used to analyse the data for interaction between process variables and responses obtained from samples 1-20 (***Table 4-2***) and results were analysed to

judge the goodness of fit. The results indicate that the designed model for MB dye removal is statistically significant for F-value of 273.8 and prob > F of <0.0001 as shown in ***Table 4-3***. R-squared coefficient is used to predict the fit of the model. ANOVA results indicate that only 0.04 % of total variables for MB removal cannot be explained by this model [118; 119]. Low Coefficient of Variation (CV%) values of the employed model describe the precision and reliability of the experiment.

A plot of actual vs predicted values is presented in *Figure 4-9*. This plot explains the effects of fitted model and compares it with the null model. It can be observed that all values are very close to the fitted line indicating a good fit of the model. The optimal design points on the basis of ***Table 4-2*** and Equation 8, were 10 *mL* TTIP, 4 *mL* EG and 1 *h* sonication time.

4.1.4 Photocatalytic Evaluation of RNP

The photocatalytic activity of RNP and P25 was investigated with 0.5 gL^{-1} dose of both photocatalysts by taking initial concentration of MB 50 mgL^{-1}. The results illustrated in *Figure 4-10* explain that the decolouration of MB follows decreasing order. It was observed that with the same dosage of RNP, dye solutions have been decoloured within 40 *min* under UV light while for P25, the dye solutions took longer time to decolour. It may be due to the fact that P25 is a mixture of rutile and anatase with a wide band gap that directed to a low photocatalytic activity. To confirm the decolouration of MB was due to the presence of RNP and not by the poor light fastness of MB dye, dye solution without photocatalyst was also exposed under UV light. This solution couldn't change its colour even after longer irradiations time. These results confirm that the higher photo activity of RNP originated due to anatase form induced by ultrasonic irradiations. So, these results revealed that RNP synthesized by Ultrasonic Acoustic Method (UAM) are more photoactive than commercially available Degussa P25 as their

minimal quantity removes dye from the dye solutions in a very short span of time. UV-Vis spectral changes in MB dye solution as a function of UV light irradiations time are illustrated in *Figure 4-10*.

Table 4-3 ANOVA results for MB removal for the synthesis of TiO_2 NPs

Source	Sum of Squares	df	Mean Square	F Value	p-value Prob > F	Remarks
Model	6536.6	9	726.2	273.8	< 0.0001	Significant
A-TTIP Conc.	4365.6	1	4365.6	1646	< 0.0001	Significant
B-EG Conc.	0.01	1	0.01	0.004	0.9506	Not significant
C-Sonication Time	204.2	1	204.2	77	< 0.0001	Significant
AB	31.7	1	31.7	11.9	0.0061	Significant
AC	243.9	1	243.9	91.9	< 0.0001	Significant
BC	732.5	1	732.5	276.2	< 0.0001	Significant
A^2	62.6	1	62.6	23.6	0.0007	Significant
B^2	497.0	1	497	187.4	< 0.0001	Significant
C^2	2.07	1	2.07	0.78	0.3968	Not significant
Residual	26.5	10	26.5			
Lack of Fit	9.0	5	1.8	0.51	0.7577	Not significant
Pure Error	17.5	5	3.5			
Cor Total	6563.2	19				

R-squared: 0.9960, adjusted R-squared: 0.9923, CV%: 2.47

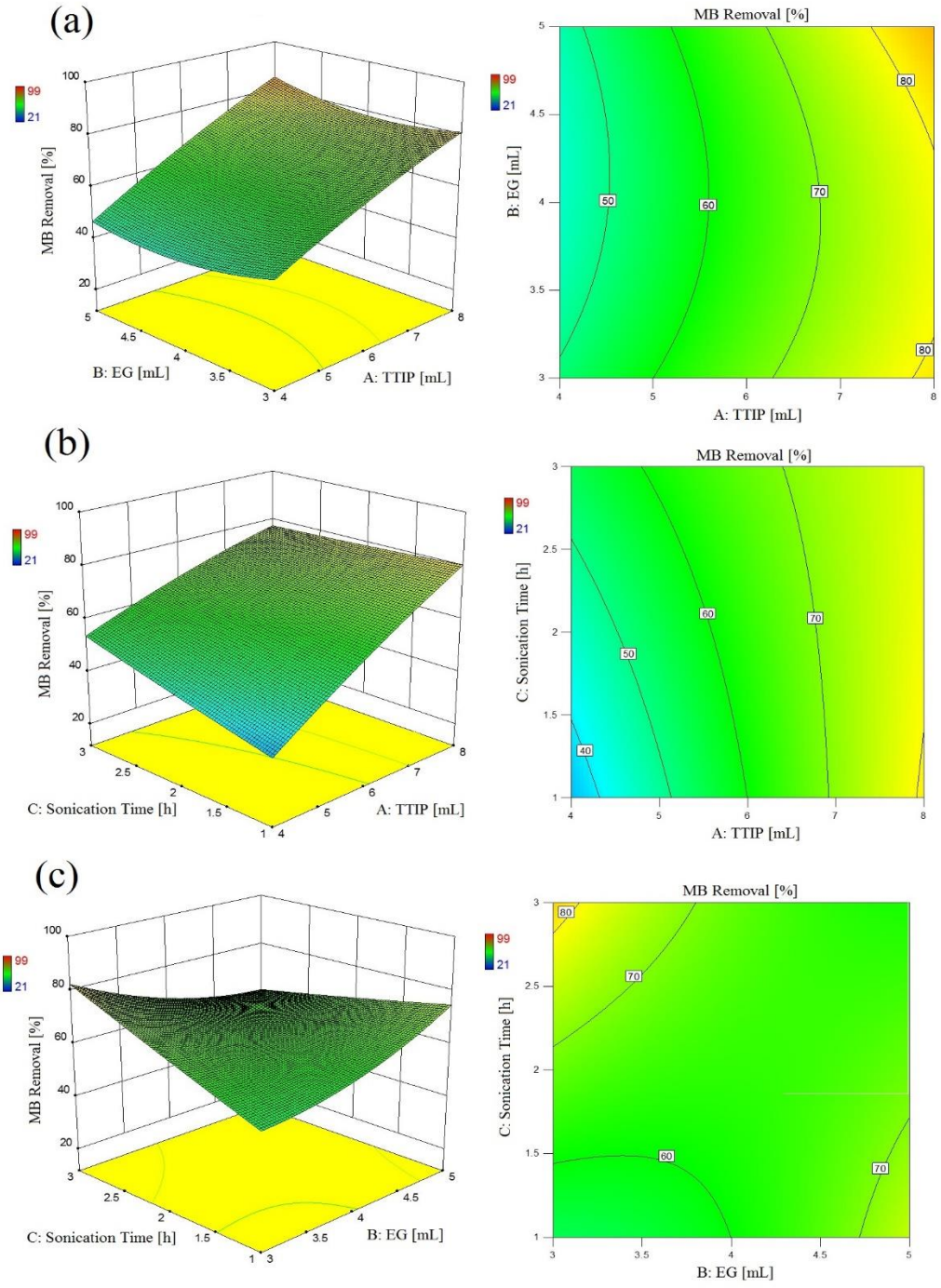

Figure 4-8 The response surfaces and contour plots for photocatalytic dye removal as a function of (a) TTIP conc., EG conc., (b) TTIP conc., Sonication time., (c) EG conc., Sonication time.

Anatase and rutile forms of TiO_2 NPs have been used in major practical applications. Zhang and Banfield reported that TiO_2 NPs in their anatase form are most stable with size less than 11 *nm* while rutile is stable above 35 *nm* [39]. So, anatase form is considered to be a better choice as a more active photocatalyst than rutile. This is also because rutile has a very lower surface affinity to most of the organic compounds as well as a high electron-hole pair recombination rate. When a photon with energy greater than the band gap energy of TiO_2 strikes its surface, electrons are released and combine with oxygen to become super oxide anion ($^{\bullet}O_2^-$). Furthermore, the surface becomes positively charged (holes) and takes electron from moisture present in the air. The moisture that has lost electron convert into hydroxyl radical ($OH^{\bullet}$). These superoxide anion ($^{\bullet}O_2^-$) and hydroxyl radical ($OH^{\bullet}$) are highly reactive species and with their strong power of oxidation, decompose organic compounds that cause staining. Agustina et al. studied heterogeneous photocatalysis and explained that hydroxyl radicals ($OH^{\bullet}$) are responsible for the degradation of pollutants. High production of radicals on the surface of photocatalyst increases its power to degrade the organic pollutants [120]. The proposed reaction mechanism is shown in *Figure 4-11*.

4.1.5 Self-cleaning Efficiency of RNP

For self-cleaning evaluation, all samples were stained in 0.01 % (*w/v*) solution of MB and colour change was calculated in RGB colour space after 24 *h* daylight irradiations as presented in Table 4-4. Significant change in colour was observed in case of RNP deposited samples as illustrated in *Figure 4-12*. However, slight colour change was observed in case of P25 treated sample and no change in untreated sample. Moreover, the values of ΔRGB were higher for samples 1-20 as compared to P25 treated sample. The results indicate that ΔRGB values are dependent on ultrasonic irradiations time and TTIP and EG concentrations. Higher colour

difference leads to better self-cleaning efficiency obtained by sample 4 with optimal conditions as illustrated in ***Table 4-4***.

The content of UV present in sunlight triggers the photocatalytic activity of TiO_2 NPs and decompose MB stains [121]. The significant influence of ultrasonic irradiations on self-cleaning property arises due to the formation of crystalline anatase phase.

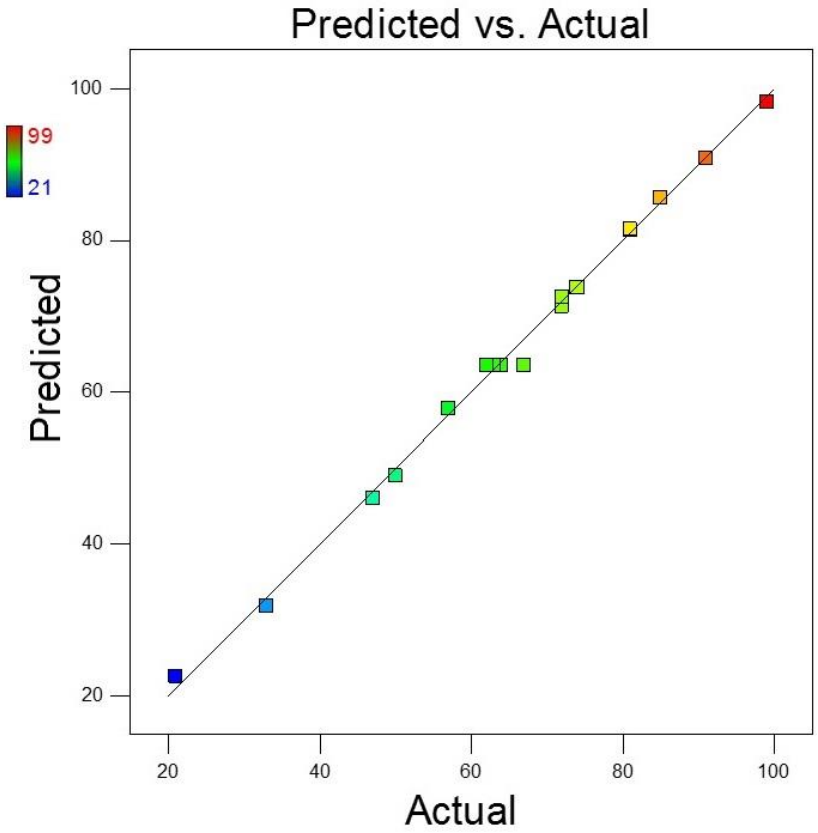

Figure 4-9 A plot of actual vs predicted responses for RNP.

4.1.6 Reusability and Sequential Application of RNP

Reusability of a catalyst is a very important property for its application point of view. The reusability of RNP and P25 was estimated in the photocatalytic removal of MB. In each cycle, photocatalysts were extracted by centrifuge process from the treated solution and washed with

distilled water. After drying at 100 $^{\circ}C$ for 1 h, they were reused again and again in the photocatalytic removal of fresh MB solution. As shown in *Figure 4-13*, after 10 reused cycles, the photocatalytic removal rate of MB had lost about 8 % and 21 % for RNP and P25 respectively. These results confirmed that the RNP with pure anatase form have much improved reusability and stability as a photocatalyst than P25 during the dye removal processes.

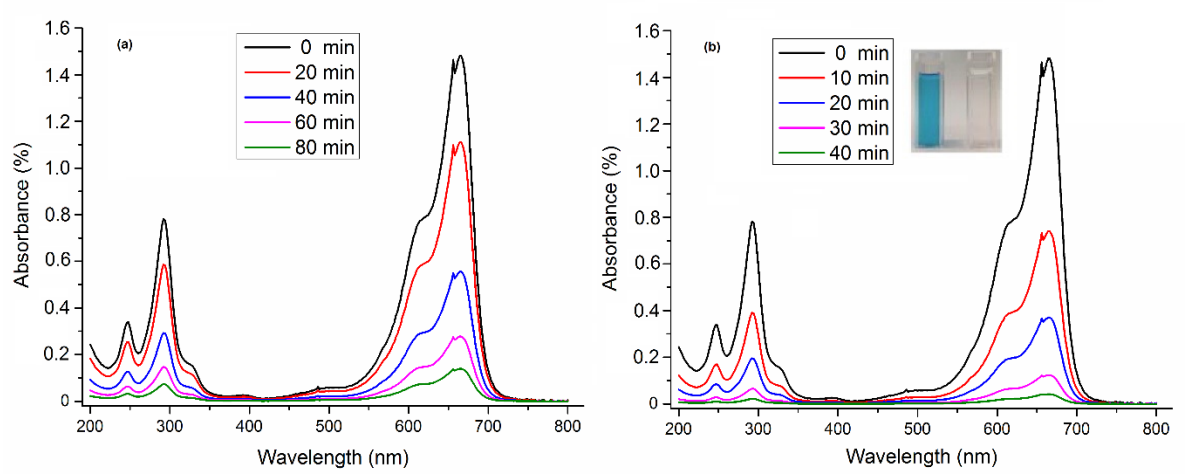

Figure 4-10 UV-Vis spectral changes in MB solution as a function of UV irradiations time. (a) P25, (b) RNP with optimal conditions TTIP 10 mL, EG 4 mL, Sonication time 1 h. The inset shows the digital photograph for colour change of MB before and after treatment.

Table 4-4 Self-cleaning (ΔRGB) results for Resulting Nanoparticles (RNP)

Sample	ΔRGB	Sample	ΔRGB
Blank	8.2	10	89.4
P25	59.4	11	88.5
1	78.1	12	87.2
2	83.2	13	91.4
3	89.5	14	86.5
4	96.6	15	90.2
5	85.2	16	87.7
6	77.1	17	93.8
7	92.4	18	90.6
8	89.8	19	85.6
9	93.2	20	91.1

4.2 Results and Discussions for Stabilization of TiO_2 NPs onto Cotton

This section explains the results for the stabilization of TiO_2 NPs (RNP) onto cotton fabric by UV light irradiations in details for further applications.

4.2.1 SEM Analysis and EDX Spectra of TiO_2 NPs Stabilized by UV Irradiations

The morphology of developed samples was investigated by SEM and EDX analysis. In *Figure 4-14*, a comparison of pristine cotton (untreated sample) with sample 14 is presented as we obtained highest incorporated amount of TiO_2 NPs for this sample (***Table 4-5***). In *Figure 4-14 (a)*, a clean and smooth surface of pristine cotton can be observed as no treatment was applied on it whereas a huge cluster of TiO_2 NPs deposited as a homogeneous thick layer on the surface of cotton fabric after padding can be seen in *Figure 4-14 (b)*. We also observed that the particles

are evenly distributed on the surface of cotton *Figure 4-14 (b)*. In *Figure 4-14 (c)*, it can be seen that after UV irradiations, most of the NPs penetrated inside the cotton fibre structure and the remaining covered the surface as a condense layer and strongly aggregated while a completely rough surface of cotton with sufficient amount of TiO_2 NPs was observed after washing the sample as illustrated in *Figure 4-14 (d)*.

Elemental analysis and detection of existing elements were characterized by EDX spectroscopy. The EDX spectrum of untreated sample and sample 14 are presented in *Figure 4-14 (e-f)* respectively. EDX spectra confirm the existence of TiO_2 NPs on cotton surface. Moreover, higher weight percentage of Ti element in sample 14 indicates higher loading of TiO_2 NPs. These results are in good agreement with SEM results.

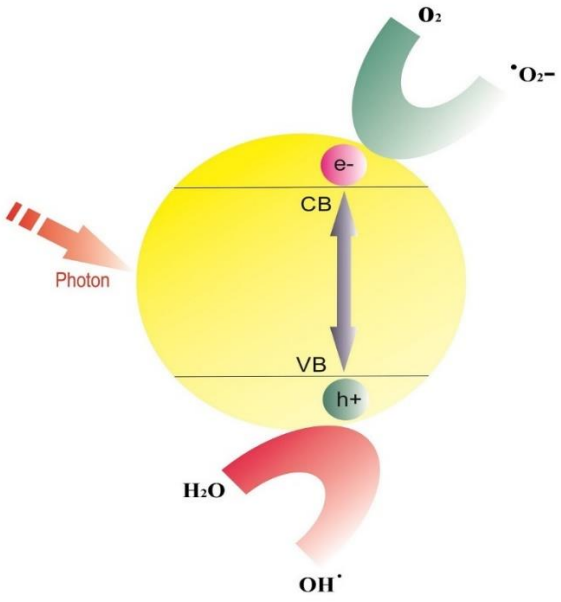

Figure 4-11 Proposed reaction mechanism on the surface of RNP under UV light (e^-, electron; h^+, hole).

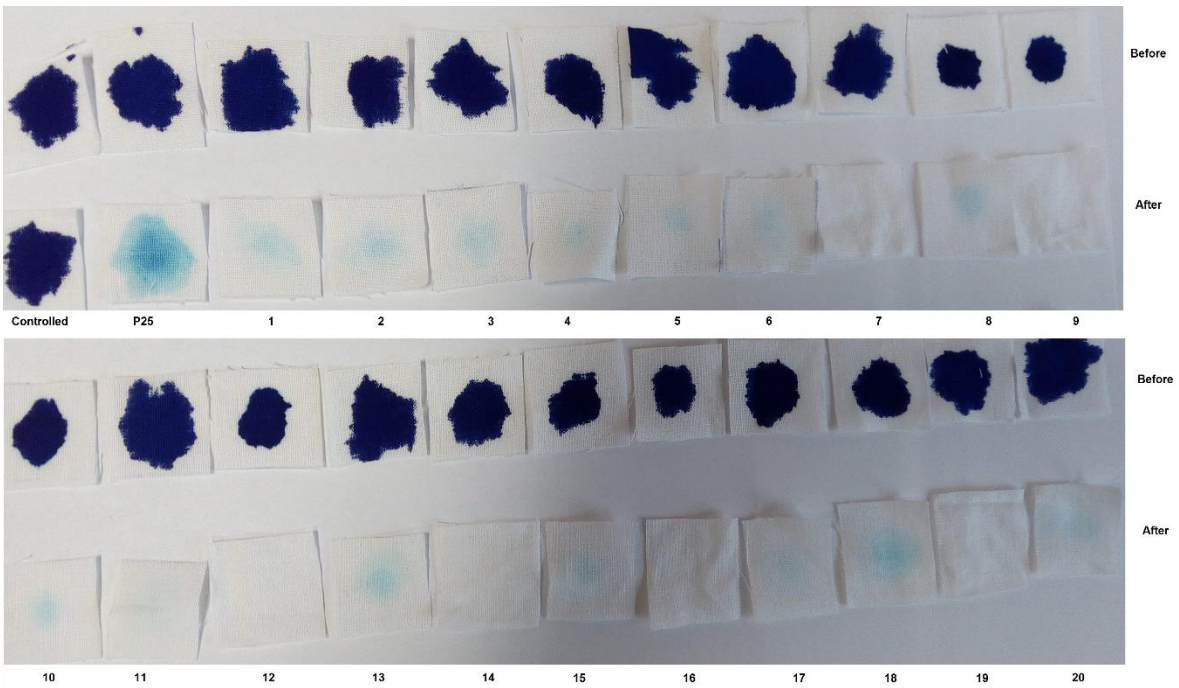

Figure 4-12 Self-cleaning efficiency after 24 h daylight irradiations for RNP.

4.2.2 ICP-AES Analysis of TiO_2 NPs Stabilized by UV Irradiations

ICP-AES analysis of samples 1-20 confirmed the presence of TiO_2 NPs on cotton. However, Ti element was not found in untreated sample. In order to estimate the incorporated amount, the characteristic peak of titanium observed in emission spectra was counted and the results were reported in ***Table 4-5***. The incorporated amount of TiO_2 NPs for samples 1, 11, 16, 17, 18 were 2123 *ppm*, 1781 *ppm*, 2895 *ppm*, 2999 *ppm*, 2756 *ppm* respectively, whereas the highest incorporated amount 3319 *ppm* was found in sample 14. The results are quite obvious as more dosage of TiO_2 NPs during padding results in more loading on cotton. These results are in good agreement with SEM and EDX results.

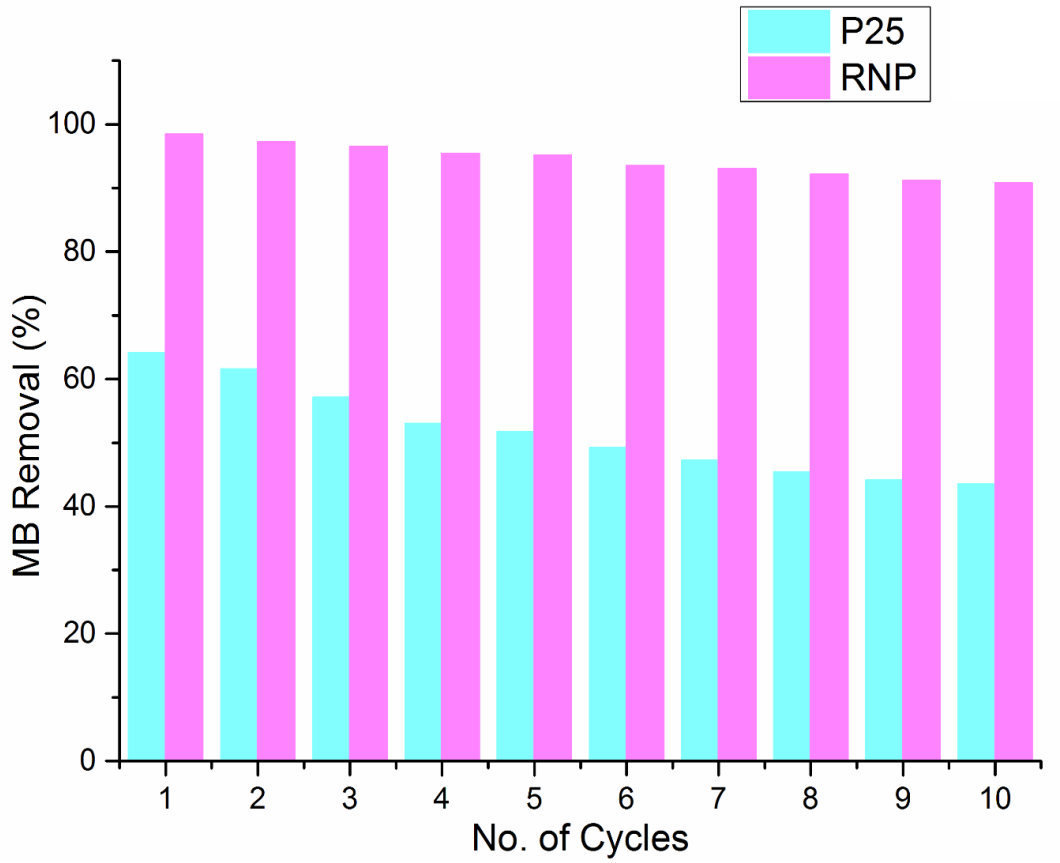

Figure 4-13 Reusability comparison of RNP vs P25 as a photocatalysts against MB removal.

4.2.3 Leaching Durability

The contents of Ti^{+4} ions present in the leaching solution were 82 *ppm*, 107 *ppm*, 102 *ppm*, 48 *ppm* and 39 *ppm* for sample 3, sample 5, sample 10, sample 14 and sample 18 respectively. These results reveal that only 5 % TiO_2 was removed from the fabric surface by leaching in case of sample 5 whereas this percentage was decreased to 1.4 % for sample 14 and sample 18. On the other side, 63 % TiO_2 was removed for TiO_2 treated sample (without UV treatment). These results indicate that TiO_2 NPs incorporated on cotton surface by UV light irradiations were strongly anchored to the textile substrate as their minimal quantity was withdrawn from the fabric even after 6 *h* of leaching process.

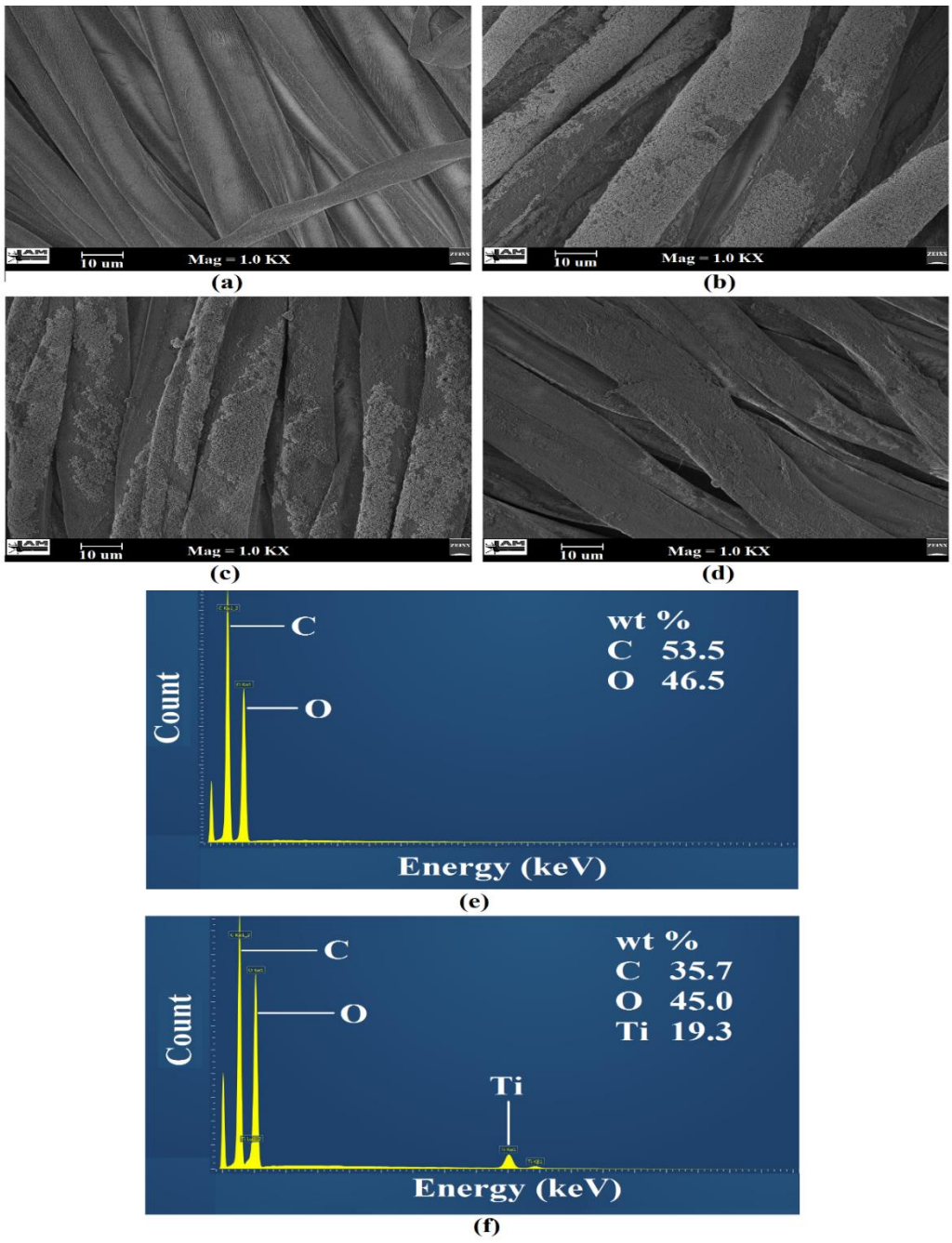

Figure 4-14 SEM analysis of (a) untreated sample, (b) sample 14 before UV treatment, (c) sample 14 after UV treatment, (d) UV treated sample after washing; and EDX spectra of (e) untreated sample (f) sample 14.

4.2.4 Washing Durability

Washing effluent analysis was used to evaluate the embedding of TiO_2 NPs on cotton fabric that provides an excellent evaluation of washing durability. The existing amount of TiO_2 NPs in the effluent is considered as durability against washing. More amount indicates lower durability. The effluent was evaluated by spectrophotometer during 6 washing cycles. During initial washing cycle, an absorption peak at 289 *nm* indicates the presence of TiO_2 NPs as illustrated in *Figure 4-15*. It happened because some of the physically attached and unstable NPs were migrated into effluent during initial washing. The results confirmed that no absorption peak was observed during subsequent washing cycles showing the absence of TiO_2 NPs in washing effluent. Furthermore, the results reveal that TiO_2 NPs are strongly attached to cotton indicating the formation of covalent bond between TiO_2 NPs and cotton fibre. TiO_2 NPs have strong affinity towards carboxyl and hydroxyl groups. The bonding between TiO_2 NPs and hydroxyl groups present in cotton play a significant role in washing durability. These results are in good agreement with the findings of Daoud et al.; Montazer et al.; and Pakdel and Daoud respectively [30; 122; 123].

4.2.5 Self-cleaning Efficiency of TiO_2 NPs Stabilized by UV Irradiations

Figure 4-16 illustrates that coffee stains were decomposed completely after 12 *h* of sunlight irradiations through photocatalytic action of TiO_2. The colour difference was calculated and the results were reported in ***Table 4-6***. Significant colour change was observed for samples 1 to 20 as presented in *Figure 4-16*. However, slight colour change was observed for TiO_2 treated sample (without UV treatment) and almost no change in untreated sample even after 12 *h* of continuous sunlight irradiations. In addition, the colour values were higher for samples 1 to 20 as compared to TiO_2 treated sample and untreated sample respectively. These results indicate

the self-cleaning efficiency of UV treated samples (samples 1 to 20) was significantly higher than TiO_2 treated sample (without UV treatment). This happens because of embedded TiO_2 NPs on cotton fabric as UV irradiations produce a covalent linkage between the OH group of TiO_2 and the OH group of cellulose that increases the durability of the treatment to impart functional properties. These results are in good agreement with the findings of Abidi et al. [25]. Moreover, the results reveal that more amount of TiO_2 NPs incorporated on the surface of cotton fabric enhances the self-cleaning properties. Higher colour difference leads to better self-cleaning efficiency obtained by sample 14 with optimal conditions as illustrated in ***Table 4-5***.

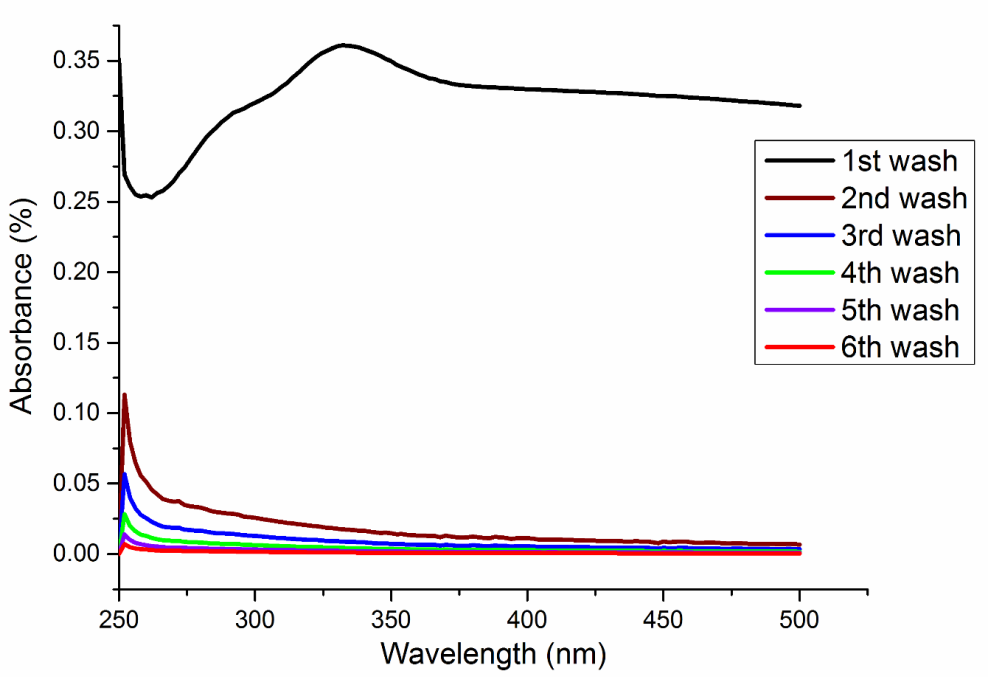

Figure 4-15 Washing effluent absorbance spectra of sample 14 during different washing cycles for the stabilization of TiO_2 NPs by UV irradiations.

4.2.6 Statistical Analysis of TiO_2 NPs Stabilized by UV Irradiations

The experimental design with different dosage of TiO_2 Nanoparticles (NPs) under varying temperature and UV irradiations time based on actual values of CCD is illustrated in ***Table 4-5***. The results include: Y_1=Incorporated amount of TiO_2 NPs onto cotton after UV irradiations and Y_2=Tensile strength of cotton after UV irradiations were adjusted by Equation 1.

CCD and RSM were used to optimize the experimental variables i.e. TiO_2 dosage, temperature and UV irradiations time. In total, 20 CCD designed samples were developed as described in ***Table 4-5***. For the evaluation of obtained results and the relationship between independent variables and response surfaces, different mathematical models (Equation 9-10) were established. In order to predict the responses for a given value of variables, the developed models are useful for further utilization. In *Figure 4-17* and *Figure 4-18*, response surfaces were drawn based on the developed mathematical models for incorporated amount of TiO_2 NPs and tensile strength respectively.

ANOVA was conducted to evaluate the interaction between the variables and the responses of the designed samples and the results are presented in ***Table 4-7*** and ***Table 4-8***. Goodness of fit was evaluated on the basis of responses analysed by ANOVA. The lack of fit explains the data variations close to the fitted model and will be significant if the proposed model unable to fit the data well. The results indicate that the designed model for incorporated amount of TiO_2 NPs on cotton after UV irradiations is statistically significant at F-value 10592.9 and p-value <0.0001 as illustrated in ***Table 4-7***. Furthermore, the developed model for tensile strength is significant at F-value 43.1 and p-value <0.0001 as described in ***Table 4-8***.

Table 4-5 The 3-factors CCD matrix based on actual values for experimental variables and responses, Y_1= Incorporated amount of TiO_2 NPs after UV irradiations, Y_2= Tensile strength after UV irradiations, for the stabilization of TiO_2 NPs by UV irradiations

Sample Name	TiO_2 Dosage [gL^{-1}]	Temperature [$^{\circ}C$]	UV Irradiations Time [*min*]	Y_1 = Incorporated TiO_2 on cotton [*ppm*]	Y_2 = Tensile Strength [*N*]
Untreated Sample	0	0	0	0	504
1	6	70	80	2123	482
2	4	30	120	1590	474
3	6	45	80	1383	434
4	6	45	80	1386	426
5	6	45	15	793	465
6	8	30	40	1590	463
7	6	45	80	1380	424
8	4	60	40	898	432
9	6	45	80	1389	427
10	4	30	40	856	498
11	8	60	40	1781	496
12	6	20	80	1763	476
13	2	45	80	759	489
14	8	60	120	3319	490
15	6	45	80	1398	428
16	8	30	120	2895	414
17	10	45	80	2999	492
18	6	45	150	2756	428
19	4	60	120	1805	425
20	6	45	80	1381	420

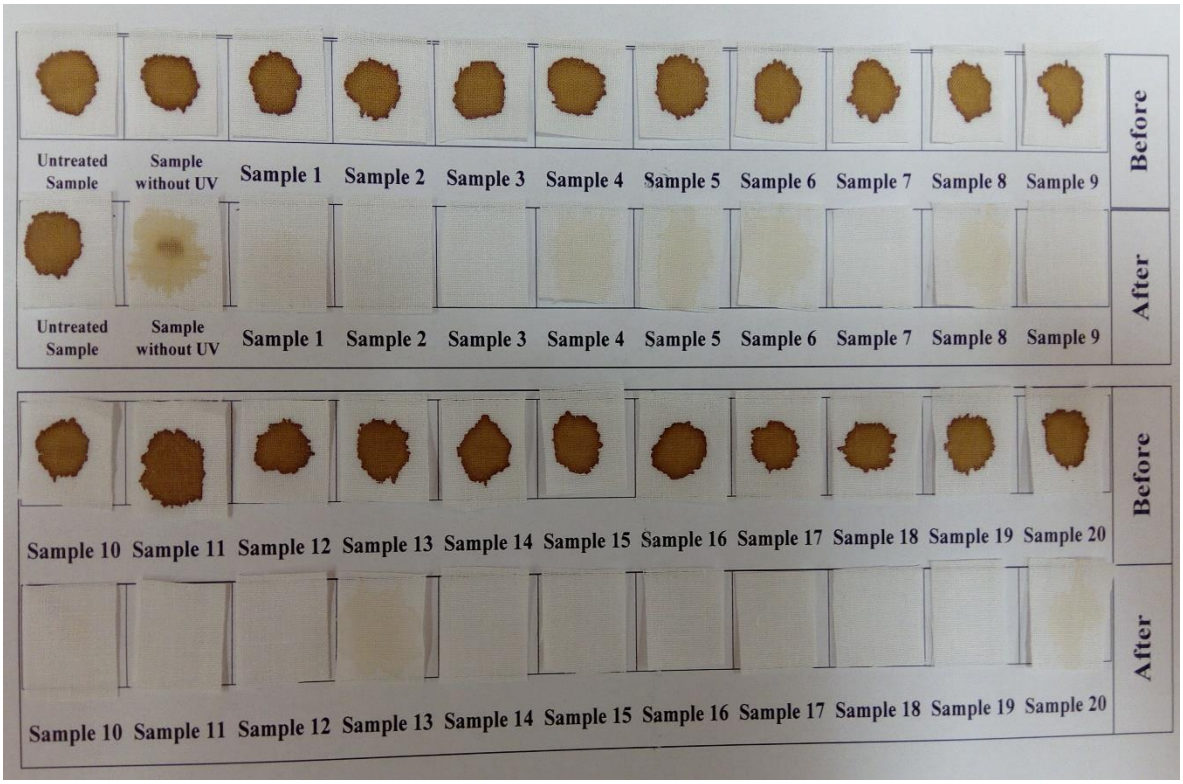

Figure 4-16 Self-cleaning efficiency after 12 h sunlight irradiations.

R-squared coefficient was used to evaluate the fit of the developed models. The results presented in ***Table 4-7*** indicate that only 0.01 % of the total variables cannot be explained through this model for incorporated amount of TiO_2 NPs on cotton after UV irradiations. Furthermore, the results of R-squared for tensile strength indicate that only 2.51 % of the total variables cannot be explained by the model (***Table 4-8***).

Table 4-6 Self-cleaning efficiency (ΔE) results for the stabilization of TiO_2 NPs by UV irradiations

Sample	(ΔE)	Sample	(ΔE)
Untreated Sample	4.9	Sample 10	83.9
TiO_2 treated sample (without UV)	48.4	Sample 11	82.6
Sample 1	81.8	Sample 12	83.2
Sample 2	79.6	Sample 13	80.1
Sample 3	80.5	Sample 14	89.7
Sample 4	82.3	Sample 15	83.5
Sample 5	78.4	Sample 16	81.7
Sample 6	79.2	Sample 17	82.6
Sample 7	81.6	Sample 18	83.3
Sample 8	82.8	Sample 19	82.9
Sample 9	80.6	Sample 20	81.8

The incorporated amount of TiO_2 NPs on cotton after UV irradiations according to the developed model is calculated by Equation 9:

$$\begin{aligned} Y_1 = {} & 3311.8 - 310.9 \times (Dosage) - 89.3 \times (Temperature) \\ & - 13.5 \times (UV\ Time) + 1.4 \times (Dosage \times Temperature) \\ & + 1.8 \times (Dosage \times UV\ Time) \\ & + 0.08 \times (Temperature \times UV\ Time) + 31.0 \times (Dosage)^2 \\ & + 0.8 \times (Temperature)^2 + 0.07 \times (UV\ Time)^2 \end{aligned} \quad [9]$$

The tensile strength after UV irradiations according to the developed model is calculated by Equation 10:

$$Y_2 = 1035.1 - 83.4 \times (Dosage) - 13.5 \times (Temperature) - 1.1 \times (UV\ Time) + 0.9 \times (Dosage \times Temperature) - 0.03 \times (Dosage \times UV\ Time) + 0.01 \times (Temperature \times UV\ Time) + 3.8 \times (Dosage)^2 + 0.07 \times (Temperature)^2 + 3.5 \times (UV\ Time)^2 \quad [10]$$

According to the above regression equations and obtained results (***Table 4-5***), the optimal points for best possible results are 8 gL^{-1} TiO_2 dosage, 60 $^{\circ}C$ temperature and 120 *min* UV irradiations time. The predicted response values for Y_1 and Y_2 under optimal conditions (Sample 14) are 3312 *ppm* and 488 *N* respectively.

The response surfaces are presented in *Figure 4-17* and *Figure 4-18* for incorporated amount of TiO_2 NPs on cotton after UV irradiations and tensile strength after UV irradiations respectively. It can be seen in *Figure 4-17* and *Figure 4-18* that increasing TiO_2 NPs dosage in the suspension results in more incorporated amount of TiO_2 NPs on the surface of cotton. Moreover, prolonged UV irradiations time leads to a higher fixation of TiO_2 NPs on cotton. This happened because UV irradiations provide most of the NPs a path to penetrate deep inside the fibre structure and strongly attached to them. The results revealed that the incorporated amount of TiO_2 NPs on cotton strongly depends on dosage of TiO_2 and UV irradiations time.

The plot of actual vs predicted values is presented in *Figure 4-19*. This plot statistically explains the effects of the fitted model and compares it with the null model. It can be observed that all the values are very close to the fitted line indicating a good fit of the model.

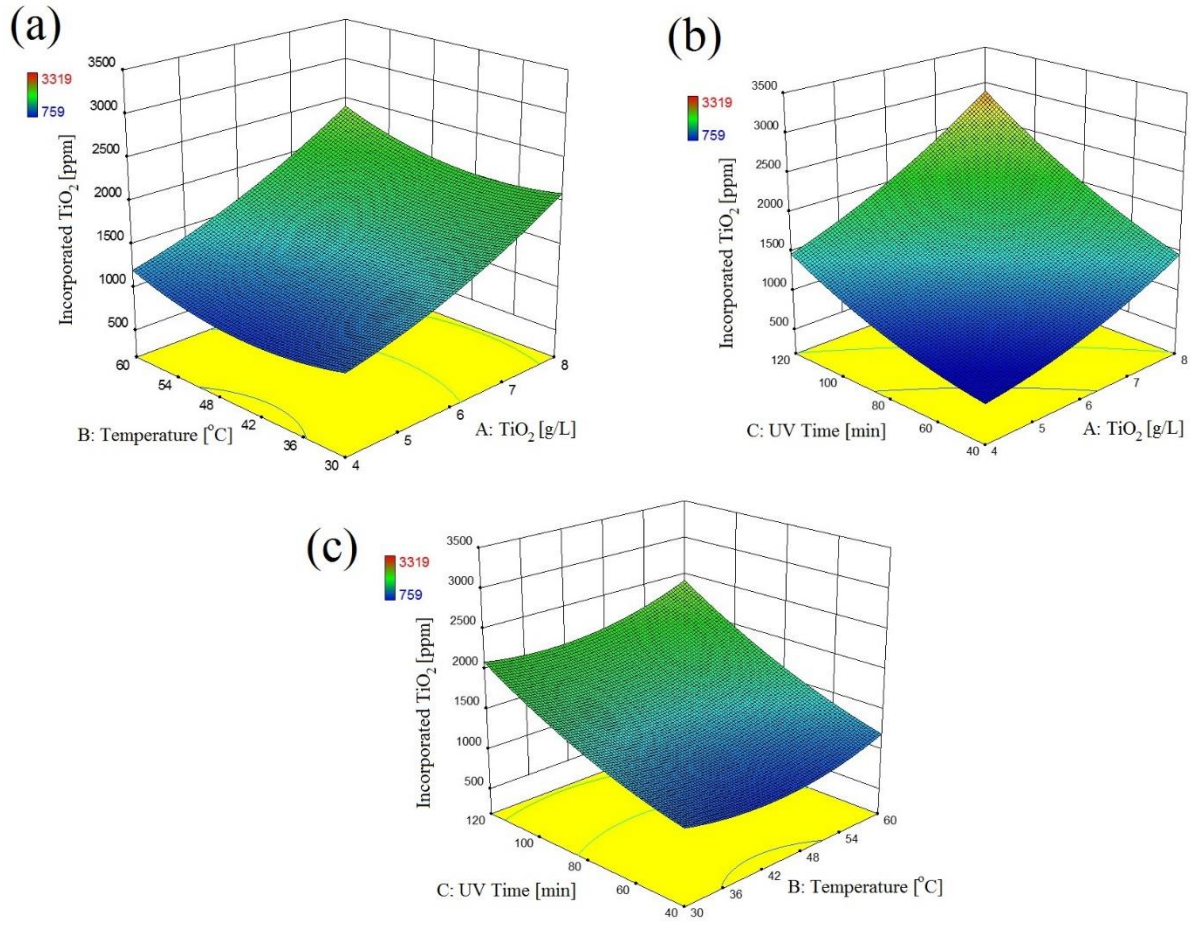

Figure 4-17 Response surfaces for incorporated amount of TiO_2 NPs on cotton after UV irradiations as a function of (a) TiO_2 dosage, Temperature, (b) TiO_2 dosage, UV time., (c) Temperature, UV time.

4.3 Results and Discussions for In-situ Developed Multifunctional CT Nanocomposites

This section explains the results for the developed multifunctional CT nanocomposites and discusses their applications.

4.3.1 SEM Images and EDX Spectra

The morphology of the developed CT nanocomposites was investigated by comparing SEM images of untreated cotton (blank sample), sample 9 and sample 18 as illustrated in *Figure 4-20*. In *Figure 4-20 (a-c)*, SEM images are showing a smooth and clean surface of blank sample as no treatment was applied on it. *Figure 4-20 (d-f)* illustrates that in sample 18, TiO_2 NPs were homogeneously deposited on cotton fabric by ultrasonic irradiations. Higher magnification of sample 18 was used to determine the distribution of particles on the surface of cotton as shown in *Figure 4-20 (f)*. In *Figure 4-20 (g-i)*, it can be seen that TiO_2 NPs covered the surface of sample 9 as a condense layer and strongly aggregated. The aggregation of nanoparticles could be due to longer ultrasonic time.

Elemental analysis and detection of involved elements in developed CT nanocomposites were characterized by EDX spectroscopy. The EDX spectrum of blank sample and sample 9 are illustrated in *Figure 4-20 (j-k)* respectively. The presence of TiO_2 NPs on cotton was confirmed by EDX spectrum. Moreover, the higher weight percentage of Ti element in sample 9 was indicating the higher loading of TiO_2 NPs. The EDX results are in good agreement with SEM results.

The difference in average particle size in the developed CT nanocomposites estimated by SEM images and in crystallite size calculated by Equation 2 was due to the aggregation of TiO_2 NPs on cotton surface due to its roughness as confirmed by Zhang et. al. [124]. Wu et.al reported that the aggregation of TiO_2 NPs on cotton occurred more quickly and easily due to its roughness [125]. These results indicate that synthesis conditions such as ultrasonic irradiations time has a substantial impact on the morphology of fabric and aggregation of deposited particles on it.

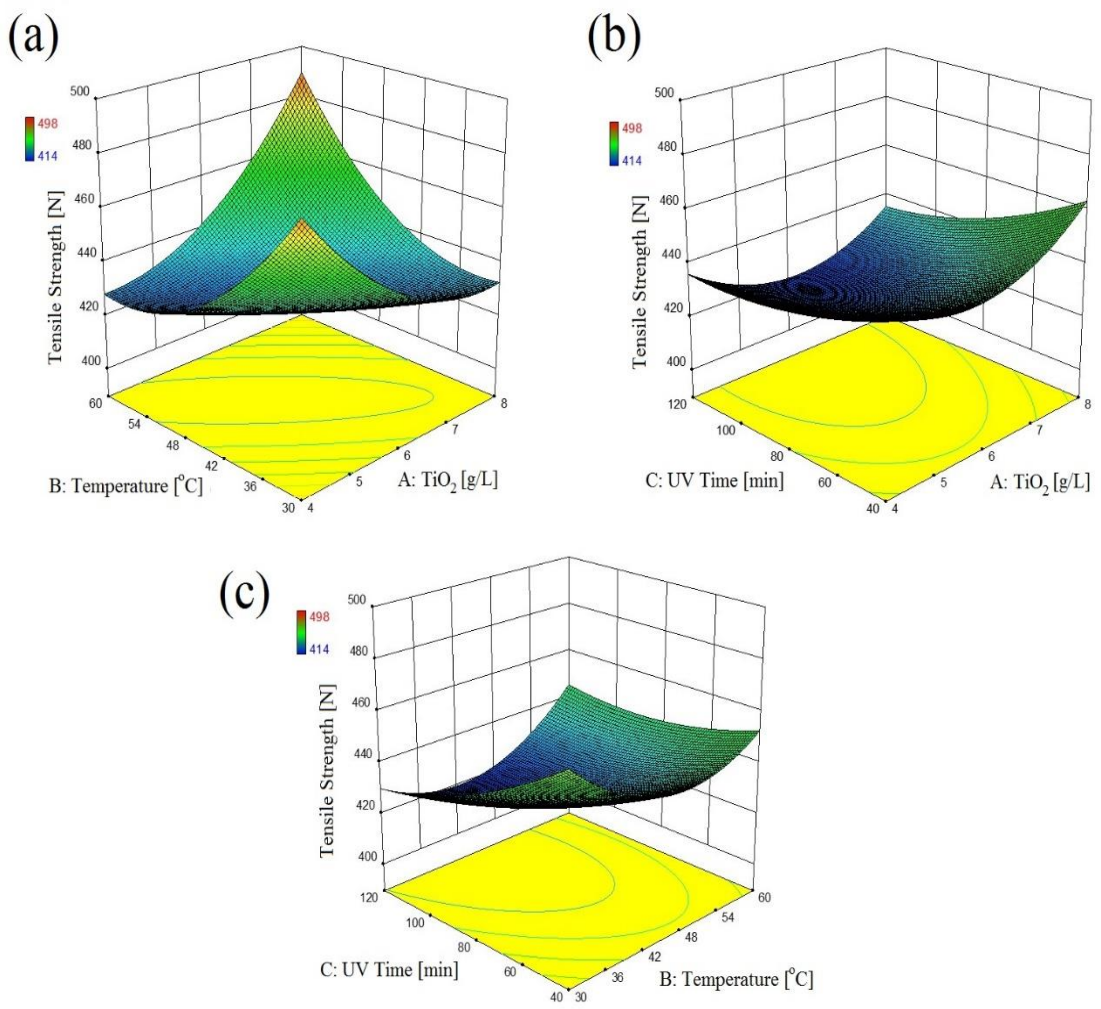

Figure 4-18 Response surfaces for tensile strength of cotton after UV irradiations as a function of (a) TiO_2 dosage, Temperature, (b) TiO_2 dosage, UV time., (c) Temperature, UV time.

Table 4-7 ANOVA results for incorporated amount of TiO_2 NPs on cotton after UV irradiations

Source	Sum of Squares	df	Mean Square	F Value	p-value Prob > F	Remarks
Model	10727146	9	1191905	10592.9	< 0.0001	Significant
A-Dosage	4968441	1	4968441	44156.6	< 0.0001	Significant
B-Temperature	159844.7	1	159845	1420.6	< 0.0001	Significant
C-UV Time	4318113.3	1	4318113	38376.8	< 0.0001	Significant
AB	16020.5	1	16020.5	142.3	< 0.0001	Significant
AC	180600.5	1	180601	1605.07	< 0.0001	Significant
BC	20604.5	1	20604.5	183.1	< 0.0001	Significant
A^2	399211.9	1	399212	3547.9	< 0.0001	Significant
B^2	563422.6	1	563423	5007.3	< 0.0001	Significant
C^2	227357.4	1	227357	2020.6	< 0.0001	Significant
Residual	1125.1	10	112.5			
Lack of Fit	902.3	5	180.4	4.05	0.075	Not significant
Pure Error	222.8	5	44.5			
Cor Total	10728271.2	19				

R-squared: 0.9999, adjusted R-squared: 0.9998, CV%: 0.62

Table 4-8 ANOVA results for tensile strength of cotton after UV irradiations

Source	Sum of Squares	df	Mean Square	F Value	p-value Prob > F	Remarks
Model	17334.2	9	1926.0	43.1	< 0.0001	Significant
A-Dosage	100	1	100	2.2	0.16533	Not significant
B-Temperature	1.1	1	1.1	0.02	0.87406	Not significant
C-UV Time	1678.8	1	1678.8	37.6	0.0001	Significant
AB	6272	1	6272	140.5	< 0.0001	Significant
AC	72	1	72	1.6	0.232	Not significant
BC	450	1	450	10.08	0.009	Significant
A^2	6028.7	1	6028.7	135.06	< 0.0001	Significant
B^2	4129.8	1	4129.8	92.5	< 0.0001	Significant
C^2	472.4	1	472.4	10.5	0.008	Significant
Residual	446.3	10	44.6			
Lack of Fit	338.8	5	67.7	3.1	0.116	Not significant
Pure Error	107.5	5	21.5			
Cor Total	17780.5	19				

R-squared: 0.9749, adjusted R-squared: 0.9523, CV%: 1.47

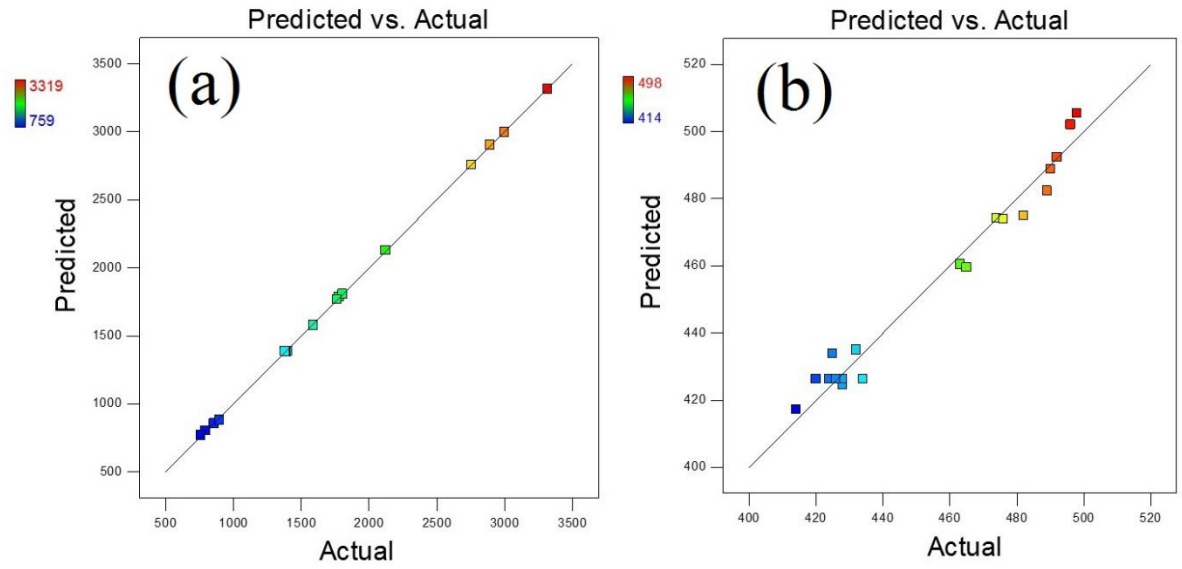

Figure 4-19 A plot of actual vs predicted responses; (a) Incorporated amount of TiO_2 on cotton after UV irradiations (b) Tensile strength of cotton after UV irradiations.

4.3.2 XRD Analysis

XRD analysis is a useful technique to determine the crystallite size and structure of the samples. The XRD patterns for extracted solid powders are described in *Figure 4-21*. Sample C prepared by conventional stirring shows amorphous nature as no sharp peak appeared in the XRD pattern which are the characteristics of crystalline phase of developed CT nanocomposites. However, a series of crystalline peaks were obtained for all other samples developed by Ultrasonic Acoustic Method (UAM). The crystalline peaks observed at $2\theta=25.4^{\circ}$, 38°, 48°, 53.8°, 55° and 62° for plane reflections (101, 004, 200, 105, 211 and 204 respectively) represent the pure anatase form of TiO_2 NPs according to JCPDS card no 21-1272. The chief influence of ultrasonication on crystallization of TiO_2 NPs was experienced by comparing sample C with sample 9 (***Table 4-9***). Ultrasonic waves are the only difference between these samples as ultrasonication plays a vital role in the crystallization mechanism of the synthesis of TiO_2 NPs.

The crystallite size of the NPs obtained from solid powder was calculated by Scherrer's equation and reported in *Figure 4-21 (a)*. The average crystallite size of all the specimen was equal to 4 *nm*. Moreover, the effect of reactants concentration (TTC and ISP) and sonication time on crystallite size and on crystallization was evaluated by XRD analysis through intensity of the peak and width of the longest peak. Comparison of XRD patterns of sample 1, 6 and 18 described that the increase in reactants concentration slightly increased the peak intensities of pure anatase form of TiO_2 NPs. Furthermore, XRD pattern and peak intensities of samples 1, 6, 9 and 18 demonstrated that an increase in sonication time led to sharper peaks. The above two discussed parameters are the signs of improved crystallinity in the synthesized TiO_2 NPs. These results indicate that more TTC and ISP concentration with prolonged sonication time have positive effects on crystallinity of NPs. However, a decrease in crystallite size was observed by increasing the sonication time *Figure 4-21 (a)*. These results are consistent with the findings of Ghows and Entezari [103]. The XRD analysis of sample 9 and untreated cotton (blank sample) is illustrated in *Figure 4-21 (b)*. The XRD pattern of untreated cotton (blank sample) showed only one characteristic peak at 21.3° which confirms a typical cotton fibre structure as concluded by Uddin et. al. [112].

Sample 9 reports a broad peak at 25.4° which confirms the XRD pattern of pure anatase form in accordance to JCPDS card data base for pure anatase phase of TiO_2. XRD is useful in determining the phase changes in crystal structures of a sample before and after treatment. In case of blank sample, the characteristic peaks or XRD pattern was not changed by ultrasonication which shows ultrasonic acoustic synthesis of TiO_2 NPs on cotton had no significant effect on phase assembly of cotton fibre. The width of the peak in XRD pattern indicates the particles size. Lower FWHM explains small particle size and vice versa. The

calculated crystallite size of the loaded TiO_2 NPs by Equation 2, was 3.982 by using FWHM at $2\theta=25.4^{\circ}$. The XRD results confirm that the crystallite size of extracted TiO_2 NPs in comparison with loaded TiO_2 NPs on cotton fabric by Ultrasonic Acoustic Method have no significant differences.

4.3.3 ICP-AES Elemental Analysis

ICP-AES analysis of samples 1-20 developed by UAM and sample C developed by conventional stirring method confirmed the presence of TiO_2 NPs on treated samples. However, in blank sample, Ti element was not detected. In order to estimate the synthesized and deposited amount of TiO_2 NPs on cotton fabric, the characteristic peak of titanium observed in emission spectra was counted and the response was reported in ***Table 4-9***. The loaded amount of TiO_2 NPs for sample 9 and sample C were 1587 *ppm* and 411 *ppm* respectively. More loading of TiO_2 NPs in sample 9 indicating the effects of ultrasonic acoustic irradiations. Moreover, a statistical study was performed to evaluate the effects of synthesis variables on deposited amount of TiO_2 NPs on cotton as reported in section 4.3.12.

4.3.4 UV-Vis Spectra

UV-vis spectra of sample 9 and blank sample after 30 washing cycles is illustrated in *Figure 4-22*. Sample 9 shows a transmittance level close to zero which confirms the excellent ability of developing CT nanocomposites as a UV absorbers or UV blocking agents. These results are consistent with the findings of Nazari et. al. [126]. Yang et. al. concluded that electronic band gap structure of TiO_2 is responsible for UV absorbance property [127]. No significant change observed on blank sample after washing *Figure 4-22*. There is a small increase in transmittance of sample 9. It could be possible that some of the deposited TiO_2 NPs are removed from cotton. So, the quantity of reactive species decreases resulting a slight increase in transmittance of

sample 9. However, UV absorption property of the developing CT nanocomposites is almost permanent even after 30 washing cycles indicating a strong bonding between cotton fabric and TiO_2 NPs. These results are in good agreement with the findings of Xin et al. and Uddin et al. [111; 112].

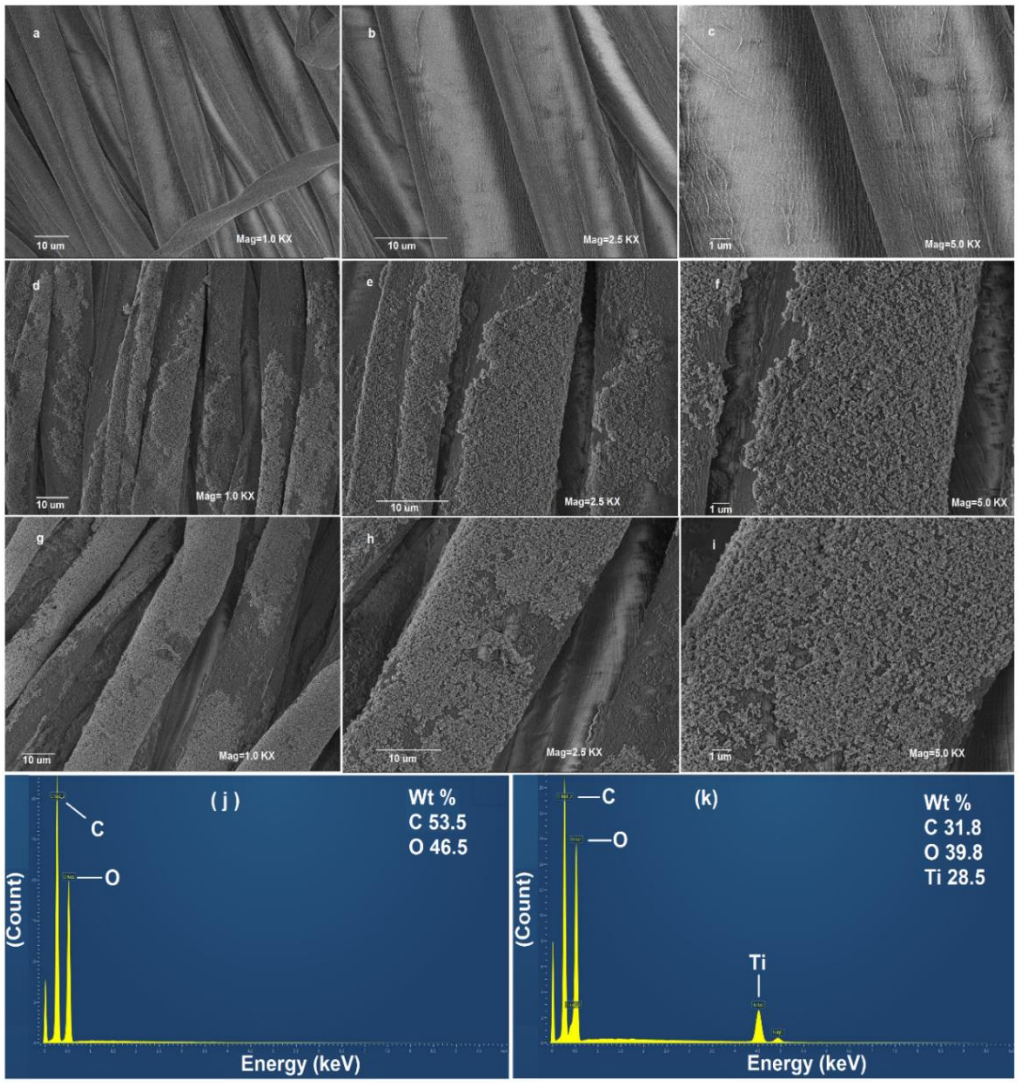

Figure 4-20 SEM analysis of blank sample (a-c), sample 18 (d-f) and sample 9 (g-i); and EDX spectrum of blank sample (j) and sample 9 (k).

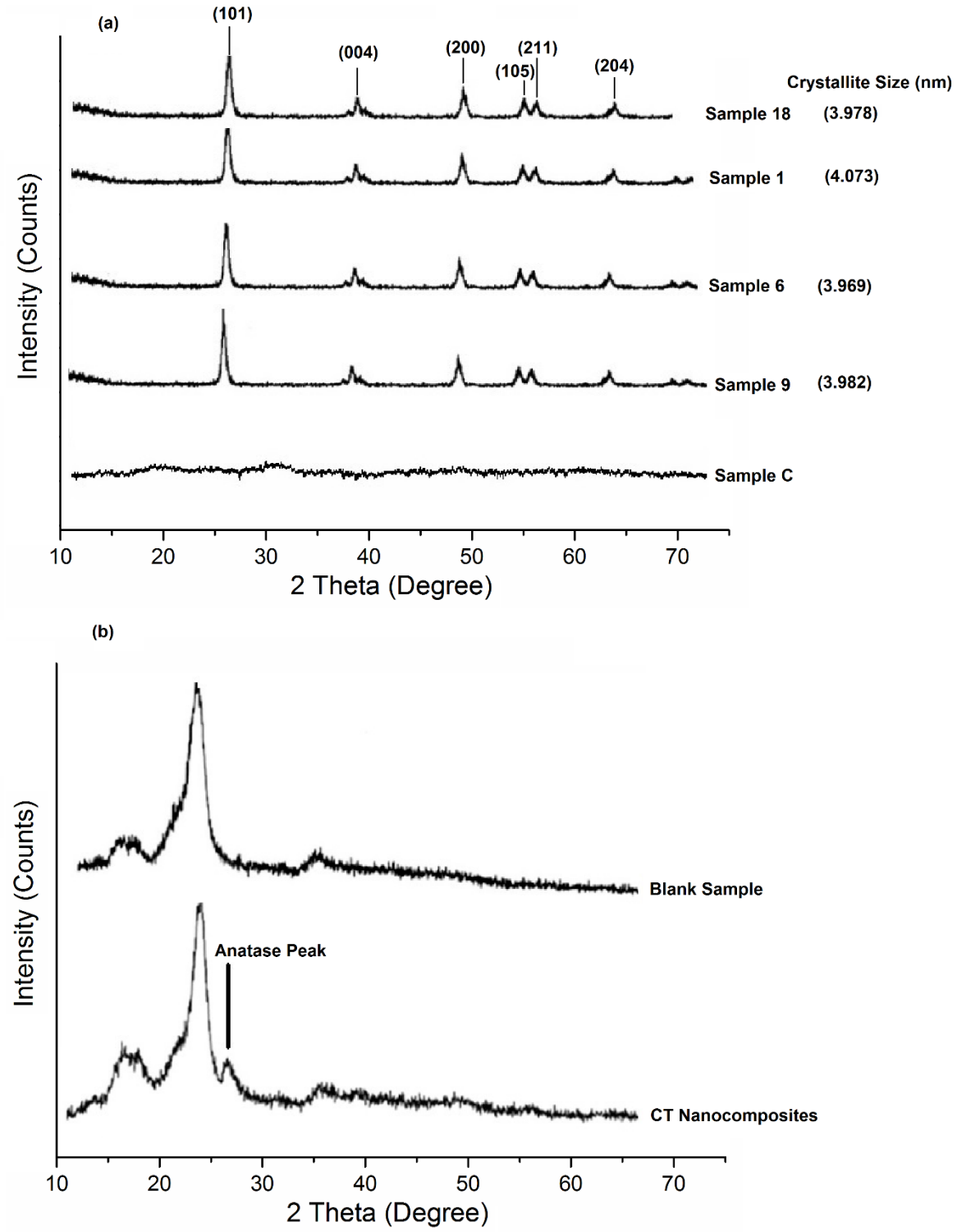

Figure 4-21 XRD pattern for (a) extracted TiO_2 NPs powder (b) blank sample and sample 9.

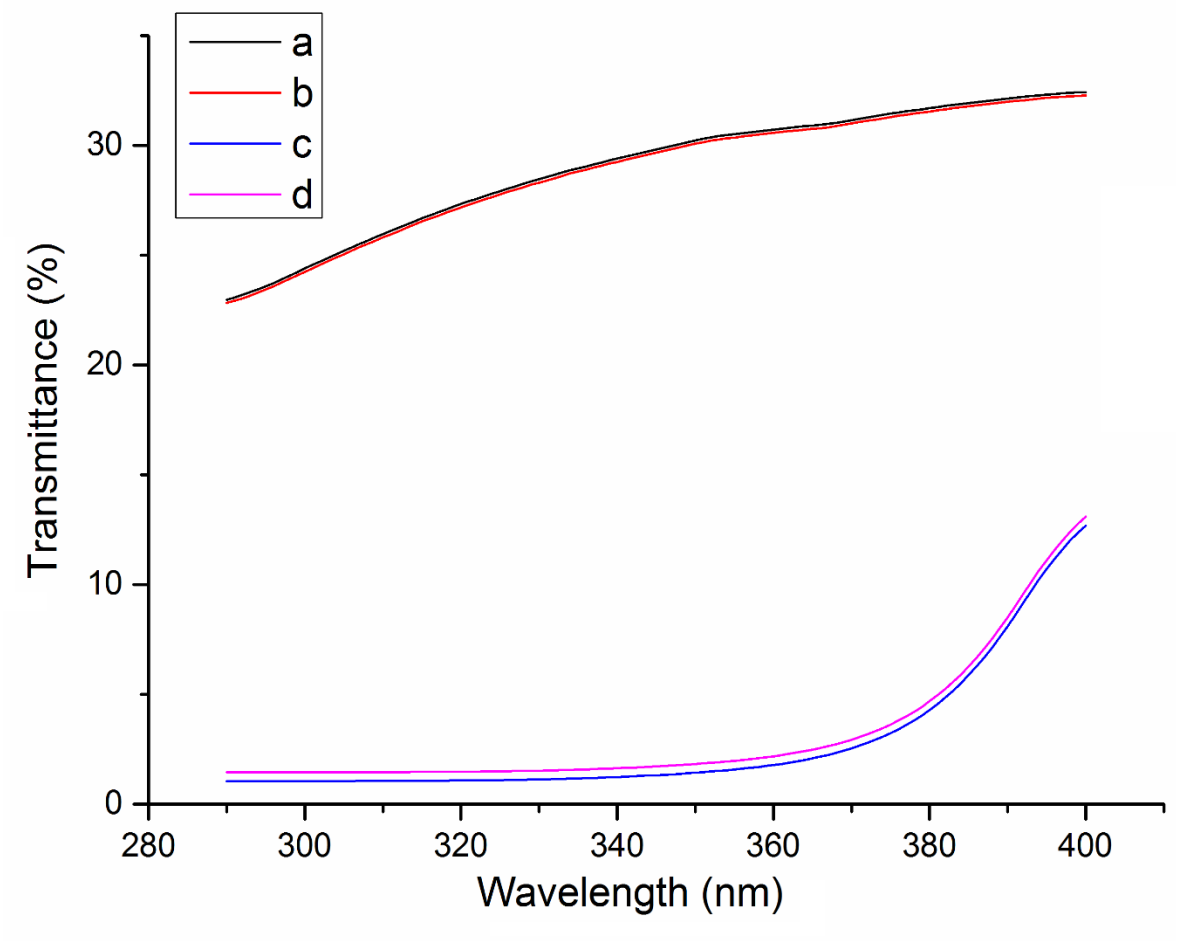

Figure 4-22 UV-Vis spectrum of (a) blank sample before washing (b) blank sample after 30 washing cycles (c) sample 9 before washing (d) sample 9 after 30 washing cycles.

4.3.5 Photocatalytic Activity of the Resulting Solution

The photocatalytic activity of the resulting solution was estimated against discoloration of MB under artificial daylight irradiations. 0.01 % (*w/v*) MB was mixed with the resulting solution containing 1 gL^{-1} TiO_2 NPs and exposed to Xenon lamp with 500 *W* power for 2 *h*. All solutions except solution obtained by sample C exhibited excellent photocatalytic activity as MB discoloured completely after irradiations. However, an incomplete discolouration was

observed in case of sample C as presented in *Figure 4-23*. This result is reasonable because Sample C was prepared by conventional stirring method having amorphous structure confirmed by XRD study. These results are in good agreement with the findings of Kaur et. al. [128].

In order to confirm the MB discolouration was due to the presence of TiO_2 NPs, a controlled 0.01 % solution of MB (without TiO_2 NPs) was exposed to irradiations. This solution showed no change in its colour even after long time of irradiations. It is confirmed through the results that photocatalytic activity of samples 1-20 was due to the presence of TiO_2 NPs induced by Ultrasonic Acoustic Method. The C/C_o plot against irradiation time for the photodegradation of MB is presented in *Figure 4-24*. In controlled sample (without TiO_2 NPs), the concentration of MB is not changed while sample C showed only 40 % change as it is prepared by conventional method. However, all other samples showed noticeable change in MB degradation. Sample 9 and sample 18 showed 100 % MB degradation as illustrated in *Figure 4-24*.

4.3.6 In-situ Synthesis and Deposition of TiO_2 NPs on Cotton

During In-situ process, TiO_2 NPs were synthesized and deposited on cotton by Ultrasonic Acoustic Method according to the following reactions as illustrated in Equations (11-12) [62; 105].

$$TiCl_4 + 4C_3H_7OH \rightarrow Ti(OC_3H_7)_4 + 4HCl \quad [11]$$

$$Ti(OC_3H_7)_4 + 2H_2O \rightarrow TiO_2 + C_3H_7OH \quad [12]$$

In ultrasonic system, an acoustic cavitation phenomenon produce a local hot spot with extreme conditions of temperature and pressure [129]. These conditions generate free $H^{\bullet}$ and $OH^{\bullet}$ radicals [130]. These radicals promote the reaction mechanism and generate TiO_2 NPs at low temperature.

In ultrasonic acoustic synthesis of CT nanocomposites, the process of acoustic cavitation takes place in bulk liquid; between boundary layer of liquid and fabric and inside the yarn [131]. During the ultrasonic irradiations, fluid flow accelerates and leads to a better adsorption of TiO_2 NPs on cotton fabric [132]. Moreover, cotton fibre swelling during ultrasonic irradiations leads to the formation of TiO_2 NPs in intramolecular chain of cotton. TiO_2 NPs have a strong affinity to hydroxyl group of cotton which results in good adhesion of TiO_2 NPs on cotton surface [32].

4.3.7 UPF Efficiency of CT Nanocomposites

The absorption of UV radiations is a natural characteristic of TiO_2. The UPF value directly evaluates the UV absorption efficiency of the synthesized samples. The high UV absorption intensity leads to higher UPF. The results of UPF efficiency are described in ***Table 4-9***. The UPF values of all samples varied from 3 (blank sample) to 63 (sample 9). The results indicate that UPF values are strongly related to TiO_2 content deposited on textile.

4.3.8 Self-cleaning Efficiency of CT Nanocomposites

For self-cleaning evaluation, samples were stained in 0.01 % (*w/v*) solution of MB and colour change was calculated in RGB colour space for all samples after 24 *h* daylight irradiations and presented in ***Table 4-9***. Significant change in colour was observed in case of sample 1-20 as presented in *Figure 4-25*. However, slight colour change was observed for sample C and almost

no change in blank (controlled) sample. In addition, the values of ΔRGB were higher for samples 1-20 as compared to sample C and blank sample. These results indicate the self-cleaning efficiency of CT nanocomposites synthesized by UAM was significantly higher than sample C. The results indicate that ΔRGB values were dependant on ultrasonic irradiation time, TTC and ISP concentrations. Higher colour difference leads to better self-cleaning efficiency that was obtained by sample 9 with optimal conditions as illustrated in ***Table 4-9***.

The content of UV present in sunlight triggers the photocatalytic activity of TiO_2 NPs and decompose MB stains [121]. The significant influence of ultrasonic irradiations on self-cleaning property arises due to the formation of crystalline anatase phase.

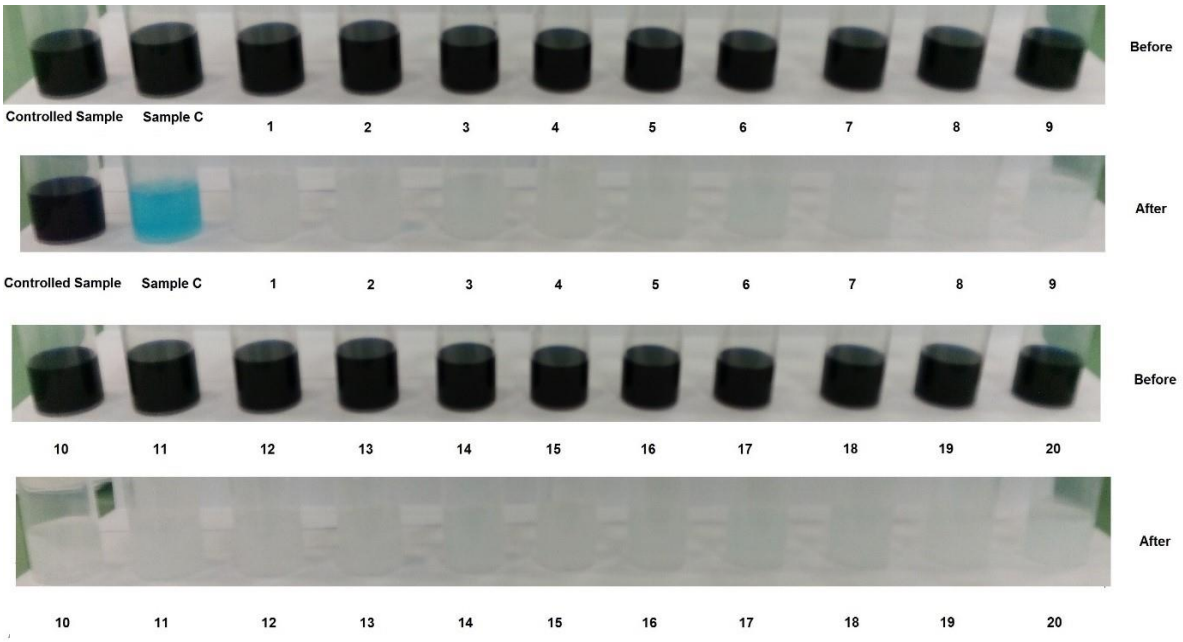

Figure 4-23 Photocatalytic efficiency of the resulting solutions against MB, before and after 2 h irradiations.

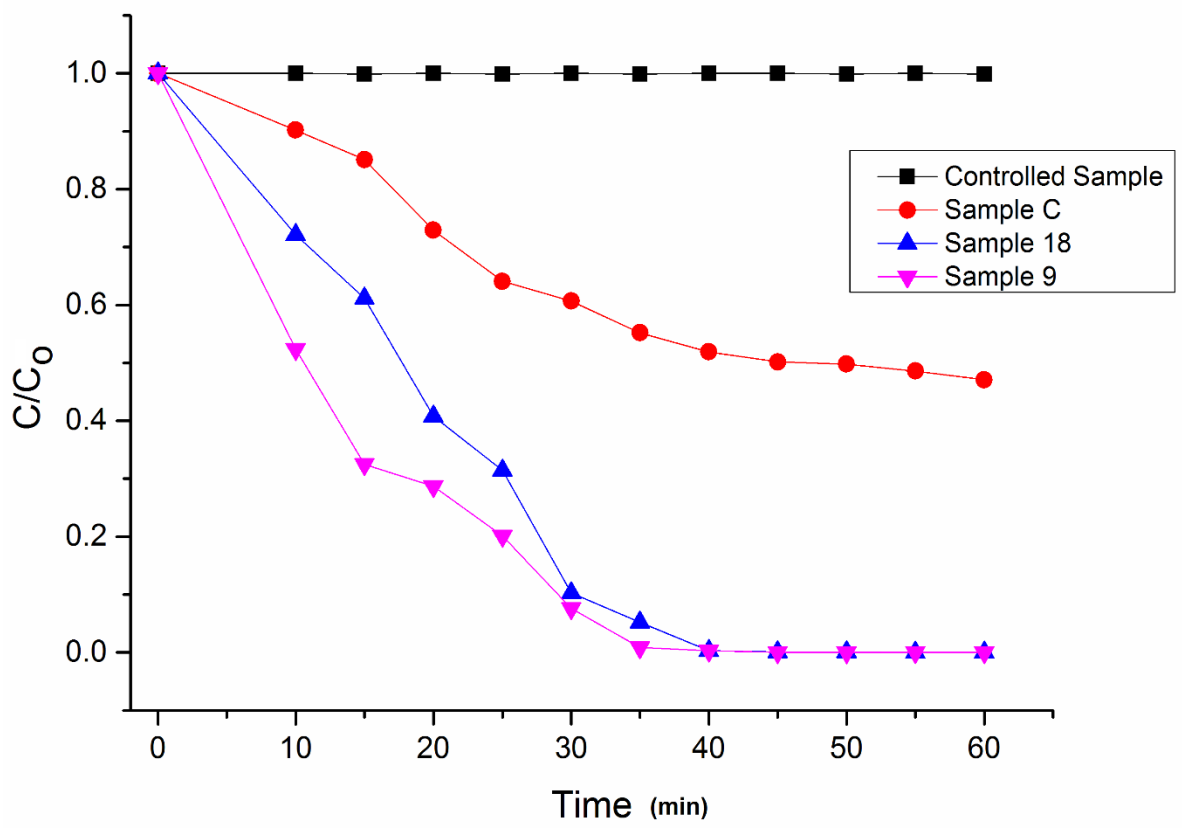

Figure 4-24 Photocatalytic degradation of MB under artificial daylight irradiations. C_o and C are the initial and final concentrations of MB at reaction time.

4.3.9 Antimicrobial Efficiency of CT Nanocomposites

The antimicrobial efficiencies of the developed CT nanocomposites are presented in ***Table 4-9***. Incubation of the blank sample (untreated cotton) did not show any significant effect on bacteria cells viability, even after 24 *h* of incubation. However, significant results were obtained for all other samples. For samples 1, 4, 8 and 18, R% against S. aureus and E. coli after 24 *h* contact time was more than 80 %. However, R% for sample 9 was 99 %. We observed that sample 9 exhibit excellent antimicrobial efficiency as compared to other samples including

sample C. It could be possible that sample 9 possess more amount of TiO_2 NPs as illustrated in ***Table 4-9*** or the larger surface area of NPs on cotton might enhance the contact area between TiO_2 and bacterial cells, which may result in a higher antimicrobial efficiency. Same results were reported by Qi et. al. [48]. Overall, the results showed excellent antimicrobial properties of CT nanocomposites synthesized by Ultrasonic Acoustic Method.

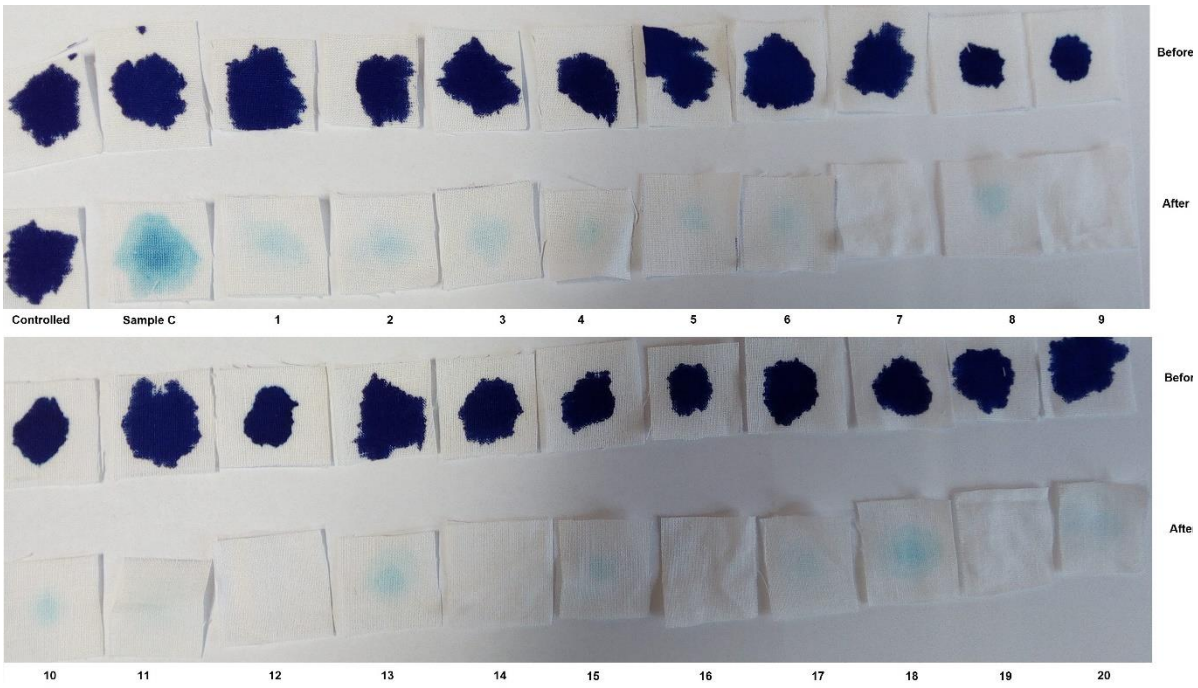

Figure 4-25 Self-cleaning efficiency of CT nanocomposites after 24 h daylight irradiations.

4.3.10 Washing Durability of CT Nanocomposites

Washing effluent analysis was used as a direct approach to evaluate washing durability besides UV-Vis absorption analysis as illustrated in section 4.3.4. This method provides an excellent evaluation of washing durability. In a typical process, the total amount of TiO_2 NPs present in the effluent was considered as durability against washing. Higher concentration of TiO_2 NPs in effluent indicates lower durability [33]. So, the effluents were evaluated by spectrophotometer

during 30 consecutive home launderings. An absorption peak at 280 *nm* during initial washing cycle indicating the presence of TiO_2 NPs as presented in *Figure 4-26* [133]. It can be possible that some of the physically attached unstable NPs were migrated into effluents during primary washing [122]. The results confirmed that no absorption peak was observed during subsequent washing cycles showing the absence of TiO_2 NPs in washing effluents. Moreover, the results show that TiO_2 NPs are strongly attached to cotton fibres. The good washing durability indicating the formation of covalent bond between TiO_2 NPs and cotton fibre [31; 123]. TiO_2 NPs have strong affinity towards carboxyl and hydroxyl groups [30; 123]. The bonding between TiO_2 NPs and hydroxyl groups present in cotton play a significant role in washing durability.

4.3.11 Tensile Strength of CT Nanocomposites

The results regarding breaking force for untreated cotton (blank sample) and sample 9 were 511 *N* and 497 *N* with standard deviation of 2.1 and 2.4 respectively. The results of breaking force for sample 9 were almost same with blank sample. This shows that the experimental conditions and ultrasonic irradiations did not damage the structure of cotton fibre to a significant level. The slight difference in sample 9 could be due to cleavage of cellulosic chain or by ultrasonic irradiations [86]. The results indicate that synthesis and deposition of TiO_2 NPs on cotton by Ultrasonic Acoustic Method have no significant damage effect to cotton fibre structure.

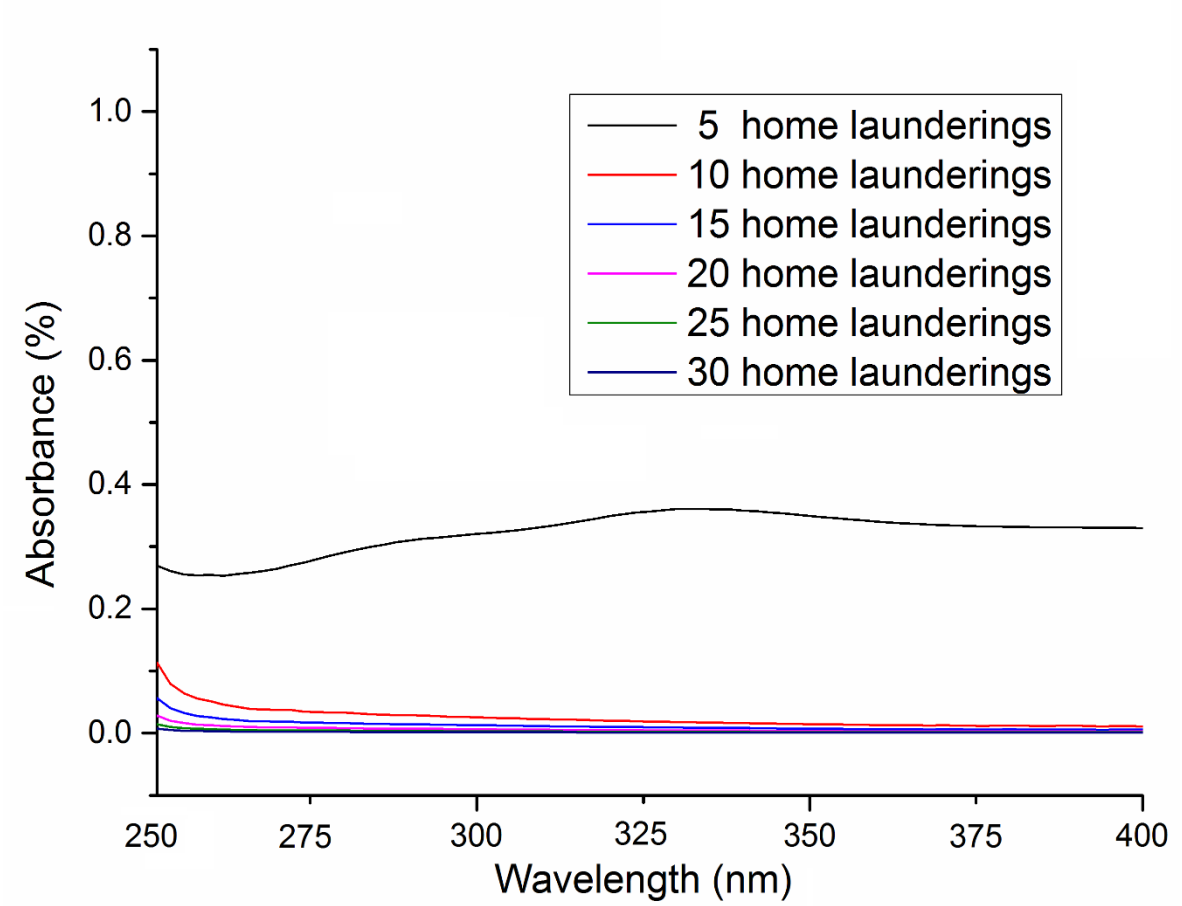

Figure 4-26 Washing effluent absorbance spectra of sample 9 after different washing cycles.

4.3.12 Statistical Analysis of CT Nanocomposites

The experimental design with different amount of TTC and ISP under varying sonication time based on the actual values of CCD for CT nanocomposites as well as sample C and blank sample (untreated cotton) is shown in ***Table 4-9***. The responses of the variables including: Y_3=Synthesized and deposited amount of TiO_2 NPs on cotton fabric; Y_4=UPF of the CT nanocomposites; Y_5=Self-cleaning efficiency after 24 h irradiations; Y_6=Antimicrobial efficiency of the CT nanocomposites, were adjusted by Equation 1.

Table 4-9 The 3-factors CCD matrix based on actual values for experimental variables and responses, Y_3=Synthesized & loaded amount of TiO_2 NPs on cotton fabric, Y_4=UPF efficiency of CT nanocomposites, Y_5=Self-cleaning efficiency of CT nanocomposites, Y_6=Antimicrobial efficiency of CT nanocomposites

Sample Name	TTC [*mL*]	ISP [*mL*]	Sonication time [*h*]	Y_3=Synthesized & loaded TiO_2 [*ppm*]	Y_4=UPF Efficiency [-]	Y_5=Self-cleaning Efficiency [-]	Y_6=Antimicrobial Efficiency [%]
Blank Sample	0	0	0	0	3	6	5
Sample C	10	6	0	411	38	61	73
1	6	4	2	830	43	83	85
2	6	4	4	839	45	85	81
3	4	2	1	749	37	70	76
4	6	4	0.25	645	44	84	85
5	6	4	2	820	43	80	80
6	6	8	2	543	40	77	79
7	8	2	3	860	47	84	83
8	8	6	1	986	50	87	87
9	10	6	2	1587	63	99	99
10	6	0.5	2	288	27	64	65
11	6	4	2	800	42	79	80
12	6	4	2	825	43	80	79
13	6	4	2	765	42	79	78
14	4	2	3	510	32	69	68
15	4	4	3	524	34	71	72
16	8	2	1	590	41	78	79
17	6	4	2	815	45	82	83
18	8	6	3	1298	58	95	94
19	4	6	1	485	37	74	73
20	2	4	2	501	25	62	65

In total, 20 samples based on CCD were developed as shown in ***Table 4-9***. The obtained responses including Y_3: Synthesized & loaded amount of TiO_2 NPs on cotton fabric, Y_4: UPF efficiency of developed CT nanocomposites, Y_5: Self-cleaning efficiency of developed CT nanocomposites, Y_6: Antimicrobial efficiency of developed CT nanocomposites, were evaluated and discussed.

For the evaluation of obtained results and the relationship between independent variables and response surfaces, several mathematical models (Equations 13-16) were established. In order to predict the responses for a given amount or value of TTC and ISP and/or ultrasonic irradiation time, these models could be useful and further utilised. In *Figure 4-27* to *Figure 4-30*, contour and response surface plots were drawn based on the mathematical models.

Statistical analysis (ANOVA) was conducted to evaluate the interaction between the variables and the responses of the designed samples 1-20 and presented in ***Table 4-10*** to ***Table 4-13***. Goodness of fit was evaluated on the basis of responses analysed by analysis of variance ANOVA. The lack of fit explains the data variations close to the fitted model and will be significant if the proposed model unable to fit the data well. The results indicate that the designed model for the synthesized and deposited amount of TiO_2 NPs on cotton is statistically significant at F-value 103.6 and p-value <0.0001 as presented in ***Table 4-10***. In addition, the developed model for UPF efficiency of the developed CT nanocomposites is significant at F-value 55 and p-value <0.0001 as presented in ***Table 4-11***. Moreover, the developed model for self-cleaning efficiency and antimicrobial efficiency of the developed CT nanocomposites were significant at F-value of 65.1 and 25.1 and p-value of <0.0001 and <0.0001 respectively as presented in ***Table 4-12*** and ***Table 4-13***.

R-squared coefficient was used to evaluate the fit of the developed models. The results presented in ***Table 4-10*** indicate that only 1.06 % of the total variables cannot be explained through this model for synthesized and deposited amount of TiO_2 NPs on cotton fabric [118; 119; 134]. Moreover, the results of R-squared for UPF, self-cleaning and antimicrobial efficiencies of the developed CT nanocomposites indicate that only 1.98 %, 1.68 % and 4.23 % of the total variables cannot be explained by the model respectively (***Table 4-11*** to ***Table 4-13***).

The synthesized and deposited amount of TiO_2 NPs on cotton according to the developed model is calculated by Equation 13:

$$Y_3 = 1442.3 - 253.8(TTC) + 4.0(ISP) - 298.5(Time) + 37.7(TTC * ISP) + 59.1(TTC * Time) + 10.7(ISP * Time) + 7.2(TTC)^2 - 26.9(ISP)^2 - 14.8(Time)^2 \quad [13]$$

The UPF efficiency of the developed CT nanocomposites is calculated by Equation 14:

$$Y_4 = 36.6 - 0.7(TTC) + 2.6(ISP) - 11.4(Time) + 0.6(TTC * ISP) + 1.4(TTC * Time) + 0.09(ISP * Time) - 0.07(TTC)^2 - 0.6(ISP)^2 + 0.6(Time)^2 \quad [14]$$

The self-cleaning efficiency of the developed CT nanocomposites is calculated by Equation 15:

$$Y_5 = 62.1 + 1.2(TTC) + 4.7(ISP) - 10.8(Time) + 0.4(TTC * ISP) + 1.2(TTC * Time) - 0.05(ISP * Time) - 0.1(TTC)^2 - 0.7(ISP)^2 + 1.1(Time)^2 \quad [15]$$

The antimicrobial efficiency is of the developed CT nanocomposites is calculated by Equation 16:

$$Y_6 = 78.0 - 0.4(TTC) + 1.9(ISP) - 12.9(Time) + 0.6(TTC * ISP) + 1.2(TTC * Time) + 0.5(ISP * Time) - 0.09(TTC)^2 - 0.6(ISP)^2 + 0.6(Time)^2 \quad [16]$$

According to the above equations and obtained results (***Table 4-9***), the optimal points for best possible results are 10 *mL* TTC, 6 *mL* ISP and 2 *h* ultrasonic irradiation time. The predicted response values for optimal conditions (Sample 9) are 1600, 63, 99 and 99 for Y_3, Y_4, Y_5 and Y_6 respectively.

The response surfaces and contour plots are illustrated in *Figure 4-27* to *Figure 4-30* for synthesized and deposited amount of TiO_2 NPs on cotton, UPF, self-cleaning and antimicrobial efficiencies of the developed CT nanocomposites respectively. It can be seen in *Figure 4-27* to *Figure 4-30* that increasing the TTC amount results in more increment in synthesized and deposited amount of TiO_2 NPs on cotton as well as other functional properties. Moreover, increasing ISP led to a higher deposition of TiO_2 NPs on cotton. In addition, with optimal TTC and ISP concentrations, prolonged ultrasonic irradiation time leads to a lower deposition of TiO_2 NPs on cotton. This is because cotton fibre provides limited surface for adsorption to TiO_2 NPs after a certain ultrasonic irradiation time. After a certain time, some of the aggregated particles were removed from cotton surface by bubble collapse but some particles penetrated deeply in the fibre and strongly attached to them. More TTC and ISP amount with a controlled irradiation time lead to more deposition of TiO_2 NPs on cotton and vice versa. Thus, the

synthesized and deposited amount of TiO_2 NPs on cotton depends on precursor concentration and ultrasonic irradiation time. These results are supported by Perelshtein et al. [86]. The functional properties i.e. UPF, self-cleaning and antimicrobial efficiencies of the developed CT nanocomposites depend on the deposition of TiO_2 NPs on cotton. These results are similar to the observations reported by Nazari et al. and Montazer et al. [126; 135].

Table 4-10 ANOVA results for synthesized and deposited amount of TiO_2 NPs on cotton fabric

Source	Sum of Squares	df	Mean Square	F Value	p-value Prob > F	Remarks
Model	1613611	9	179290	103.6	< 0.0001	Significant
A-TTC	596350	1	596350	344.8	< 0.0001	Significant
B-ISP	68037.9	1	68037.9	39.3	< 0.0001	Significant
C-Sonication Time	22931.5	1	22931.5	13.2	0.004	Significant
AB	173460	1	173460	100.2	< 0.0001	Significant
AC	104852	1	104852	60.6	< 0.0001	Significant
BC	2902.06	1	2902.06	1.6	0.224	Not significant
A^2	18357.3	1	18357.3	10.6	0.008	Significant
B^2	233198	1	233198	134.8	< 0.0001	Significant
C^2	4453.5	1	4453.5	2.5	0.139	Not significant
Residual	17294.6	10	1729.4			
Lack of Fit	14423.7	5	2884.7	5.02	0.0505	Not significant
Pure Error	2870.8	5	574.1			
Cor Total	1630906	19				

R-squared: 0.9894, adjusted R-squared: 0.9799, CV%: 5.45

Table 4-11 ANOVA results for UPF efficiency of the developed CT nanocomposites

Source	Sum of Squares	df	Mean Square	F Value	p-value Prob > F	Remarks
Model	1513.2	9	168.139	55	< 0.0001	Significant
A-TTC	832.1	1	832.1	272.4	< 0.0001	Significant
B-ISP	133.6	1	133.6	43.7	< 0.0001	Significant
C-Sonication Time	1.4	1	1.4	0.5	0.502	Not significant
AB	50.1	1	50.1	16.4	0.002	Significant
AC	65.8	1	65.8	21.5	0.0009	Significant
BC	0.2	1	0.2	0.07	0.796	Not significant
A^2	2.07	1	2.07	0.6	0.429	Not significant
B^2	130.8	1	130.8	42.8	< 0.0001	Significant
C^2	7.6	1	7.6	2.5	0.144	Not significant
Residual	30.5	10	30.5			
Lack of Fit	24.5	5	4.9	4.09	0.074	Not significant
Pure Error	6	5	1.2			
Cor Total	1543.8	19				

R-squared: 0.9802, adjusted R-squared: 0.9624, CV%: 4.17

4.3.13 Reusability and Sequential Application of CT Nanocomposites

Reusability of a catalyst is a significantly important property for application point of view. The reusability of the developed CT nanocomposites was estimated by repeating their application in the photocatalytic removal of MB. The experiment was repeated for seven cycles. In each cycle, a piece of sample 9 was immersed in an aliquot of fresh MB solution. As shown in *Figure 4-31*, after 7 reuse cycles, the removal rate of MB had lost only 7.5 % for sample 9

which was developed with optimal conditions. The results confirmed that the developed CT nanocomposites are very stable and reusable as a catalyst.

The behaviour of MB under different conditions i.e. in the presence of dark; in the presence of light only; in the presence of TiO_2 only; and in the presence of TiO_2 and light has also been evaluated and the results are presented in *Figure 4-32*. Under dark conditions and in the absence of TiO_2, the MB colour remained unchanged, while with TiO_2, only 8 % change in MB colour was found. Whereas 99.6 % results were obtained with TiO_2 under light.

Table 4-12 ANOVA results for self-cleaning efficiency of the developed CT nanocomposites

Source	Sum of Squares	df	Mean Square	F Value	p-value Prob > F	Remarks
Model	1594.6	9	177.2	65.1	< 0.0001	Significant
A-TTC	884.2	1	884.2	325.2	< 0.0001	Significant
B-ISP	172.9	1	172.9	63.6	< 0.0001	Significant
C-Sonication Time	4.7	1	4.7	1.7	0.216	Not significant
AB	28.6	1	28.6	10.5	0.008	Significant
AC	43.4	1	43.4	15.9	0.002	Significant
BC	0.08	1	0.08	0.02	0.866	Not significant
A^2	6.6	1	6.6	2.4	0.149	Not significant
B^2	163.6	1	163.6	60.1	< 0.0001	Significant
C^2	24.9	1	24.9	9.1	0.0127	Significant
Residual	27.2	10	27.2			
Lack of Fit	13.6	5	2.7	1.01	0.494	Not significant
Pure Error	13.5	5	2.7			
Cor Total	1621.8	19				

R-squared: 0.9832, adjusted R-squared: 0.9681, CV%: 2.08

Table 4-13 ANOVA results for antimicrobial efficiency of the developed CT nanocomposites

Source	Sum of Squares	df	Mean Square	F Value	p-value Prob > F	Remarks
Model	1341.6	9	149	25.1	< 0.0001	Significant
A-TTC	691.1	1	691.1	116.5	< 0.0001	Significant
B-ISP	139.5	1	139.5	23.5	0.0007	Significant
C-Sonication Time	3.3	1	3.3	0.5	0.4705	Not significant
AB	45.1	1	45.1	7.6	0.0201	Significant
AC	49.6	1	49.6	8.3	0.016	Significant
BC	7.2	1	7.2	1.2	0.296	Not significant
A^2	2.9	1	2.9	0.4	0.498	Not significant
B^2	126.6	1	126.6	21.3	0.0009	Significant
C^2	8.2	1	8.2	1.3	0.265	Not significant
Residual	59.2	10	59.2			
Lack of Fit	24.4	5	4.8	0.70198	0.646	Not significant
Pure Error	34.8	5	6.9			
Cor Total	1400.9	19				

R-squared: 0.9577, adjusted R-squared: 0.9196, CV%: 3.06

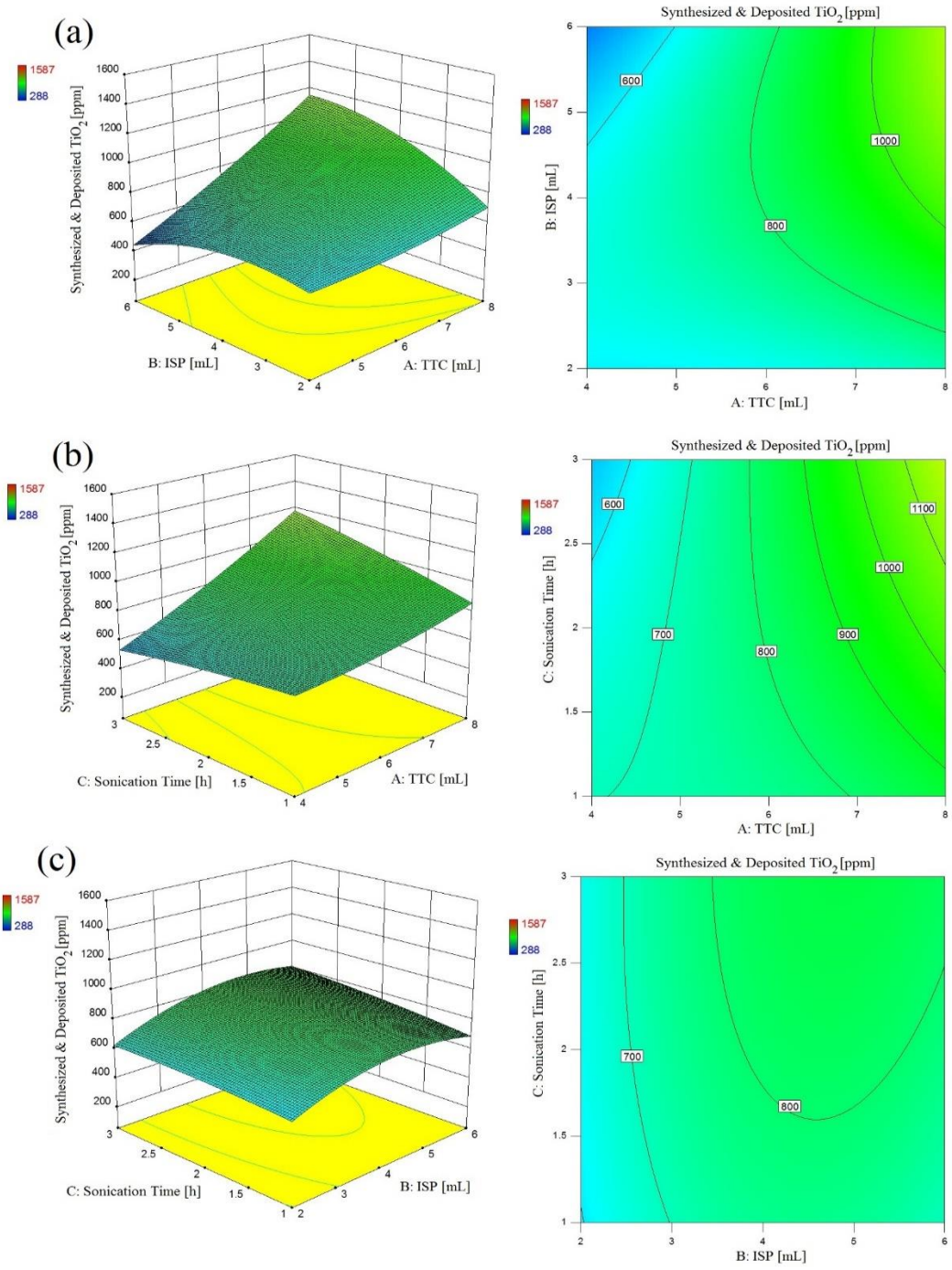

Figure 4-27 Response surfaces and contour plots for synthesized and deposited amount of TiO_2 NPs on cotton as a function of (a) TTC conc., ISP conc., (b) TTC conc., Sonication time, (c) ISP conc., Sonication time.

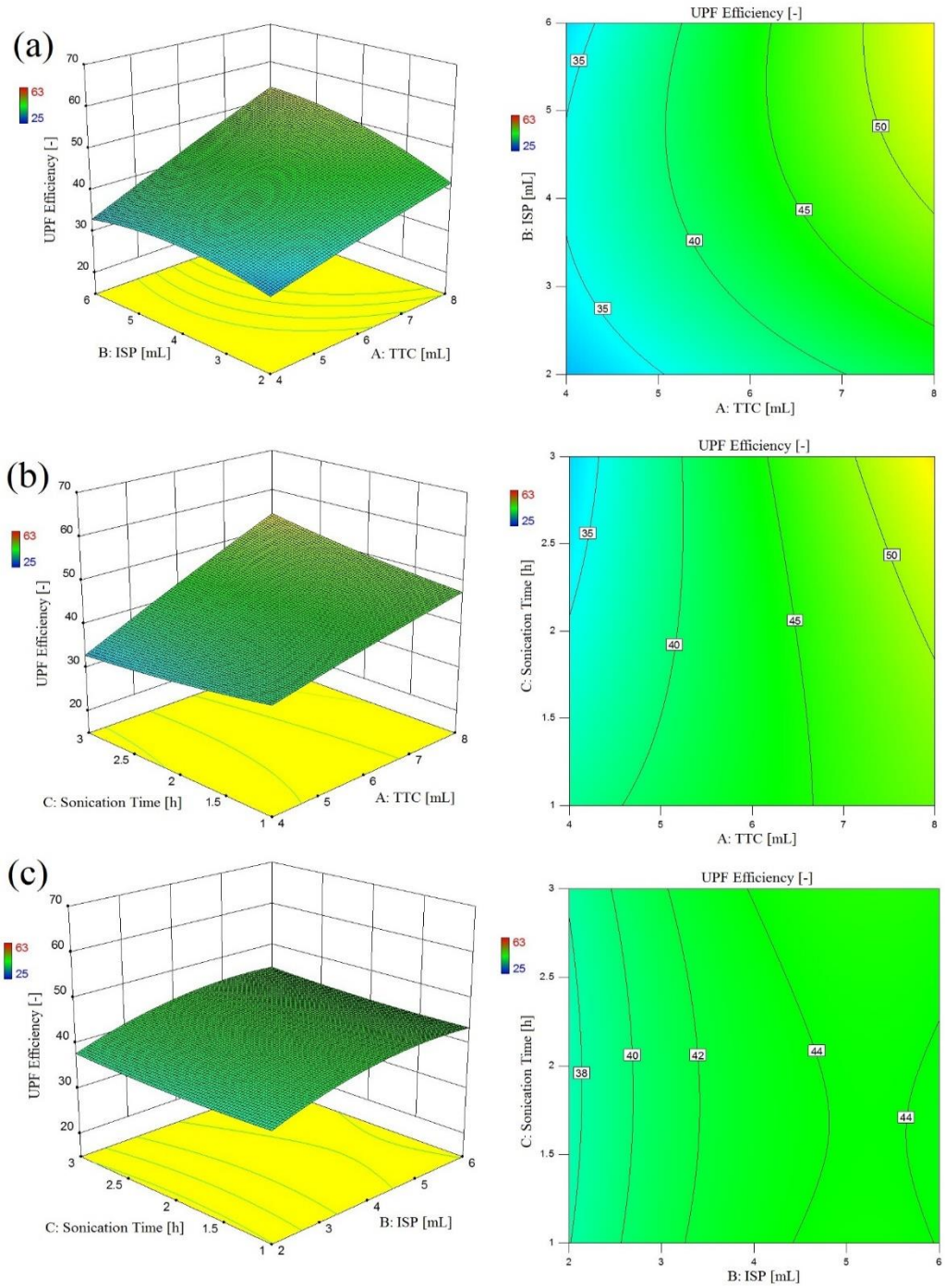

Figure 4-28 Response surfaces and contour plots for UPF efficiency of developed CT nanocomposites as a function of (a) TTC conc., ISP conc., (b) TTC conc., Sonication time, (c) ISP conc., Sonication time.

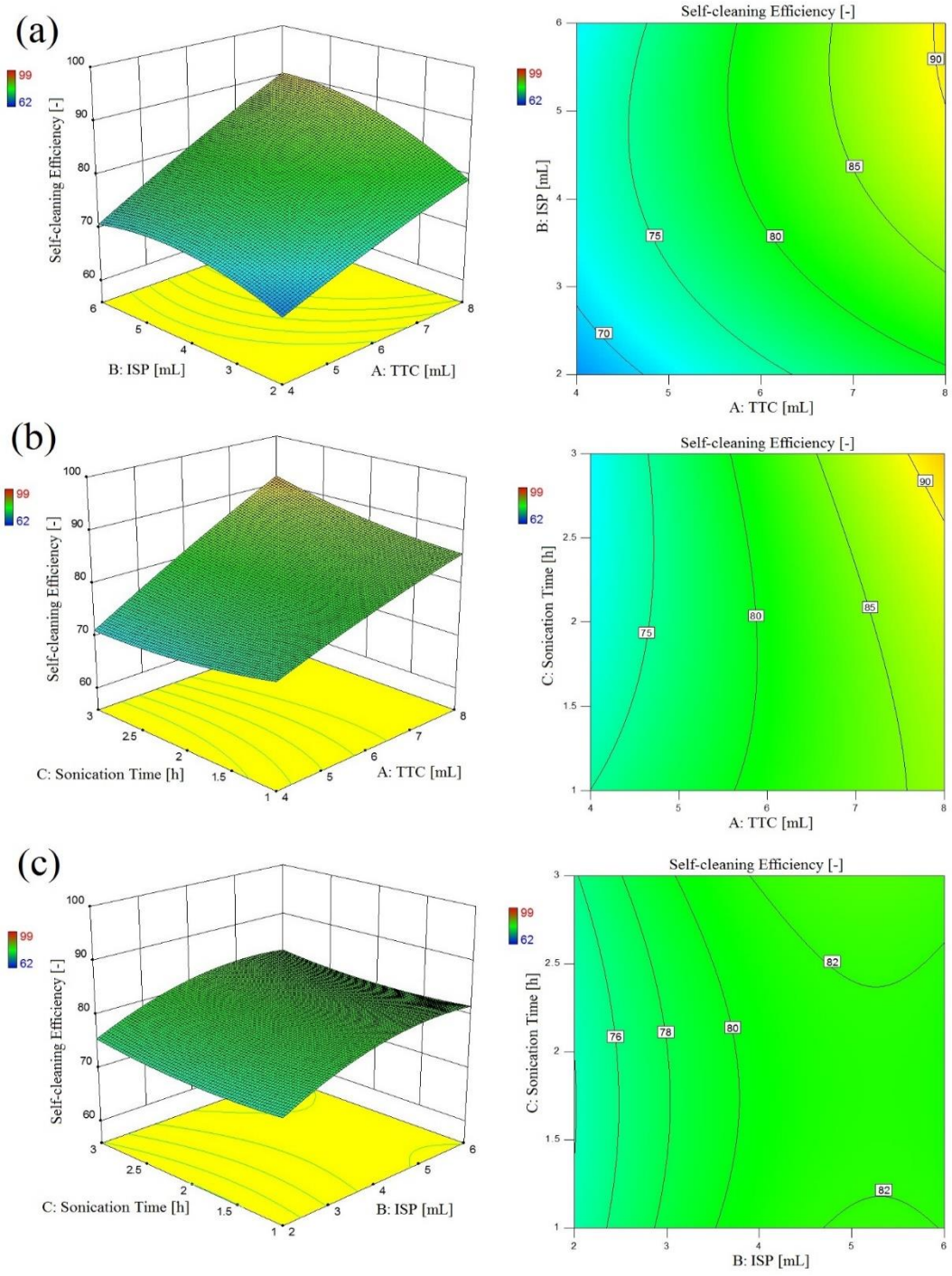

Figure 4-29 Response surfaces and contour plots for self-cleaning efficiency of developed CT nanocomposites as a function of (a) TTC conc., ISP conc., (b) TTC conc., Sonication time, (c) ISP conc., Sonication time.

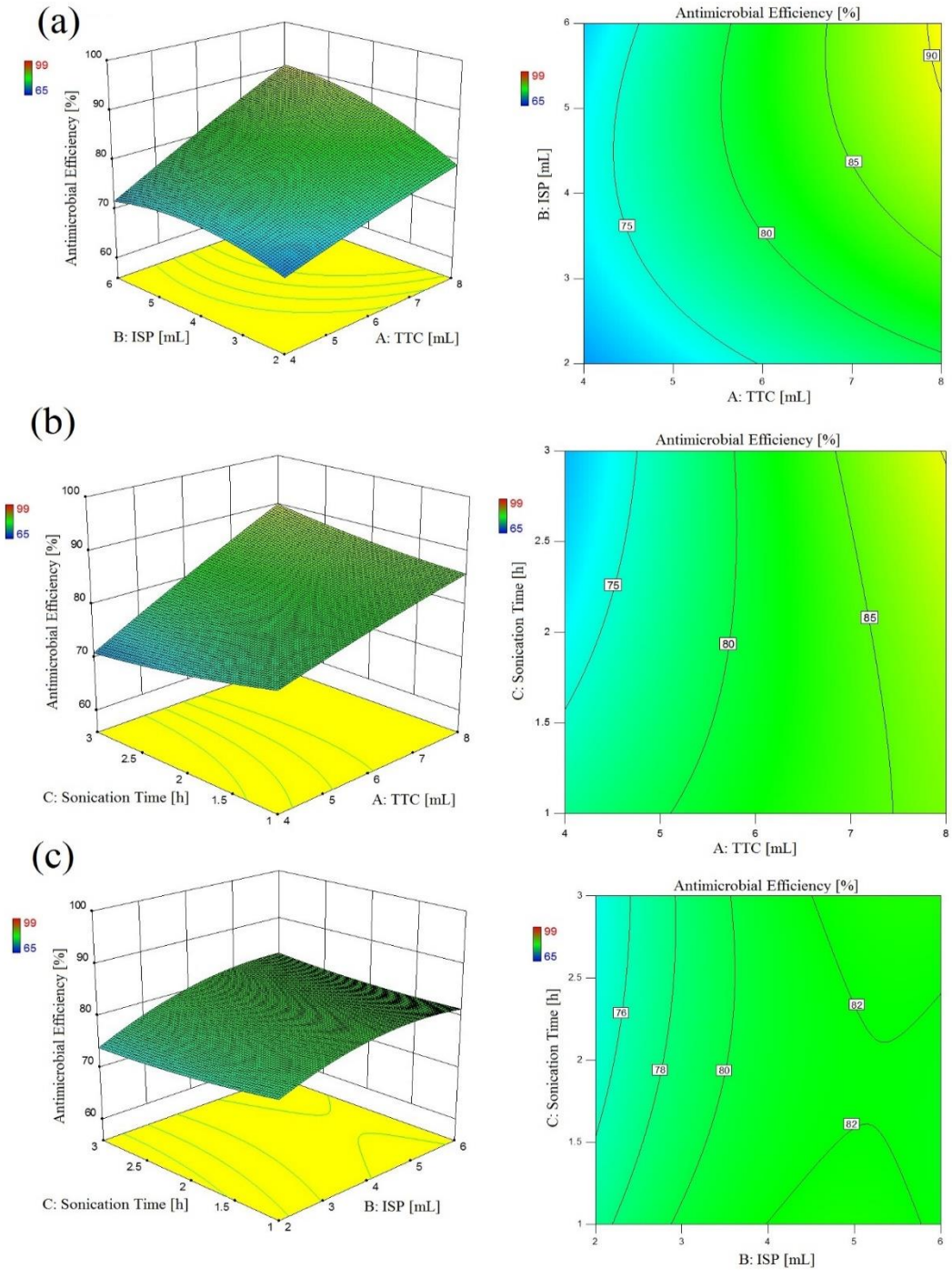

Figure 4-30 Response surfaces and contour plots for antimicrobial efficiency of developed CT nanocomposites as a function of (a) TTC conc., ISP conc., (b) TTC conc., Sonication time, (c) ISP conc., Sonication time.

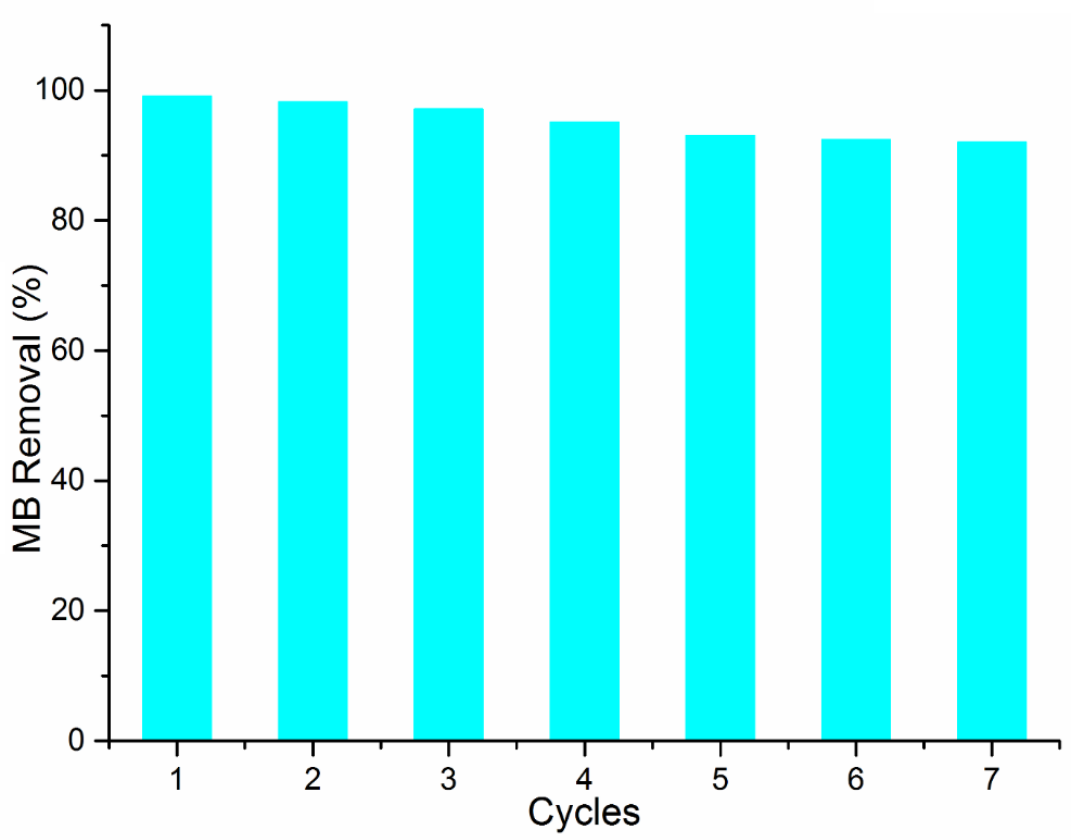

Figure 4-31 Reusability of the developed CT nanocomposites.

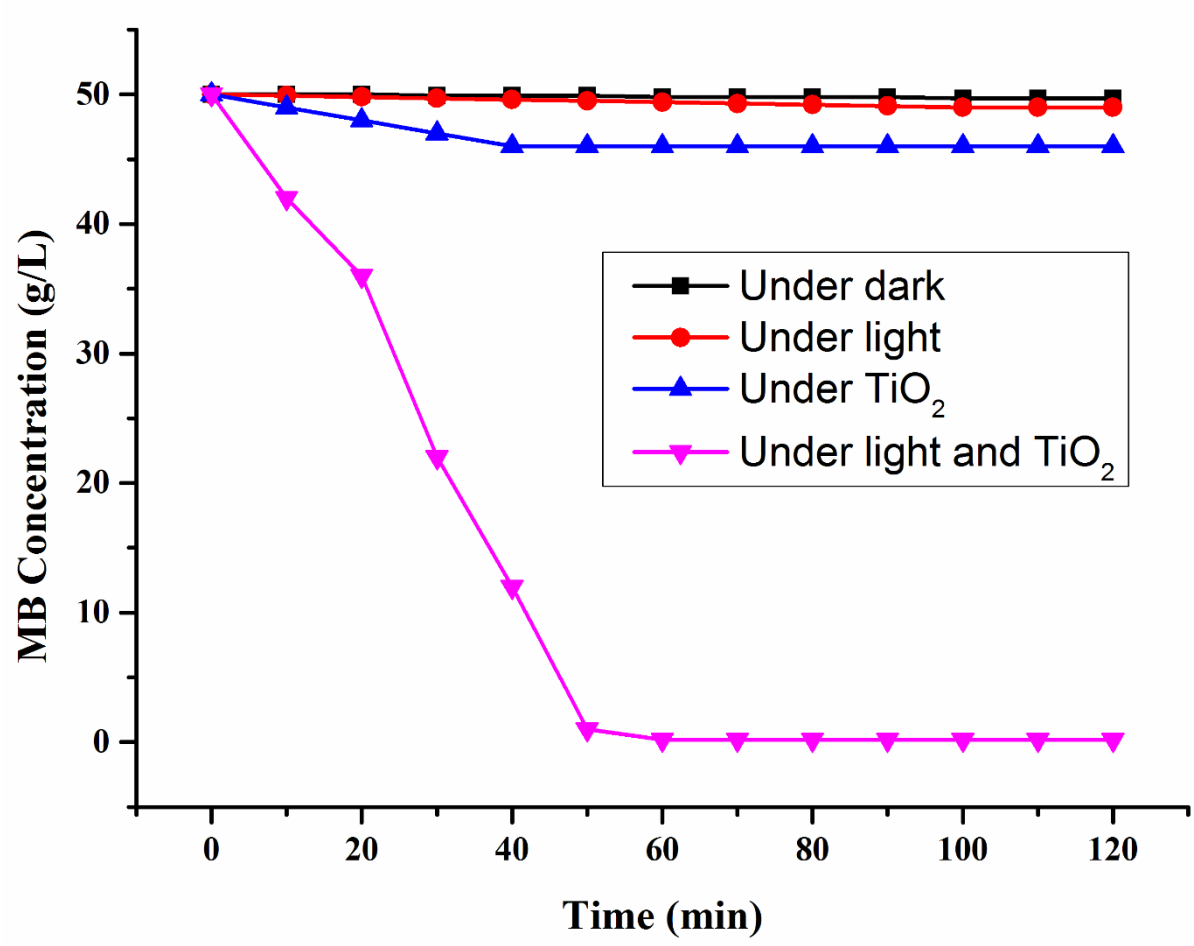

Figure 4-32 Behaviour of MB degradation under different conditions i.e. Under dark; Under light; Under TiO_2; Under light and TiO_2.

Chapter 5

5 Summary of the Results

The overall summary of this dissertation comprises the conclusion of the obtained results and the recommendations for future work.

5.1 Conclusion

After a comprehensive introduction and discussion about the related work, **Chapter 3** explained the bulk of the work deriving important materials and used methods. The data was further used in **Chapter 4** to perform chemical analysis and statistical calculations.

TiO_2 NPs (RNP) with pure anatase form were successfully synthesized by Ultrasonic Acoustic Method (UAM) using TTIP and EG as synthesis variables. The RNP were found to be more photoactive than commercially available photo catalyst P25. The average particle size for RNP was relatively small as compared to P25. The photo degradation of MB dye showed excellent dye removal ability for the RNP. The role of ultrasonic irradiations time and precursors concentration was very crucial in order to synthesize highly crystalline NPs with smaller particle and higher photocatalytic activity. The use of EG suppressed the crystal growth as well as anatase-rutile phase transformation. Self-cleaning of cotton fabrics recommends the potential use of RNP in textile industry. Reusability of the RNP confirmed their durability during photocatalytic processes. The RNP could be further utilized in many other textile applications.

In another experiment, the developed TiO_2 NPs were successfully embedded on cotton fabric by UV light. SEM, EDX and ICP-AES analysis confirmed the deposition of TiO_2 NPs on cotton. Higher incorporated amount of TiO_2 NPs onto cotton led to higher self-cleaning

efficiency. Washing and leaching durability of UV treated samples (samples 1 to 20) confirmed the role of UV light irradiations for the stabilization of TiO_2 NPs onto cotton through covalent bonding. Moreover, almost similar tensile strength of untreated samples and samples 1 to 20 verified the fitting of the used method. Statistical analysis confirmed that the obtained results solely rely on TiO_2 dosage, temperature and UV irradiations time. Optimal conditions for obtaining best possible results were attained by using 8 gL^{-1} TiO_2, 60 $^{\circ}C$ temperature and 120 *min* UV irradiations time.

In another study, an in-situ Ultrasonic Acoustic Method is developed to simultaneously synthesize and deposit TiO_2 NPs on cotton fabric in a single step. Pure anatase crystals were detected on XRD analysis indicating the crucial effects of ultrasonic irradiations at low temperature (70 $^{\circ}C$) synthesis. In addition, more amount of TTC and prolonged sonication time led to more crystals of TiO_2. SEM, EDX and ICP-AES analysis confirmed the presence of TiO_2 NPs on cotton. The deposited particles on cotton fabric possessed pure anatase crystals with average size 4 *nm* as confirmed by XRD analysis. High amount of TiO_2 NPs deposited on cotton led to higher functional properties such as UPF, self-cleaning and antimicrobial properties. Washing durability of the ultrasonic irradiated samples confirmed the role of acoustic cavitation and covalent bonding between TiO_2 and hydroxyl groups of cotton. Moreover, ultrasonic irradiations had no negative effect on the tensile strength of the developed CT nanocomposites verifying the fitting of the used method. Statistical analysis confirmed that the obtained results solely relied on TTC concentration, ultrasonic irradiation time and ISP amount. The optimal conditions for obtaining the best results were obtained by using 10 *mL* TTC, 6 *mL* ISP and 2 *h* ultrasonic irradiation time.

5.2 Follow-up Work

Working on this dissertation has uncovered many worthy avenues for future investigations. The inquisitive readers will no-doubt have ideas of their own, but there are some suggestions for research of possible interest:

- Synthesis of other metal oxides nanoparticles e.g. Fe, Zn, Cu, Ag, Au etc. through Ultrasonic Acoustic Method (UAM).

- Some other polymeric textile fibres i.e. polypropylene, polyester, polyamide can be utilized to make nanocomposites through UAM that can be more beneficial to investigate the effects of ultrasonic irradiations on different textile substrates.

6 References

1. DREXLER, K. E. Molecular directions in nanotechnology. *Nanotechnology*, 1991, **2** (3), 113.

2. DREXLER, K. E. Molecular tip arrays for molecular imaging and nanofabrication. *Journal of Vacuum Science & Technology B: Microelectronics and Nanometer Structures Processing, Measurement, and Phenomena*, 1991, **9** (2), 1394-1397.

3. ATES, M. Graphene and its nanocomposites used as an active materials for supercapacitors. *Journal of Solid State Electrochemistry*, 2016, **20** (6), 1509-1526.

4. BOGART, L. K., G. POURROY, C. J. MURPHY, V. PUNTES, T. PELLEGRINO, D. ROSENBLUM, D. PEER and R. LÉVY. Nanoparticles for imaging, sensing, and therapeutic intervention. *ACS Nano*, 2014, **8** (4), 3107-3122.

5. CAI, P., W. R. LEOW, X. WANG, Y. L. WU and X. CHEN. Programmable Nano-Bio Interfaces for Functional Biointegrated Devices. *Advanced Materials*, 2017, **29** (26), 1-26.

6. NOUR, E., A. BONDAREVS, P. HUSS, M. SANDBERG, S. GONG, M. WILLANDER and O. NUR. Low-frequency self-powered footstep sensor based on ZnO nanowires on paper substrate. *Nanoscale Research Letters*, 2016, **11** (1), 1-7.

7. OELHAFEN, P. and A. SCHÜLER. Nanostructured materials for solar energy conversion. *Solar Energy*, 2005, **79** (2), 110-121.

8. SAWHNEY, A., B. CONDON, K. SINGH, S. PANG, G. LI and D. HUI. Modern applications of nanotechnology in textiles. *Textile Research Journal*, 2008, **78** (8), 731-739.

9. SOLANKI, A., J. D. KIM and K.-B. LEE. Nanotechnology for regenerative medicine: nanomaterials for stem cell imaging. *Nanomedicine,* 2008, **3** (4), 567-578.

10. WANG, L., Q. XIONG, F. XIAO and H. DUAN. 2D nanomaterials based electrochemical biosensors for cancer diagnosis. *Biosensors and Bioelectronics,* 2017, **89**, 136-151.

11. WHITESIDES, G. M. Nanoscience, nanotechnology, and chemistry. *Small,* 2005, **1** (2), 172-179.

12. YIN, J. and B. DENG. Polymer-matrix nanocomposite membranes for water treatment. *Journal of Membrane Science,* 2015, **479**, 256-275.

13. DREXLER, K. E. Nanotechnology: from Feynman to funding. *Bulletin of Science, Technology & Society,* 2004, **24** (1), 21-27.

14. ASAHI, R., T. MORIKAWA, H. IRIE and T. OHWAKI. Nitrogen-doped titanium dioxide as visible-light-sensitive photocatalyst: designs, developments, and prospects. *Chemical Reviews,* 2014, **114** (19), 9824-9852.

15. BAI, J. and B. ZHOU. Titanium dioxide nanomaterials for sensor applications. *Chemical Reviews,* 2014, **114** (19), 10131-10176.

16. COPPENS, P., Y. CHEN and E. B. TRZOP. Crystallography and properties of polyoxotitanate nanoclusters. *Chemical Reviews,* 2014, **114** (19), 9645-9661.

17. DAHL, M., Y. LIU and Y. YIN. Composite titanium dioxide nanomaterials. *Chemical Reviews,* 2014, **114** (19), 9853-9889.

18. EL-SHAFEI, A., M. ELSHEMY and A. ABOU-OKEIL. Eco-friendly finishing agent for cotton fabrics to improve flame retardant and antibacterial properties. *Carbohydrate Polymers*, 2015, **118**, 83-90.

19. FATTAKHOVA-ROHLFING, D., A. ZALESKA and T. BEIN. Three-dimensional titanium dioxide nanomaterials. *Chemical Reviews*, 2014, **114** (19), 9487-9558.

20. GAMINIAN, H. and M. MONTAZER. Enhanced Self-Cleaning Properties on Polyester Fabric Under Visible Light Through Single-Step Synthesis of Cuprous Oxide Doped Nano-TiO_2. *Photochemistry and Photobiology*, 2015, **91** (5), 1078-1087.

21. GRÄTZEL, M. Conversion of sunlight to electric power by nanocrystalline dye-sensitized solar cells. *Journal of Photochemistry and Photobiology A: Chemistry*, 2004, **164** (1), 3-14.

22. GU, F., W. HUANG, S. WANG, X. CHENG, Y. HU and C. LI. Improved photoelectric conversion efficiency from titanium oxide-coupled tin oxide nanoparticles formed in flame. *Journal of Power Sources*, 2014, **268**, 922-927.

23. XU, J., Y. CHEN, L. DENG, J. LIU, Y. CAO, P. LI, H. RAN, Y. ZHENG and Z. WANG. Microwave-activated nanodroplet vaporization for highly efficient tumor ablation with real-time monitoring performance. *Biomaterials*, 2016, **106**, 264-275.

24. ABBASI, A. R. and A. MORSALI. Ultrasound-assisted coating of silk yarn with silver chloride nanoparticles. *Colloids and Surfaces A: Physicochemical and Engineering Aspects*, 2010, **371** (1), 113-118.

25. ABIDI, N., E. HEQUET, S. TARIMALA and L. L. DAI. Cotton fabric surface modification for improved UV radiation protection using sol-gel process. *Journal of Applied Polymer Science,* 2007, **104** (1), 111-117.

26. ARAIN, R. A., Z. KHATRI, M. H. MEMON and I.-S. KIM. Antibacterial property and characterization of cotton fabric treated with chitosan/AgCl–TiO_2 colloid. *Carbohydrate Polymers,* 2013, **96** (1), 326-331.

27. BEHZADNIA, A., M. MONTAZER, A. RASHIDI and M. MAHMOUDI RAD. Rapid Sonosynthesis of N-Doped Nano TiO_2 on Wool Fabric at Low Temperature: Introducing Self-cleaning, Hydrophilicity, Antibacterial/Antifungal Properties with low Alkali Solubility, Yellowness and Cytotoxicity. *Photochemistry and Photobiology,* 2014, **90** (6), 1224-1233.

28. BEHZADNIA, A., M. MONTAZER, A. RASHIDI and M. M. RAD. Sonosynthesis of nano TiO_2 on wool using titanium isopropoxide or butoxide in acidic media producing multifunctional fabric. *Ultrasonics Sonochemistry,* 2014, **21** (5), 1815-1826.

29. CASCHERA, D., F. FEDERICI, T. DE CARO, B. CORTESE, P. CALANDRA, A. MEZZI, R. L. NIGRO and R. G. TORO. Fabrication of Eu-TiO_2 NCs functionalized cotton textile as a multifunctional photocatalyst for dye pollutants degradation. *Applied Surface Science,* 2018, **427**, 81-91.

30. DAOUD, W. A., S. LEUNG, W. TUNG, J. XIN, K. CHEUK and K. QI. Self-cleaning keratins. *Chemistry of Materials,* 2008, **20** (4), 1242-1244.

31. DAOUD, W. A. and J. H. XIN. Nucleation and growth of anatase crystallites on cotton fabrics at low temperatures. *Journal of the American Ceramic Society,* 2004, **87** (5), 953-955.

32. DAOUD, W. A., J. H. XIN and Y.-H. ZHANG. Surface functionalization of cellulose fibers with titanium dioxide nanoparticles and their combined bactericidal activities. *Surface Science,* 2005, **599** (1), 69-75.

33. DASTJERDI, R., M. MONTAZER and S. SHAHSAVAN. A novel technique for producing durable multifunctional textiles using nanocomposite coating. *Colloids and Surfaces B: Biointerfaces,* 2010, **81** (1), 32-41.

34. NOMAN, M. T., J. WIENER, J. SASKOVA, M. A. ASHRAF, M. VIKOVA, H. JAMSHAID and P. KEJZLAR. In-situ development of highly photocatalytic multifunctional nanocomposites by ultrasonic acoustic method. *Ultrasonics Sonochemistry,* 2018, **40**, 41-56.

35. PERELSHTEIN, I., G. APPLEROT, N. PERKAS, G. GUIBERT, S. MIKHAILOV and A. GEDANKEN. Sonochemical coating of silver nanoparticles on textile fabrics (nylon, polyester and cotton) and their antibacterial activity. *Nanotechnology,* 2008, **19** (24), 1-6.

36. PERELSHTEIN, I., G. APPLEROT, N. PERKAS, E. WEHRSCHETZ-SIGL, A. HASMANN, G. GUEBITZ and A. GEDANKEN. Antibacterial properties of an in situ generated and simultaneously deposited nanocrystalline ZnO on fabrics. *ACS Applied Materials & Interfaces,* 2008, **1** (2), 361-366.

37. PERELSHTEIN, I., G. APPLEROT, N. PERKAS, E. WEHRSCHUETZ-SIGL, A. HASMANN, G. GUEBITZ and A. GEDANKEN. CuO-cotton nanocomposite: Formation, morphology, and antibacterial activity. *Surface and Coatings Technology,* 2009, **204** (1), 54-57.

38. SARAVANAN, R., S. KARTHIKEYAN, V. GUPTA, G. SEKARAN, V. NARAYANAN and A. STEPHEN. Enhanced photocatalytic activity of ZnO/CuO nanocomposite for the degradation of textile dye on visible light illumination. *Materials Science and Engineering: C,* 2013, **33** (1), 91-98.

39. ZHANG, H. and J. F. BANFIELD. Kinetics of crystallization and crystal growth of nanocrystalline anatase in nanometer-sized amorphous titania. *Chemistry of Materials,* 2002, **14** (10), 4145-4154.

40. JAĆIMOVIĆ, J., C. VÂJU, R. GAÁL, A. MAGREZ, H. BERGER and L. FORRÓ. High-pressure study of anatase TiO_2. *Materials,* 2010, **3** (3), 1509-1514.

41. MATTHEWS, A. The crystallization of anatase and rutile from amorphous titanium dioxide under hydrothermal conditions. *American Mineralogist,* 1976, **61** (5-6), 419-424.

42. BOURIKAS, K., C. KORDULIS and A. LYCOURGHIOTIS. Titanium dioxide (anatase and rutile): surface chemistry, liquid–solid interface chemistry, and scientific synthesis of supported catalysts. *Chemical Reviews,* 2014, **114** (19), 9754-9823.

43. BAI, Y., I. MORA-SERO, F. DE ANGELIS, J. BISQUERT and P. WANG. Titanium dioxide nanomaterials for photovoltaic applications. *Chemical Reviews,* 2014, **114** (19), 10095-10130.

44. CHEN, H., C. E. NANAYAKKARA and V. H. GRASSIAN. Titanium dioxide photocatalysis in atmospheric chemistry. *Chemical Reviews,* 2012, **112** (11), 5919-5948.

45. GOKILAMANI, N., N. MUTHUKUMARASAMY, M. THAMBIDURAI, A. RANJITHA and D. VELAUTHAPILLAI. Basella alba rubra spinach pigment-sensitized TiO_2 thin film-based solar cells. *Applied Nanoscience*, 2014, **5** (3), 297.

46. LOTA, W. and A. WALAWSKA. Evaluation of the Photocatalytic Properties of Textile Fabrics Modified with Titanium Dioxide of Anatase Structure. *FIBRES & TEXTILES in Eastern Europe*, 2011, **19** (2), 85.

47. MILLS, A., R. H. DAVIES and D. WORSLEY. Water purification by semiconductor photocatalysis. *Chemical Society Reviews*, 1993, **22** (6), 417-425.

48. QI, K., W. A. DAOUD, J. H. XIN, C. MAK, W. TANG and W. CHEUNG. Self-cleaning cotton. *Journal of Materials Chemistry*, 2006, **16** (47), 4567-4574.

49. RAM, C., R. K. PAREEK and V. SINGH. Photocatalytic degradation of textile dye by using titanium dioxide nanocatalyst. *International Journal of Theoratical and Applied Sciences*, 2012, **4** (2), 82-88.

50. XU, M., Y. WANG, J. GENG and D. JING. Photodecomposition of NOx on Ag/TiO_2 composite catalysts in a gas phase reactor. *Chemical Engineering Journal*, 2017, **307**, 181-188.

51. ANDERSSON, M., L. ÖSTERLUND, S. LJUNGSTRÖM and A. PALMQVIST. Preparation of nanosize anatase and rutile TiO_2 by hydrothermal treatment of microemulsions and their activity for photocatalytic wet oxidation of phenol. *The Journal of Physical Chemistry B*, 2002, **106** (41), 10674-10679.

52. ARAMI, H., M. MAZLOUMI, R. KHALIFEHZADEH and S. SADRNEZHAAD. Sonochemical preparation of TiO_2 nanoparticles. *Materials Letters,* 2007, **61** (23), 4559-4561.

53. ARENAS, M., L. F. RODRÍGUEZ-NÚNEZ, D. RANGEL, O. MARTÍNEZ-ÁLVAREZ, C. MARTÍNEZ-ALONSO and V. CASTAÑO. Simple one-step ultrasonic synthesis of anatase titania/polypyrrole nanocomposites. *Ultrasonics Sonochemistry,* 2013, **20** (2), 777-784.

54. BESSEKHOUAD, Y., D. ROBERT and J. V. WEBER. Synthesis of photocatalytic TiO_2 nanoparticles: optimization of the preparation conditions. *Journal of Photochemistry and Photobiology A: Chemistry,* 2003, **157** (1), 47-53.

55. BLEŠIĆ, M. D., Z. ŠAPONJIĆ, J. NEDELJKOVIĆ and D. USKOKOVIĆ. TiO_2 films prepared by ultrasonic spray pyrolysis of nanosize precursor. *Materials Letters,* 2002, **54** (4), 298-302.

56. CAI, H., W. MU, W. LIU, X. ZHANG and Y. DENG. Sol-gel synthesis highly porous titanium dioxide microspheres with cellulose nanofibrils-based aerogel templates. *Inorganic Chemistry Communications,* 2015, **51**, 71-74.

57. CARATTO, V., F. LOCARDI, S. ALBERTI, S. VILLA, E. SANGUINETI, A. MARTINELLI, T. BALBI, L. CANESI and M. FERRETTI. Different sol-gel preparations of iron-doped TiO_2 nanoparticles: characterization, photocatalytic activity and cytotoxicity. *Journal of Sol-Gel Science and Technology,* 2016, **80**, 152-159.

58. CARGNELLO, M., T. R. GORDON and C. B. MURRAY. Solution-phase synthesis of titanium dioxide nanoparticles and nanocrystals. *Chemical Reviews,* 2014, **114** (19), 9319-9345.

59. CHIBAC, A. L., V. MELINTE, T. BURUIANA, I. MANGALAGIU and E. C. BURUIANA. Preparation of photocrosslinked sol-gel composites based on urethane-acrylic matrix, silsesquioxane sequences, TiO_2, and Ag/Au Nanoparticles for use in photocatalytic applications. *Journal of Polymer Science Part A: Polymer Chemistry,* 2015, **53** (10), 1189-1204.

60. FAN, Z., F. MENG, J. GONG, H. LI, Z. DING and B. DING. One-step hydrothermal synthesis of mesoporous Ce-doped anatase TiO_2 nanoparticles with enhanced photocatalytic activity. *Journal of Materials Science: Materials in Electronics,* 2016, **11** (27), 11866-11872.

61. GUO, J., S. ZHU, Z. CHEN, Y. LI, Z. YU, Q. LIU, J. LI, C. FENG and D. ZHANG. Sonochemical synthesis of TiO_2 nanoparticles on graphene for use as photocatalyst. *Ultrasonics Sonochemistry,* 2011, **18** (5), 1082-1090.

62. GUO, W., Z. LIN, X. WANG and G. SONG. Sonochemical synthesis of nanocrystalline TiO_2 by hydrolysis of titanium alkoxides. *Microelectronic Engineering,* 2003, **66** (1), 95-101.

63. HOSSAIN, M. K., U. S. AKHTAR, A. R. KOIRALA, I. C. HWANG and K. B. YOON. Steam-assisted synthesis of uniformly mesoporous anatase and its remarkably superior photocatalytic activities. *Catalysis Today,* 2015, **243**, 228-234.

64. JHUANG, Y.-Y. and W.-T. CHENG. Fabrication and characterization of silver/titanium dioxide composite nanoparticles in ethylene glycol with alkaline solution through sonochemical process. *Ultrasonics Sonochemistry*, 2016, **28**, 327-333.

65. KADAM, A., R. DHABBE, M. KOKATE, Y. GAIKWAD and K. GARADKAR. Preparation of N doped TiO_2 via microwave-assisted method and its photocatalytic activity for degradation of malathion. *Spectrochimica Acta Part A: Molecular and Biomolecular Spectroscopy*, 2014, **133**, 669-676.

66. KALE, R. and C. R. MEENA. Synthesis of Titanium dioxide Nanoparticles and Application on Nylon fabric using Layer by Layer technique for Antimicrobial Property. *Advances in Applied Science Research*, 2012, **3** (5), 3073-3080.

67. LI, D., H. WANG, W. JING, Y. FAN and W. XING. Fabrication of mesoporous TiO_2 membranes by a nanoparticle-modified polymeric sol process. *Journal of Colloid and Interface Science*, 2014, **433**, 43-48.

68. LI, M., Y. JIANG, R. DING, D. SONG, H. YU and Z. CHEN. Hydrothermal synthesis of anatase TiO_2 nanoflowers on a nanobelt framework for photocatalytic applications. *Journal of Electronic Materials*, 2013, **42** (6), 1290.

69. MUTUMA, B. K., G. N. SHAO, W. D. KIM and H. T. KIM. Sol-gel synthesis of mesoporous anatase-brookite and anatase-brookite-rutile TiO_2 nanoparticles and their photocatalytic properties. *Journal of Colloid and Interface Science*, 2015, **442**, 1-7.

70. SHAHMORADI, B., M. NEGAHDARY and A. MALEKI. Hydrothermal synthesis of surface-modified, manganese-doped TiO_2 nanoparticles for photodegradation of methylene blue. *Environmental Engineering Science*, 2012, **29** (11), 1032-1037.

71. SUGIMOTO, T., X. ZHOU and A. MURAMATSU. Synthesis of uniform anatase TiO_2 nanoparticles by gel-sol method: 4. Shape control. *Journal of Colloid and Interface Science*, 2003, **259** (1), 53-61.

72. SUN, Y. and Y. XIA. Shape-controlled synthesis of gold and silver nanoparticles. *Science*, 2002, **298** (5601), 2176-2179.

73. TEOH, W. Y., L. MÄDLER, D. BEYDOUN, S. E. PRATSINIS and R. AMAL. Direct (one-step) synthesis of TiO_2 and Pt/TiO_2 nanoparticles for photocatalytic mineralisation of sucrose. *Chemical Engineering Science*, 2005, **60** (21), 5852-5861.

74. VALENCIA, S., X. VARGAS, L. RIOS, G. RESTREPO and J. M. MARÍN. Sol-gel and low-temperature solvothermal synthesis of photoactive nano-titanium dioxide. *Journal of Photochemistry and Photobiology A: Chemistry*, 2013, **251**, 175-181.

75. WANG, P., T. XIE, L. PENG, H. LI, T. WU, S. PANG and D. WANG. Water-assisted synthesis of anatase TiO_2 nanocrystals: mechanism and sensing properties to oxygen at room temperature. *The Journal of Physical Chemistry C*, 2008, **112** (17), 6648-6652.

76. SUSLICK, K. S. Ultrasound in synthesis. In *Modern Synthetic Methods 1986.* Springer, 1986, p. 1-60.

77. MESKIN, P. E., V. K. IVANOV, A. E. BARANTCHIKOV, B. R. CHURAGULOV and Y. D. TRETYAKOV. Ultrasonically assisted hydrothermal synthesis of nanocrystalline

ZrO_2, TiO_2, $NiFe_2O_4$ and $Ni_{0.5}$ $Zn_{0.5}$ Fe_2O_4 powders. *Ultrasonics Sonochemistry,* 2006, **13** (1), 47-53.

78. SADR, F. A. and M. MONTAZER. In-situ sonosynthesis of nano TiO_2 on cotton fabric. *Ultrasonics Sonochemistry,* 2014, **21** (2), 681-691.

79. FUJISHIMA, A., T. N. RAO and D. A. TRYK. Titanium dioxide photocatalysis. *Journal of Photochemistry and Photobiology C: Photochemistry Reviews,* 2000, **1** (1), 1-21.

80. SCHNEIDER, J., M. MATSUOKA, M. TAKEUCHI, J. ZHANG, Y. HORIUCHI, M. ANPO and D. W. BAHNEMANN. Understanding TiO_2 photocatalysis: mechanisms and materials. *Chemical Reviews,* 2014, **114** (19), 9919-9986.

81. CHENG, Q., C. LI, V. PAVLINEK, P. SAHA and H. WANG. Surface-modified antibacterial TiO_2/Ag^+ nanoparticles: preparation and properties. *Applied Surface Science,* 2006, **252** (12), 4154-4160.

82. EL-RAFIE, M., A. MOHAMED, T. I. SHAHEEN and A. HEBEISH. Antimicrobial effect of silver nanoparticles produced by fungal process on cotton fabrics. *Carbohydrate Polymers,* 2010, **80** (3), 779-782.

83. HEBEISH, A., M. ABDELHADY and A. YOUSSEF. TiO_2 nanowire and TiO_2 nanowire doped Ag-PVP nanocomposite for antimicrobial and self-cleaning cotton textile. *Carbohydrate Polymers,* 2013, **91** (2), 549-559.

84. KARIMI, L., M. E. YAZDANSHENAS, R. KHAJAVI, A. RASHIDI and M. MIRJALILI. Optimizing the photocatalytic properties and the synergistic effects of graphene

and nano titanium dioxide immobilized on cotton fabric. *Applied Surface Science,* 2015, **332**, 665-673.

85. LONG, M., L. ZHENG, B. TAN and H. SHU. Photocatalytic self-cleaning cotton fabrics with platinum (IV) chloride modified TiO_2 and N-TiO_2 coatings. *Applied Surface Science,* 2016, **386**, 434-441.

86. PERELSHTEIN, I., G. APPLEROT, N. PERKAS, J. GRINBLAT and A. GEDANKEN. A One-Step Process for the Antimicrobial Finishing of Textiles with Crystalline TiO_2 Nanoparticles. *Chemistry-A European Journal,* 2012, **18** (15), 4575-4582.

87. FIEVET, F., J. LAGIER, B. BLIN, B. BEAUDOIN and M. FIGLARZ. Homogeneous and heterogeneous nucleations in the polyol process for the preparation of micron and submicron size metal particles. *Solid State Ionics,* 1989, **32**, 198-205.

88. KURIHARA, L., G. CHOW and P. SCHOEN. Nanocrystalline metallic powders and films produced by the polyol method. *Nanostructured Materials,* 1995, **5** (6), 607-613.

89. SUN, Y., Y. YIN, B. T. MAYERS, T. HERRICKS and Y. XIA. Uniform silver nanowires synthesis by reducing $AgNO_3$ with ethylene glycol in the presence of seeds and poly (vinyl pyrrolidone). *Chemistry of Materials,* 2002, **14** (11), 4736-4745.

90. KHUSHALANI, D., G. A. OZIN and A. KUPERMAN. Glycometallate surfactants. Part 1: non-aqueous synthesis of mesoporous silica. *Journal of Materials Chemistry,* 1999, **9** (7), 1483-1489.

91. OZIN, G. Glycometallate surfactants Part 2: non-aqueous synthesis of mesoporous titanium, zirconium and niobium oxides. *Journal of Materials Chemistry,* 1999, **9** (7), 1491-1500.

92. SCOTT, R. W., N. COOMBS and G. A. OZIN. Non-aqueous synthesis of mesostructured tin dioxide. *Journal of Materials Chemistry,* 2003, **13** (4), 969-974.

93. MO, T.-C. and S.-Y. CHEN. Physical characterization and electrical properties of chelating-agents added PZT films. *Ferroelectrics,* 2001, **259** (1), 305-310.

94. KAKIHANA, M., M. ARIMA, M. YOSHIMURA, N. IKEDA and Y. SUGITANI. Synthesis of high surface area $LaMnO_{3+d}$ by a polymerizable complex method. *Journal of Alloys and Compounds,* 1999, **283** (1), 102-105.

95. LEE, S., M. BIEGALSKI and W. KRIVEN. Powder synthesis of barium titanate and barium orthotitanate via an ethylene glycol complex polymerization route. *Journal of Materials Research,* 1999, **14** (07), 3001-3006.

96. HASSANI, A., A. KHATAEE, S. KARACA, C. KARACA and P. GHOLAMI. Sonocatalytic degradation of ciprofloxacin using synthesized TiO_2 nanoparticles on montmorillonite. *Ultrasonics Sonochemistry,* 2017, **35**, 251-262.

97. FATHINIA, M., A. KHATAEE, S. ABER and A. NASERI. Development of kinetic models for photocatalytic ozonation of phenazopyridine on TiO_2 nanoparticles thin film in a mixed semi-batch photoreactor. *Applied Catalysis B: Environmental,* 2016, **184**, 270-284.

98. HEBEISH, A., M. EL-NAGGAR, M. M. FOUDA, M. RAMADAN, S. S. AL-DEYAB and M. EL-RAFIE. Highly effective antibacterial textiles containing green synthesized silver nanoparticles. *Carbohydrate Polymers*, 2011, **86** (2), 936-940.

99. GASHTI, M. P. and A. ALMASIAN. UV radiation induced flame retardant cellulose fiber by using polyvinylphosphonic acid/carbon nanotube composite coating. *Composites Part B: Engineering*, 2013, **45** (1), 282-289.

100. GASHTI, M. P., A. ELAHI and M. P. GASHTI. UV radiation inducing succinic acid/silica-kaolinite network on cellulose fiber to improve the functionality. *Composites Part B: Engineering*, 2013, **48**, 158-166.

101. MALEKI, A., M. SAFARI, R. REZAEE, R. D. CHESHMEH SOLTANI, B. SHAHMORADI and Y. ZANDSALIMI. Photocatalytic degradation of humic substances in the presence of ZnO nanoparticles immobilized on glass plates under ultraviolet irradiation. *Separation Science and Technology*, 2016, **51** (14), 2484-2489.

102. HUANG, W., X. TANG, Y. WANG, Y. KOLTYPIN and A. GEDANKEN. Selective synthesis of anatase and rutile via ultrasound irradiation. *Chemical Communications*, 2000, (15), 1415-1416.

103. GHOWS, N. and M. H. ENTEZARI. Ultrasound with low intensity assisted the synthesis of nanocrystalline TiO_2 without calcination. *Ultrasonics Sonochemistry*, 2010, **17** (5), 878-883.

104. PRASAD, K., D. PINJARI, A. PANDIT and S. MHASKE. Synthesis of titanium dioxide by ultrasound assisted sol-gel technique: effect of amplitude (power density) variation. *Ultrasonics Sonochemistry*, 2010, **17** (4), 697-703.

105. PRASAD, K., D. PINJARI, A. PANDIT and S. MHASKE. Phase transformation of nanostructured titanium dioxide from anatase-to-rutile via combined ultrasound assisted sol–gel technique. *Ultrasonics Sonochemistry*, 2010, **17** (2), 409-415.

106. BABU, S. G., R. VINOTH, D. P. KUMAR, M. V. SHANKAR, H.-L. CHOU, K. VINODGOPAL and B. NEPPOLIAN. Influence of electron storing, transferring and shuttling assets of reduced graphene oxide at the interfacial copper doped TiO_2 p-n heterojunction for increased hydrogen production. *Nanoscale*, 2015, **7** (17), 7849-7857.

107. VINOTH, R., P. KARTHIK, C. MUTHAMIZHCHELVAN, B. NEPPOLIAN and M. ASHOKKUMAR. Carrier separation and charge transport characteristics of reduced graphene oxide supported visible-light active photocatalysts. *Physical Chemistry Chemical Physics*, 2016, **18** (7), 5179-5191.

108. KARTHIK, P., R. VINOTH, P. SELVAM, E. BALARAMAN, M. NAVANEETHAN, Y. HAYAKAWA and B. NEPPOLIAN. A visible-light active catechol-metal oxide carbonaceous polymeric material for enhanced photocatalytic activity. *Journal of Materials Chemistry A*, 2017, **5** (1), 384-396.

109. XU, Y., W. WEN, M.-Z. TANG and J.-M. WU. Photocatalytically active TiO_2 microtubes assembled with radially aligned nanowires. *Materials Chemistry Frontiers*, 2017, **1**, 1453-1458.

110. ZHANG, J., G. XIAO, F.-X. XIAO and B. LIU. Revisiting one-dimensional TiO_2 based hybrid heterostructures for heterogeneous photocatalysis: a critical review. *Materials Chemistry Frontiers*, 2017, **1**, 231-250.

111. XIN, J., W. DAOUD and Y. KONG. A new approach to UV-blocking treatment for cotton fabrics. *Textile Research Journal*, 2004, **74** (2), 97-100.

112. UDDIN, M., F. CESANO, F. BONINO, S. BORDIGA, G. SPOTO, D. SCARANO and A. ZECCHINA. Photoactive TiO_2 films on cellulose fibres: synthesis and characterization. *Journal of Photochemistry and Photobiology A: Chemistry*, 2007, **189** (2), 286-294.

113. LESSAN, F., M. MONTAZER and M. MOGHADAM. A novel durable flame-retardant cotton fabric using sodium hypophosphite, nano TiO_2 and maleic acid. *Thermochimica Acta*, 2011, **520** (1), 48-54.

114. NAZARI, A., M. MONTAZER, A. RASHIDI, M. YAZDANSHENAS and M. B. MOGHADAM. Optimization of cotton crosslinking with polycarboxylic acids and nano TiO_2 using central composite design. *Journal of Applied Polymer Science*, 2010, **117** (5), 2740-2748.

115. BIRKS, L. and H. FRIEDMAN. Particle size determination from X-ray line broadening. *Journal of Applied Physics*, 1946, **17** (8), 687-692.

116. NOMAN, M. T., J. MILITKY, J. WIENER, J. SASKOVA, M. A. ASHRAF, H. JAMSHAID and M. AZEEM. Sonochemical Synthesis of Highly Crystalline Photocatalyst For Industrial Applications. *Ultrasonics*, 2018, **83**, 203-213.

117. MONTAZER, M., A. BEHZADNIA, E. PAKDEL, M. K. RAHIMI and M. B. MOGHADAM. Photo induced silver on nano titanium dioxide as an enhanced antimicrobial agent for wool. *Journal of Photochemistry and Photobiology B: Biology,* 2011, **103** (3), 207-214.

118. AMINI, M., H. YOUNESI, N. BAHRAMIFAR, A. A. Z. LORESTANI, F. GHORBANI, A. DANESHI and M. SHARIFZADEH. Application of response surface methodology for optimization of lead biosorption in an aqueous solution by Aspergillus niger. *Journal of Hazardous materials,* 2008, **154** (1), 694-702.

119. BOX, G. E. and N. R. DRAPER *Empirical model-building and response surfaces*. Wiley New York, 1987.

120. AGUSTINA, T. E., H. ANG and V. VAREEK. A review of synergistic effect of photocatalysis and ozonation on wastewater treatment. *Journal of Photochemistry and Photobiology C: Photochemistry Reviews,* 2005, **6** (4), 264-273.

121. HARIFI, T. and M. MONTAZER. Free carrier dyeing of polyester fabric using nano TiO_2. *Dyes and Pigments,* 2013, **97** (3), 440-445.

122. MONTAZER, M., F. ALIMOHAMMADI, A. SHAMEI and M. K. RAHIMI. Durable antibacterial and cross-linking cotton with colloidal silver nanoparticles and butane tetracarboxylic acid without yellowing. *Colloids and Surfaces B: Biointerfaces,* 2012, **89**, 196-202.

123. PAKDEL, E. and W. A. DAOUD. Self-cleaning cotton functionalized with TiO_2/SiO_2: focus on the role of silica. *Journal of Colloid and Interface Science,* 2013, **401**, 1-7.

124. ZHANG, H., H. ZHU and R. SUN. Fabrication of photocatalytic TiO_2 nanoparticle film on PET fabric by hydrothermal method. *Textile Research Journal*, 2012, **82** (8), 747-754.

125. WU, D., M. LONG, J. ZHOU, W. CAI, X. ZHU, C. CHEN and Y. WU. Synthesis and characterization of self-cleaning cotton fabrics modified by TiO_2 through a facile approach. *Surface and Coatings Technology*, 2009, **203** (24), 3728-3733.

126. NAZARI, A., M. MONTAZER, M. MOGHADAM and M. ANARY-ABBASINEJAD. Self-cleaning properties of bleached and cationized cotton using nanoTiO_2: A statistical approach. *Carbohydrate Polymers*, 2011, **83** (3), 1119-1127.

127. YANG, H., S. ZHU and N. PAN. Studying the mechanisms of titanium dioxide as ultraviolet-blocking additive for films and fabrics by an improved scheme. *Journal of Applied Polymer Science*, 2004, **92** (5), 3201-3210.

128. KAUR, K. and C. V. SINGH. Amorphous TiO_2 as a photocatalyst for hydrogen production: a DFT study of structural and electronic properties. *Energy Procedia*, 2012, **29**, 291-299.

129. PATIL, M. N. and A. B. PANDIT. Cavitation-a novel technique for making stable nano-suspensions. *Ultrasonics Sonochemistry*, 2007, **14** (5), 519-530.

130. BANG, J. H. and K. S. SUSLICK. Applications of ultrasound to the synthesis of nanostructured materials. *Advanced Materials*, 2010, **22** (10), 1039-1059.

131. MOHOLKAR, V. S. *Intensification of textile treatments: sonoprocess engineering*. Twente University Press, 2002. ISBN 9036517516.

132. MOHOLKAR, V. and M. WARMOESKERKEN. Investigations in mass transfer enhancement in textiles with ultrasound. *Chemical Engineering Science*, 2004, **59** (2), 299-311.

133. REDDY, K. M., C. G. REDDY and S. MANORAMA. Preparation, characterization, and spectral studies on nanocrystalline anatase TiO_2. *Journal of Solid State Chemistry*, 2001, **158** (2), 180-186.

134. GHORBANI, F., H. YOUNESI, S. M. GHASEMPOURI, A. A. ZINATIZADEH, M. AMINI and A. DANESHI. Application of response surface methodology for optimization of cadmium biosorption in an aqueous solution by Saccharomyces cerevisiae. *Chemical Engineering Journal*, 2008, **145** (2), 267-275.

135. MONTAZER, M., F. LESSAN and M. MOGHADAM. Nano-TiO_2/maleic acid/triethanol amine/sodium hypophosphite colloid on cotton to produce cross-linking and self-cleaning properties. *Journal of the Textile Institute*, 2012, **103** (8), 795-805.

7 List of Publications

7.1 Publications in Impact Factor Journals

1. M.T. Noman, J. Wiener, J. Saskova, M.A. Ashraf, M. Vikova, H. Jamshaid, P. Kejzlar, "In-situ development of highly photocatalytic multifunctional nanocomposites by ultrasonic acoustic method". ***Ultrasonics Sonochemistry***, 40 (2018), 41-56. **Impact factor: 6.012**.
2. M.T. Noman, J. Militky, J. Wiener, J. Saskova, M.A. Ashraf, H. Jamshaid, M. Azeem, "Sonochemical synthesis of highly crystalline photocatalyst for industrial applications". ***Ultrasonics***, 83 (2018), 203-213. **Impact factor: 2.377.**
3. M.T. Noman, M.A. Ashraf, H. Jamshaid, A. Ali, A novel green stabilization of TiO_2 nanoparticles onto cotton, ***Fibers and Polymers***, (Accepted). **Impact factor: 1.353.**
4. H. Jamshaid, R. Mishra, J. Militky, M. Pechociakova, M.T. Noman, "Mechanical, thermal and interfacial properties of green composites from basalt and hybrid woven fabrics". ***Fibers and Polymers***, 17 (2016), 1675-1686. **Impact factor: 1.353.**
5. H. Jamshaid, R. Mishra, J. Militky, M.T. Noman, "Interfacial Performance and Durability of Textile Reinforced Concrete". ***The Journal of the Textile Institute***, 109 (2017), 879-890. **Impact factor: 1.174.**
6. A. Ali, N.H.A. Nguyen, V. Baheti, M. Ashraf, J. Militky, T. Mansoor, M.T. Noman, S. Ahmad, "Electrical conductivity and physiological comfort of silver coated cotton fabrics". ***The Journal of the Textile Institute***, 109 (2017), 620-628. **Impact factor: 1.174.**

7. M.A. Ashraf, J. Wiener, A. Farooq, J. Saskova, M.T. Noman, "Development of Maghemite Glass Fibre Nanocomposite for Adsorptive Removal of Methylene Blue". ***Fibers and Polymers***, 19 (2018), 1735-1746. **Impact factor: 1.353.**
8. M.T. Noman, M.A. Ashraf, H. Jamshaid, A. Ali, Synthesis and Applications of Nano TiO_2: A Review, ***Environmental Science and Pollution Research***, (Under Review). **Impact factor: 2.80.**
9. M.A. Ashraf, J. Wiener, A. Farooq, M.T. Noman, J. Saskova, S. Naeem, "Selective synthesis of iron oxide nanoparticles for efficient adsorption of methylene blue". ***Desalination and Water Treatment***, (Under Review). **Impact factor: 2.327.**

7.2 Publications in International Conferences

1. M.T. Noman, J. Wiener, J. Saskova, M.A. Ashraf, H. Jamshaid., "Synthesis and characterization of highly crystalline anatase form titania by ultrasonic cavitation method". 8th International Textile, Clothing & Design Conference, October 02nd to 05th 2016, Dubrovnik, Croatia.
2. M.A. Ashraf, J. Wiener, M.S. Naeem, M.T. Noman., "Synthesis and application of iron oxide nanoparticles for efficient adsorption of acid red dye from water". 8th International Conference on Nanomaterials - Research and Application, NANOCON 2016; Hotel Voronez IBrno; Czech Republic; 19 October 2016 through 21 October 2016; Code 126915.
3. H. Jamshaid, R. Mishra, M.T. Noman., "Effect of basalt nanoparticles on mechanical and thermal characterization". 8th International Conference on Nanomaterials - Research and Application, NANOCON 2016; Hotel Voronez IBrno; Czech Republic; 19 October 2016 through 21 October 2016; Code 126915.

4. N.A. Jamil, B. Shahbaz, M.T. Noman., "Performance Evaluation of Ultrasonic Assisted Reactive Dyeing of Cotton Under Multiple Variables". The Fiber Society Spring 2010, International Conference, May 12-14, 2010. Merinos Congress Center, Bursa, Turkey.

7.3 Book Chapters

1. "Synthesis and Characterization of Anatase Phase Nanoparticles". **Advances in Fibrous Material Science.**
2. "New generation of flame-resistant woven fabrics from green material". **Advances in Fibrous Material Science.**

TECHNICAL UNIVERSITY OF LIBEREC
Faculty of Textile Engineering

Resume

MUHAMMAD TAYYAB NOMAN MSc
15th Feb 1986, Pakistan

Vision & Skills

- An enthusiastic, adaptive and fast-learning individual with a broad and acute interest in textiles, nanocomposites, ultrasonics and discovery of new innovations
- I particularly enjoy collaborating with scientists from different disciplines to develop new skills and solve new challenges

Education

PhD (Textile Engineering) **Continue**
Technical University of Liberec, **Czech Republic**

MSc (Fibre Technology) **2009**
University of Agriculture, Faisalabad, **Pakistan**

Languages

English: Professional proficiency
Urdu: Native proficiency
Punjabi: Native proficiency

Personal Info

Email: tayyab_noman411@yahoo.com
Mobile: 00420-776396302
Country of stay: Czech Republic
Nationality: Pakistani

Publications

M.T. Noman, J. Wiener, J. Saskova, M.A. Ashraf, M. Vikova, H. Jamshaid, P. Kajzlar., "In-situ development of highly photocatalytic multifunctional nanocomposites by ultrasonic acoustic method", *Ultrasonics Sonochemistry*, 40 (2018), 41-56. **Impact factor: 6.012**

M.T. Noman, J. Militky, J. Wiener, J. Saskova, M.A. Ashraf, H. Jamshaid, M. Azeem., "Sonochemical synthesis of highly crystalline photocatalyst for industrial applications", Ultrasonics 83 (2018), 203-213. **Impact factor: 2.377**

Conference Papers

Muhammad Tayyab Noman, Jakub Wiener, Jana Saskova, Muhammad Azeem Ashraf, Hafsa Jamshaid., "Synthesis and characterization of highly crystalline anatase form titania by ultrasonic cavitation method". 8th International Textile, Clothing & Design Conference, October 02nd to 05th 2016, Dubrovnik, Croatia.

Muhammad Azeem Ashraf, Jakub Wiener, Muhammad Salman Naeem, Muhammad Tayyab Noman., "Synthesis and application of iron oxide nanoparticles for efficient adsorption of acid red dye from water". 8th International Conference on Nanomaterials - Research and Application, NANOCON 2016; Hotel Voronez IBrno; Czech Republic; 19 October 2016 through 21 October 2016; Code 126915.